REPORT DOCUMENTATION PAGE

Form Approved
OMB NO. 0704-0188

1. AGENCY USE ONLY (Leave Blank)	2. REPORT DATE	3. REPORT TYPE AND DATES COVERED
	19 October 2004	Final 01 Sep02 - 31 May04

4. TITLE AND SUBTITLE

Adaptation of Advanced Diesel Engines for Military Requirements Under Severe Environmental Conditions

5. FUNDING NUMBERS

G: DAAD19-02-1-0372

6. AUTHOR(S)

Naeim A. Henein, Dinu Taraza and Nabil Chalhoub

7. PERFORMING ORGANIZATION NAME(S) AND ADDRESS(ES)

Wayne State University Office of Sponsored Programs, 656 West Kirby, 4001 Faculty Admin. Bldg, Detroit, MI 48202-3629

8. PERFORMING ORGANIZATION REPORT NUMBER

9. SPONSORING / MONITORING AGENCY NAME(S) AND ADDRESS(ES)

U. S. Army Research Office
P.O. Box 12211
Research Triangle Park, NC 27709-2211

10. SPONSORING / MONITORING AGENCY REPORT NUMBER

43997.1-EG

11. SUPPLEMENTARY NOTES

The views, opinions and/or findings contained in this report are those of the author(s) and should not be construed as an official Department of the Army position, policy or decision, unless so designated by other documentation.

12 a. DISTRIBUTION / AVAILABILITY STATEMENT

Approved for public release; distribution unlimited.

12 b. DISTRIBUTION CODE

13. ABSTRACT (Maximum 200 words)

The overall goal of this program is to adapt commercially produced heavy duty diesel engines to meet the goals the military engines for maximum power, better fuel economy, and low signature in the field by white or black smoke and compactness for mobility. The commercial advanced heavy-duty diesel engines are produced to meet stringent emission standards, causing penalties in peak power and fuel economy. This project addressed three major thrust areas. The first area is to determine the effect of replacing the commercially available fuel with JP8 fuel. The second area is to examine the different control strategies used in advanced diesel engines to meet the emission goals and their effect on engine performance, fuel economy and exhaust emissions. This requires a basic understanding of the different strategies used in the commercial vehicles to meet the emission standards and to develop new strategies to optimize the fuel economy and maximize the power density without exceeding the low smoke limits allowable in the field. The third area is a fundamental investigation on the lubrication of the main engine bearings. Four codes have been developed in Matlab to calculate the loading of the engine main bearings and, determine the journal orbit and the oil film thickness.

14. SUBJECT TERMS

Diesel engines, JP8 fuel, DF2 Fuel, Cold start, Cranking period, Control strategies, Common rail Injection system, Cylinder gas pressure trace.

15. NUMBER OF PAGES

75

16. PRICE CODE

17. SECURITY CLASSIFICATION OR REPORT	18. SECURITY CLASSIFICATION ON THIS PAGE	19. SECURITY CLASSIFICATION OF ABSTRACT	20. LIMITATION OF ABSTRACT
UNCLASSIFIED	**UNCLASSIFIED**	**UNCLASSIFIED**	**UL**

NSN 7540-01-280-5500

Standard Form 298 (Rev.2-89)
Prescribed by ANSI Std. 239-18
298-102

FINAL REPORT

Contract: DAAD19-02-1-0372, (09-01-02 to 02/29/2004)

ADAPTATION OF ADVANCED DIESEL ENGINES FOR MILITARY REQUIREMENTS UNDER SEVERE ENVIRONMENTAL CONDITIONS

By

Naeim. A. Henein, Ph.D.
Tel. (313) 577 3887
Fax. (313) 577 878
Email: henein@wayne.edu

Dinu Taraza, Ph.D.
Tel.(313) 5773701
Fax. (313) 577 8789
email: taraza@eng.wayne.edu

Nabil Chalhoub, Ph.D.
Tel. (313) 577 3753
Fax. (313) 577 8789
email:nchalhooub@eng.wayne.edu

Wayne State University
Engineering building
5050 Anthony Wayne Drive
Detroit, Michigan 48202

To
U. S. Army Research Office
Research Triangle Park, NC 27709-2211

October 15, 2004

Table of Contents **Page**

List of Figures

List of Appendixes

ABSTRACT

Advanced heavy-duty commercial diesel engines are produced to meet stringent emission standards, causing penalties in peak power and fuel economy. Since future military engines are expected to be obtained from the commercial sector, there is a need to adapt the commercial engines to the military requirements.

This project addressed three major thrust areas. The first area is to determine the effect of replacing the commercially available fuel with JP8 fuel. The main differences between the two fuels are: (a) JP 8 is a more volatile fuel than DF2, and (b) The cetane number for JP8 is 37, compared to 45 for DF2. A review of the literature indicates that most of the cold start investigations on diesel engines had been experimental and emphasized the effect of cetane number. In this project a mathematical model has been developed to account for the combined effects of the fuel volatility and cetane number on the cold start process and the cranking period. The model predictions are compared with the experimental results obtained on a single cylinder direct injection diesel engine at different ambient temperatures. The tests were conducted in a cold room, where the engine is soaked for at least 8 hours before conducting the cold start test. The predictions showed a fairly good agreement with the experimental data.

The second area is to examine the different control strategies used in advanced diesel engines to meet the emission goals and their effect on engine performance, fuel economy and exhaust emissions. For the commercial engines, one of the major goals is to control the combustion process by the OPERAS (Optimizing fuel injection Pressure, EGR %, injection timing: Retard or Advance, and the Swirl ratio) to achieve the engine-out emission goals. .The strategies used in commercial diesel engines are not available in the literature and are impossible to get from the manufacturer. There fore, the modification of the current and future strategies requires a basic understanding of the diesel combustion process in advanced diesel engines and an awareness of the several strategies needed to meet specific emission standards. To achieve this, a detailed analysis is made of the experimental traces of the cylinder gas pressure to determine the rate of burning of the fuel (Rate of Heat Release, RHR), from which we can determine the different modes of diesel combustion, and the strategies that produce them. The validity of such an analysis depends on of the accuracy of the cylinder gas pressure trace. This required a study of the effect of smoothing the pressure trace on the interpretation of experimental data for diesel combustion. Also, the effect of the characteristics of the common rail injection system, which will be widely used in advanced diesel engines, is investigated. Finally, illustrations are made for the integrated OPERAS strategies for low emissions in high speed direct injection engines.

The third area is a fundamental investigation on the lubrication of the main engine bearings. Four codes have been developed in Matlab to calculate the loading of the engine main bearings and, determine the journal orbit and the oil film thickness. The model predictions will be compared with the experimental data obtained on a single cylinder diesel engine instrumented with a pressure transducer and gap sensors to measure the journal orbit. The model will be used to compute the maximum load the bearings can stand in high power density heavy military diesel engines.

GOAL

The overall goal of this program is to adapt the commercially produced heavy duty diesel engines to meet the goals the military engines for maximum power, better fuel economy, and low signature in the field by white or black smoke and compactness for mobility. This requires a basic understanding of the different strategies used in the commercial vehicles to meet the emission standards and to develop new strategies to optimize the fuel economy and maximize the power density without exceeding the low smoke limits allowable in the field.

MOTIVATION

Commercial diesel engines are subjected to very strict emission regulations. The measures taken by industry to meet these standards might affect the power density and fuel economy of the engine. Further more, commercial vehicles are designed to run on the commercially available diesel fuel DF2. Meanwhile, the military engines might be required to use JP8 fuel instead of DF2. One of the problems that need to be addressed is the cold starting on JP8. This will require new strategies for fuel injection to ensure a reliable cold starting without hesitation and the emission of white smoke that produces an undesirable signal in the field. Another issue to be addressed is the electronic controls of the engine to meet the military needs of high power and best fuel economy. In commercial engines, the injection parameters are adjusted to meet the emission standards. To modify the strategy in commercial engines to meet the military needs requires a basic understanding of different control strategies. In this project, a detailed analysis of the effect of the different engine operating parameters on performance, fuel economy and engine-out emissions is made and the different strategies are examined.

Further more, the commercial engines are designed with a large factor of safety, in order to avoid the expensive recalls and warranties. In the case of military engines, the highest priority is in maximum power and best fuel economy. It is clear then that different engine components in military engines can stand a heavier load than that allowed in commercial engines. The main engine bearings represent the component that might fail under heavier loads. In this project computer models have been developed to compute the orbit of the journal in the bearing. If the clearance between the journal and bearing gets below a certain value, metal to metal contact will take place and end in failure. The models are put in a Simulink Format for easy access and application in different engine types.

APPROACH

The program consists of two interacting research areas:

I. Control strategies for maximum power density and fuel economy
   1. Adaptation of the commercially produced diesel engine to operate on JP8 fuel.
   2. Effect of Cycle-to-Cycle Variation in the Injection Pressure in a common rail injection system
   3. Effect of Smoothing the Cylinder Gas Pressure Trace on the Computed Tare of Energy Release

II. Tribology of the Main Engine bearings

2. Effect of Cycle-to-Cycle Variation in the Injection Pressure in a common rail injection system
3. Effect of Smoothing the Cylinder Gas Pressure Trace on the Computed Tare of Energy Release

II. Tribology of the Main Engine bearings

I. CONTROL STRATEGY FOR MAXIMUM POWER DENSITY and FUEL ECONOMY

1. Adaptation of the commercially produced diesel engine to operate on JP8 fuel:

Commercial diesel engines are designed and developed to run on the commercially available DF2 fuel. But military diesel engines might be required to run on JP8 fuel which has different properties than DF2. The main differences between the two fuels are the volatility and Cetane Number, both of which affect the cold starting process. Figures 1and 2 show the gas chromatographs for DF2 and JP8 fuels respectively. It is clear that JP8 contains higher fractions of lower carbon contents than DF2.

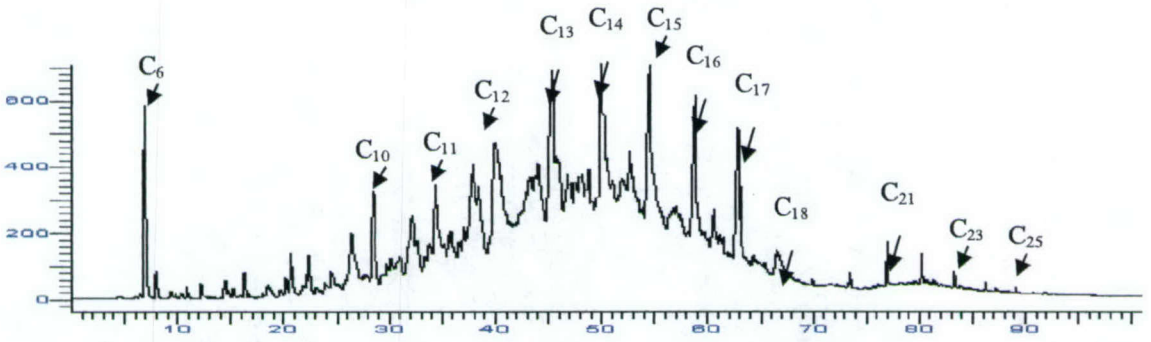

Figure 1. Gas Chromatograph for DF2 fuel.

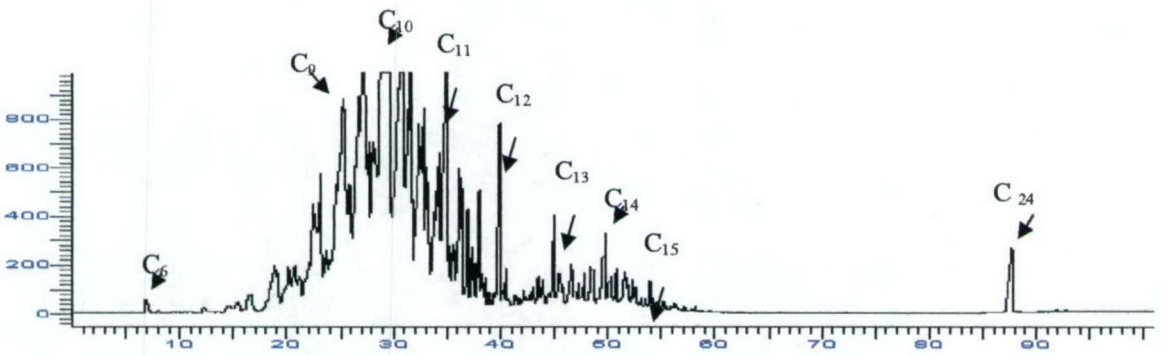

Figure 2. Gas Chromatograph for JP8 fuel.

Unreliable cold starting of diesel engines can result in long cranking periods, misfiring and hesitation after the first firing, and the emission of white smoke or complete failure of the engine to start. All of these conditions are not desirable in the field. Most of the previous investigations were experimental, aimed at finding practical techniques to improve the cold starting of diesel engines.

The goal of this part of this work is to develop a mathematical model that simulates the physical and chemical processes that take place in the engine cylinder, from the start of motoring to the end of the cranking period when the engine fires. In this study, a zero-dimension model is developed to simulate the overall engine performance under cold starting conditions. The model consists of many sub models: (a) Heat transfer model, (b) Fuel penetration model, (c) Liquid droplet evaporation model, (d) Liquid fuel film evaporation model and (e) and an autoignition index model. The model predictions for the length of the cranking period are compared with experimental results. The model produced is built on the previous work done in this area at Wayne State University, and published in references (1- 4). The experimental work was conducted on a single-cylinder, naturally aspirated, direct-injection, air-cooled, four-stroke, diesel engine. The engine was soaked in the cold room for at least 8 hours before each cold start test. The details of this investigation are given in Appendix A. Figure (3) shows a comparison between the experimental and the predicted results for the length of the cranking period at different room

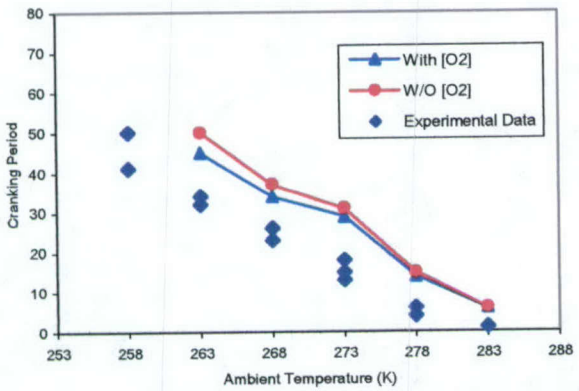

Figure 3. Comparison between predicted and experimental data of number of cranking cycle before the first firing.

temperature. This figure shows that the predicted data follow the trend as the experimental data, but produce longer cranking periods. The reason for this discrepancy is under investigation, and more accurate models are being developed.

2. Effect of Cycle-to-Cycle Variation in the Injection Pressure in a common rail Diesel Injection System on Engine Performance

The performance of the Common Rail diesel injection system (CRS) is investigated experimentally in a single cylinder engine and a test rig to determine the cycle-to-cycle variation

in the injection pressure and its effects on the needle opening and rate of fuel delivery. The engine used is a single cylinder, simulated-turbocharged diesel engine. Data for the different injection and performance parameters are collected under steady state conditions for 35 consecutive cycles. A mathematical model has been developed to calculate the instantaneous fuel delivery rate at various injection pressures. The experimental results supported with the model computations indicated the presence of cycle-to-cycle variations in the fuel injection pressure and needle lift. The variations in the peak-cylinder gas pressure, rate of heat release, cylinder gas temperature and IMEP are

correlated with the variation in the injection rate. The effect of these variations on NOx emission and soot are also discussed in Appendix B.

3. Effect of Smoothing the Cylinder Gas Pressure Trace on the Computed Tare of Energy Release

To adapt a diesel engine to run on JP8 instead of DF2, there is a need to adjust the injection timing and its rate to avoid any deterioration in power output and fuel economy. The proper injection timing can be determined from the rate of chemical energy release, (RCER) of the fuel air mixture, commonly known as ARHR (Apparent Rate of Heat Release). This is computed from the rate of change in cylinder gas pressure. Due to the sensitivity of the slope of the pressure trace to any waves in the pressure trace, many errors in RCER have been experienced. There fore, it is necessary to smooth the pressure trace before carrying out the RCER and make any interpretations for the autoignition and combustion processes.

Different smoothing methods are analyzed and their features compared. Furthermore, the selection of the smoothing starting point and its effect on the smoothing quality of the pressure data are described. The Fast Fourier Transform (FFT) analysis is applied to determine the frequency of the disturbances in power spectrum and obtain the optimal specified smoothing parameter (SSP).
The experimental data was obtained on a single-cylinder, small-bore, high-speed, direct-injection diesel engine equipped with a CRS. The experiments were conducted under simulated turbocharged steady state conditions and covered engine speeds of 1500rpm and 2000rpm; and injection pressures of 600bar, 800bar and 1000bar. A Hi-Tech data acquisition system was used to collect data in consecutive cycles for the fuel pressure, needle lift and cylinder pressure.

The investigation showed that the natural frequency of the cylinder gas pressure is around 3000 Hertz and the oscillations in the pressure trace are closely related to the rate of pressure rise due to combustion. This rate increases at higher injection pressures, EGR rates, and engine load. Among the smoothing methods discussed in this paper, the Spline function is the most effective one under the steady and transient states. Meanwhile, the point where the smoothing starts has a significant effect on the accuracy to RER. The optimum starting smoothing point is at the ¼ the natural period in crank angle degree before the rapid rising peak of cylinder pressure. This point can be obtained from the power spectrum of smoothed pressure trace.
The details of this work are given in Appendix C.

II. Tribology of the Main Engine bearings

Summary.

Four codes have been developed in Matlab to calculate the loading of the engine main bearings and, based on the loading to determine the journal orbit and the oil film thickness. In parallel, a

single cylinder diesel engine was instrumented with a pressure transducer and gap sensors to measure the journal orbit

Background

Engine bearings are one of the most vulnerable parts in high power density diesel engines. If the minimum oil film thickness (OFT) becomes less than 2 μm damage of the bearing could occur. The accurate determination of the OFT must consider bearing and shaft deformation.
The following computer codes have been developed:
(a) The code "Polar Diagram" calculate the loading of the bearings and displays the polar diagram of the bearing according to two separate assumptions:

a) Statically determined cranks
b) Statically Undetermined crankshaft structure

The inputs needed for the code are: the cylinder pressure variation and basic engine dimensions (bore, stroke, connecting rod length, mass of the piston assembly, mass of the connecting rod, dimensions and mass of the crankshaft).

(b) The code "Journal Orbit" calculates the orbit of the journal using the mobility method and displays the orbit inside the clearance circle showing also the variation of the oil film thickness

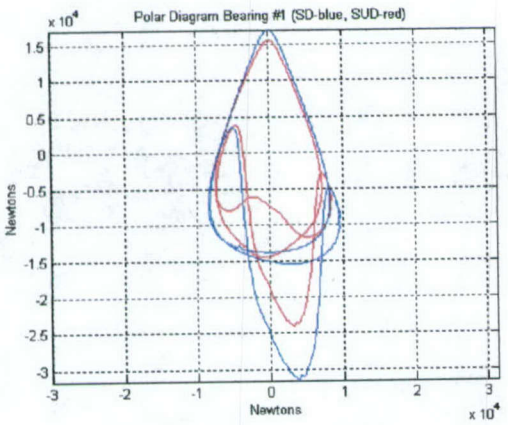

Fig. 4. Polar diagrams of the first main bearing four-stroke, four-cylinder diesel engine (2500 rpm)

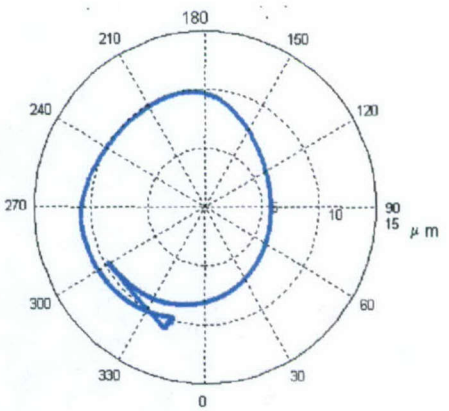

Fig. 5. Journal orbit calculated for the Bearing load shown in Fig.1

(c) The code "Oil Pressure" uses a finite difference method to integrate the Reynolds equation and calculate the oil pressure variation inside the bearing. This code is used for a more accurate determination of the oil film thickness and also to obtain the detailed bearing load for the Finite Element model of the bearing to determine the deformation of the bearing. The code is capable to simulate the oil-feeding groove in the bearing and the effect of the shaft misalignment. The following figures show the influence of these parameters on the minimum oil film thickness.

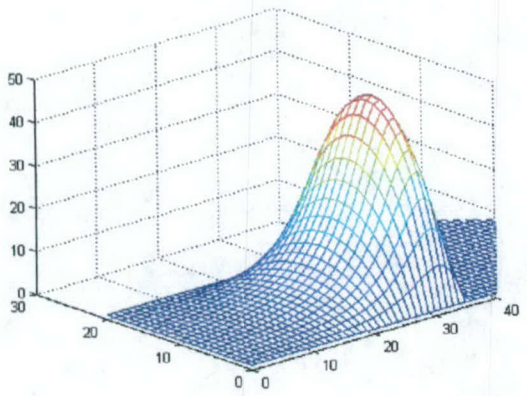

Fig. 6.a. Minimum OFT 3.5 μm

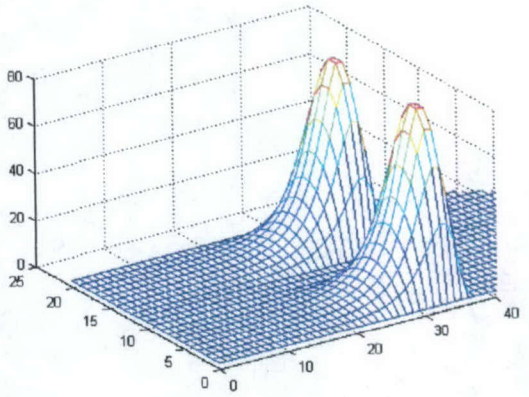

Fig. 6. b. Minimum OFT 1.8 μm

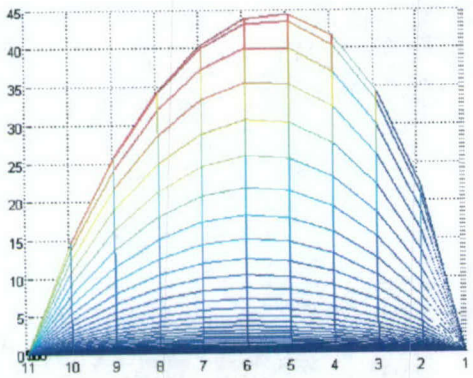

Fig. 6.c. Minimum OFT 2.82 μm
Load center offset 0.645 mm

Fig. 6. Oil film pressure variation in the bearing for the load of 42,500 N at 1500 rpm

The main bearing at the flywheel end of the crankshaft of the experimental engine has been instrumented with two gap sensors for the measurement of the journal orbit. Preliminary measurements have shown a very good repeatability and the sensors are now calibrated for the validation of the simulation model. Also the finite element model (FEM) of the bearing has been generated and the deformation of the bearing under oil pressure load was determined.

The code "Oil Pressure" has been coupled to the finite element model of the bearing housing to correlate the oil film thickness with the bearing deformation and investigate the effect of deformation on the pressure distribution in the bearing. It was determined that the deformation increases the loaded area of the bearing and reduces the peak pressure.

Two additional gap sensors were procured and the bearing housing has been equipped with four sensors to measure the oil film thickness and validate the mathematical models. The calibration of the measuring system is underway.

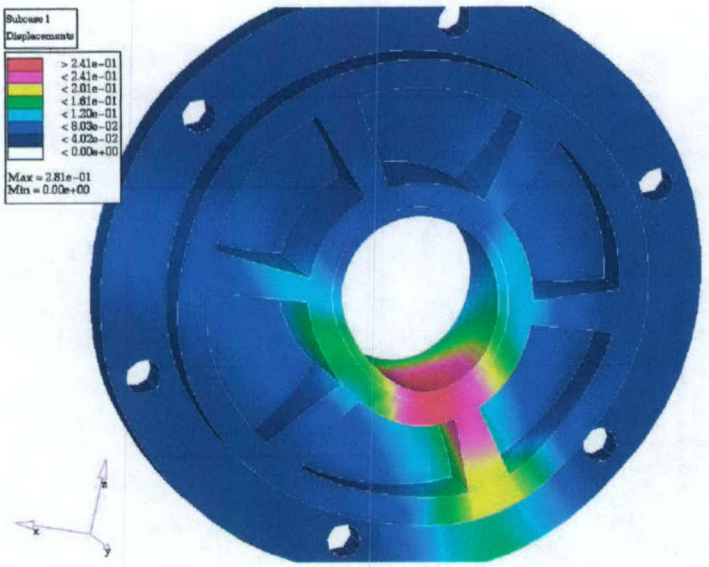

Fig. 7. The deformation of the bearing housing (amplified 20 times)

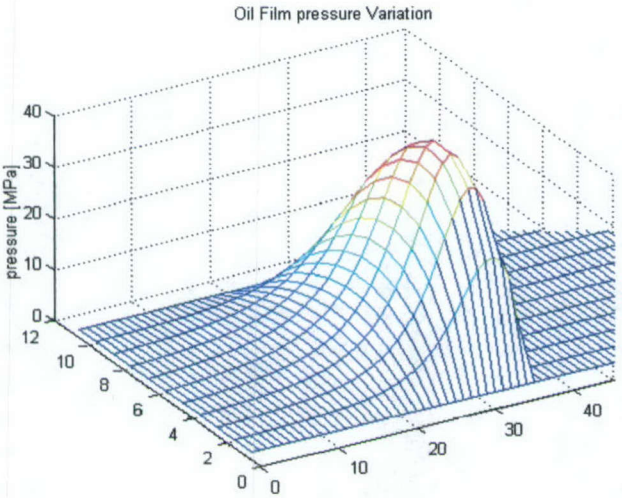

Fig.8. The oil film pressure distribution in the deformed bearing

Summary of the most important results

1. A simulation model for the cold-start cranking-period is developed in this investigation. The model predictions agreed with the experimental on the following conclusions: (a) CN alone is not a good indicator of the number of cranking cycles and (b) Fuel volatility is as important as CN in controlling the cranking period at the low ambient temperatures.
2. The cycle-to-cycle variation in the fuel pressure in the common rail injection can cause variations in fuel delivery, rate of combustion energy release, indicated mean effective pressure, and engine out emissions.

3. The rate of combustion energy release, known as Apparent Rate of Heat Release, calculated from the pressure trace, can give useful information about the autoignition and combustion processes of different fuels in diesel engines. An evaluation of the smoothing techniques of the pressure trace are examined and evaluated.
4. A computer simulation model, in MATLAB, has been developed to calculate the loading of the engine main bearings and, determine the journal orbit and the oil film thickness. The model can be used to compute the maximum load the bearings can stand in high power density heavy military diesel engines.

List of publications

1 Zhong,L., Henein, N. A., Liu, H., Bryzik, W., »A Mathematical Modelo for the Cranking Period in the Cold Start of Diesel Engines, : Proceedings of 2003 IMECE 2003-43990, 2003.
2. Henein, N. A., Singh, I. P., Zhong, L., Lai, M-C, Bryzik, W.,"New Integrated "O.P.E.R.A.S." Strategies for Low Emissions in HSDI Diesel Engines," SAE 2003-01-0261, 2003.
3. Zhong, L., Singh, I. P., Han, J., Lai, M-C., Henein, N. A., Bryzik, W.,"Effect of Cycle-to-Cycle Variation in the Injection Pressure in a Common Rail Diesel Injection System on Engine Performance,"SAE 2003-01-0699, 2003.
4. Zhong, L., Henein, N. A., Bryzik, W.,"Effect of Smoothing the Pressure Trace on the Interpretation of Experimental Data for Combustion in Diesel Engines," SAE2004-01-0931, 2004.

Scientific personnel supported by this project

1. Lurun Zhong, Ph.D. Candidate, Wayne State University
2. Inderpal Singh, Ph. D Applicant, Wyne State University
3. Naeim A. Henein, Professor and Director of Center for Automotive Research , WSU.
4. Dinu Taraza, Professor of Mechanical Engineering, WSU.
5. Nabil Chalhoub, Professor of Mechanical Engineering, Wayne State University.

Report of Inventions

None

Appendix A.

Proceedings of 2003 IMECE:
2003 ASME International Mechanical Engineering Congress and R&RD Expo
November 15-21,2003 Washington D.C. USA

IMECE2003-43990

A MATHEMATICAL MODEL FOR THE CRANKING PERIOD IN THE COLD START OF DIESEL ENGINES

Lurun Zhong
Mechanical Engineering Department
Wayne State University, 48202

Naeim A. Henein
Mechanical Engineering Department
Wayne State University, 48202

Hengqing Liu
General Motor Company

Walter Bryzik
US Army TARDEC

ABSTRACT

A mathematical model is developed to predict the length of the cranking period of direct injection diesel engines at low ambient temperatures. The model takes into consideration the physical and chemical processes that develop in the cylinder over the whole cranking period. The model accounts for the variation in the following: (a) fuel accumulated in the cylinder in both the liquid and the vapor phases, (b) gas temperature and pressure, (c) wall temperature and (d) the autoignition reactions rate. An "Autoignition Index" (AI) is developed to account for the combined effects of fuel volatility and its Cetane Number. The model considers that autoignition starts in the cycle where AI reaches a critical value at the end of the cranking period. The model predictions are compared with the experimental data obtained on a single cylinder diesel engine tested in a cold room using four distillate fuels having different volatilities and Cetane numbers.

INTRODUCTION

Long cranking periods, hesitation and the emission of white smoke are among the problems experienced during the cold stating of diesel engines. The factors that affect engine cold startability[1-12] include the ambient temperature, fuel properties, mass of fuel injected, fuel injection timing, and cranking speed. For decades, researchers have worked on this problem and tried to find ways to improve engine cold startability. Most of the investigations were experimental, aimed at finding practical techniques to improve the cold starting of diesel engines. . Other studies included zero-dimensional (11-13) models and multi-dimensional computer simulation (14,22). In many cases, pure hydrocarbon compounds were used in the analysis. However, the actual diesel fuel consists of many hydrocarbons of different structures and number of carbon atoms. Also, because of the long computational time, many models were limited to one or a few number of cycles.

The goal of this paper is to develop a mathematical model that simulates the physical and chemical processes that take place in the engine cylinder, from the start of motoring to the end of the cranking period when the engine fires.

In this study, a zero-dimension model is developed to simulate the overall engine performance under cold starting conditions. The model consists of many sub models: (a) Heat transfer model, (b) Fuel penetration model, (c) Liquid droplet evaporation model, (d) Liquid fuel film evaporation model and (e) an autoignition index model. The model predictions for

the length of the cranking period are compared with experimental results. The model is then applied to find the effects of the fuelling rate , cranking speed, injection timing and fuel properties on the length of the cranking period.

EXPERIMENTAL SETUP

A single-cylinder, naturally aspirated, direct-injection, air-cooled, four-stroke, diesel engine was tested in a cold room at different ambient temperatures. The specifications of the engine are given in appendix A. The cylinder gas pressure was measured by using a water-cooled piezo-electronic pressure transducer flush mounted on the cylinder head, and a charge amplifier. The fuel line pressure was measured by using an inline strain gauge pressure transducer. The angular velocity of the engine was measured by using an optic shift encoder with one crank angle degree resolution. The tests covered two diesel fuels of different volatilities and cetane numbers. The fuel properties are given in Appendix B.

NOMENCLATURE

C_d discharge coefficient, --

C_L heat capacity of liquid fuel, J/kg·K

C_{ls} concentration of fuel vapor at fuel film surface, kg/m^3

C_p constant pressure specific heat, J/kg·K

C_∞ concentration of fuel vapor at distance, kg/m^3

d_0 diameter of injector nozzle, m

D_0 initial fuel droplet diameter, m

D_{ij} diffusivity of fuel in air, m^2/s

D_j fuel droplet diameter, m

E activation energy, kJ/kg

FA air fuel ratio, --

h_c heat transfer coefficient, w/m^2·K

h_l heat transfer coefficient at the inner side of the wall, w/m^2·K

h_n heat transfer coefficient at outer side of the wall, w/m^2·K

h_m mass transfer coefficient, m/s

ID ignition delay, ms

K thermal conductivity, w/m·K

K_l thermal conductivity, w/m·K

Le Lewis number, --

m_{drop} mass of a fuel droplet, kg

m_f mass of fuel injected, kg

P pressure, or total pressure, kPa

P_{fs} partial pressure at droplet surface, kPa

P_v fuel vapor pressure in cylinder, kPa

Pr Prandtl number, --

Q_c convective heat transfer, J/m^2

R gas constant, kJ/kg·K

rpm revolutions per minute

S spray penetration, m

SMD Sauter Mean Diameter, micron

t time, second

T_0 gas temperature in cylinder, K

T_{fs} temperature at fuel surface, K

T_g cylinder gas temperature, K

T_l temperature of liquid fuel, K

T_L temperature in cooling chamber, K

TDC top dead center, crank angle degree

V_f fuel injected per cycle, mm^3

W_a molecular weight of air, g/mol

W_f molecular weight of fuel, g/mol

α thermal diffusivity, m^2/s

ρ_a density of gas, kg/m^3

ρ_f density of fuel, kg/m^3

Δh_{ev} latent heat of fuel, J/kg

ΔP pressure difference cross the fuel injector nozzle, kPa

MATHEMATIC MODELS

The filling and emptying approach is used to describe the mass flow processes in and out of the cylinder, blow-by, intake manifolds and exhaust manifolds. An optimization method was used to calibrate the engine models [11~13].

Heat Transfer Model in Cylinder

Assuming uniform material properties and one-dimensional heat conduction in the wall, the temperature T(x,t), at any point x in the wall, and at any time t, should satisfy the heat conduction equation i.e. Fourier's Law:

$$\frac{\partial T}{\partial t} = \alpha \frac{\partial^2 T}{\partial x^2} \quad (1)$$

The boundary condition at the inner side of the wall is

$$\rho c \frac{\partial T}{\partial t} = K \frac{\partial T}{\partial x} + h_1 (T_0 - T) \quad (2)$$

The boundary condition at the outer side of the wall is

$$\rho c \frac{\partial T}{\partial t} = K \frac{\partial T}{\partial x} + h_n (T - T_L) \quad (3)$$

The finite difference scheme was applied to solve equations (1-3) and to calculate the temperature transient in the cylinder liner, piston and cylinder head. Generally, under typical engine operating conditions, the cyclic transients do not penetrate into the wall structure for a distance greater than a few millimeters. Thus the boundary conditions at the outside walls do not affect the transient processes at the inner side of the wall, providing the penetrating time period is short. This is the case of engine cold start where the typical time for engine from motoring to idle speed is only in the neighborhood of twenty seconds.

The validity and accuracy of the finite difference computations are verified by comparing the results with and these obtained from the exact solution method as shown in Appendix C.

Fuel Penetration Model

At low ambient temperature, during starting the cylinder pressure is low because of the relatively high blow by losses at the low cranking speeds. The cylinder temperature and combustion chamber temperature will be very close to the ambient air conditions. When the fuel is injected into cylinder, part of it will evaporate and mix with air, the rest will deposit on the wall or be exhausted with the cylinder gases and appear as white smoke. Part of the fuel deposited on the wall will evaporate, and the rest will be left over for the next cycle. The accumulated fuel in the combustion chamber increases the actual compression ratio [13], hence it boosts the compression pressure and temperature. Therefore, the fuel penetration model is critical to predict fuel evaporation and accumulation in the combustion chamber.

A two-zone penetration model proposed by Hiroyasu and Arai [15] based on jet instability analysis will be used in this investigation. It can be summarized as:

$$S = 0.39\left(\frac{2\Delta P}{\rho_f}\right)^{0.5} t \quad \text{for } t < t_b \quad (4)$$

$$S = 2.95\left(\frac{\Delta P}{\rho_a}\right)^{0.25} (d_0 t)^{0.5} \quad \text{for } t > t_b \quad (5)$$

Where

Spray breakup time t_b is given by

$$t_b = 28.6(\Delta P \cdot \rho_a)^{-0.5} \rho_f \cdot d_0 \quad (6)$$

ΔP is pressure difference, ρ_f and ρ_a are fuel and air density, t is time, d_0 is nozzle orifice diameter.

Liquid Droplet Evaporation Model

The high-pressure sprays encountered in diesel engines have fairly short breakup lengths, so that almost the entire spray evaporation may be treated as a droplet with a Sauter mean diameter, (SMD). SMD is calculated by using the correlations developed by Hiroyasu and Kadota[18]:

$$D_0 = 23.9(\Delta P)^{-0.135} \rho_a^{\ 0.121} V_f^{\ 0.131} \quad (7)$$

D_0 is SMD in micron, ΔP is the pressure difference in MPa, V_f is the fuel injected per cycle in mm^3.

The number of fuel droplets formed from the injected fuel,

$$N = \frac{6 m_f}{\pi D_0^3 \rho_f} \quad (8)$$

The fuel droplet evaporation rate [20] is

$$\frac{dm_{drop}}{dt} = -\pi D_j D_{ij} Sh \frac{P}{R T_{fs}} \ln\left(\frac{P - P_v}{P - P_{fs}}\right) \quad (9)$$

and convective heat transfer [20] is

$$Q_c = \pi D_j k (T_g - T_l) Nu \frac{z}{e^z - 1} \quad (10)$$

$$z = \frac{C_{pv}\dfrac{dm_{drop}}{dt}}{\pi D_j k Nu}$$

Droplet temperature equation:

$$m_{drop} C_L \frac{dT_l}{dt} = Q_c - \Delta h_{ev} \frac{dm_{drop}}{dt} \qquad (11)$$

Fuel Film Evaporation Model

Once the fuel droplets impinge on the combustion chamber wall, a fuel film is formed. The film surface temperature, and evaporation are computed from the following equations [13]:

$$\frac{dm_{ev}}{dt} = \frac{h_c(T_g - T_{ls}) + K_l \dfrac{dT_{ls}}{dx}}{\Delta h_{ev}} \qquad (12)$$

$$\frac{dm_{ev}}{dt} = h_m (C_{ls} - C_\infty) \qquad (13)$$

$$h_m = \frac{h_c}{\rho C_p Le^{\frac{2}{3}}}$$

$$C_{ls} = \frac{P_{ls}}{R_f T_{ls}}$$

$$C_\infty = \frac{P_f}{R_f T}$$

$$P_f = \frac{P}{1 + FA\dfrac{W_a}{W_f}} FA \frac{W_a}{W_f} = \frac{P}{1 + AF\dfrac{W_f}{W_a}}$$

Auto-ignition Index (AI) Model

In a previous investigation [13], autoignition is considered to occur in the cycle where the AI reaches a certain critical value. AI combines the effects of the following parameters as shown in equation (14): (a) the concentration of the fuel vapor [F] which is related to fuel volatility, (b) the concentration of the oxygen molecules [O_2], (c) the activation energy of the global autoignition reactions [E], which is considered to be related to the cetane number (CN) of the fuel, (d) the temperature of the reacting mixture [T], and the time [t] calculated from the start of injection to the point when AI reaches the critical value. In a previous investigation [13], [O_2] was not concluded in the AI equation.

$$AI = \int_{t_{inj}}^{t_{end}} k_0 [F][O2] \exp(-\frac{E}{RT}) dt \qquad (14)$$

VALIDATION OF THE MATHEMATIC MODEL

Figures 1~2 show a fair agreement between the computed and measured cylinder gas pressure and the instantaneous engine speed during motoring at 0°C ambient temperature. Also, Figure 3 shows a fair agreement between the computed and measured cranking speeds at different ambient temperatures.

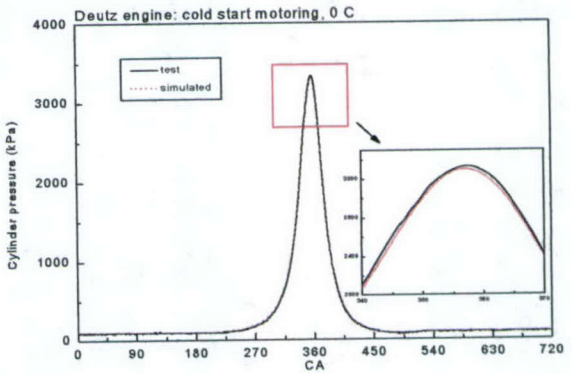

Figure 1 Comparison between simulated cylinder pressure and test data, Deutz engine, motoring, 0 C.

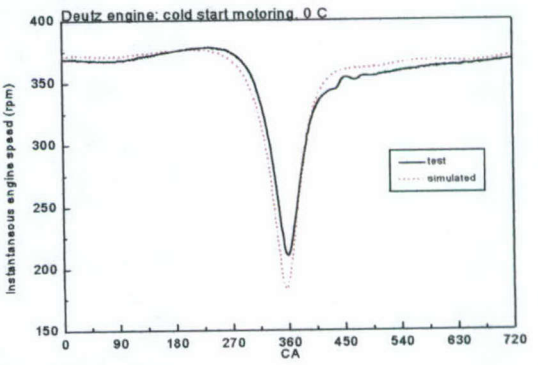

Figure 2 Comparison between simulated instantaneous engine speed and test data, Deutz engine, motoring, 0 C.

PARAMETRIC ANALYSIS AND AI FOR CONSECUTIVE CYCLES DURING THE CRANKING PERIOD

During the cranking period, many key thermodynamic and heat transfer parameters vary from one cycle to the next cycle as the engine speed increases from zero to the motoring speed. These parameters include the wall temperature, cylinder gas compression pressure and temperature, and the fuel vapor-air ratio. Figures 4-7 show the variation in the different parameters as the engine speed increased from zero to 320 RPM at an ambient temperature of 5°C (268K). Figure 4 is for the variation in the wall temperature at three locations: the cylinder head, piston crown and cylinder liner. Notice that the temperatures at cylinder head and piston are higher than that of cylinder liner because they are exposed to cylinder gas all the time. The cylinder liner, however, is partly exposed. Therefore, its temperature is lower. Figure 5 is for the cylinder gas pressure and temperature at two fuelling rates. The 110% fuelling produced slightly higher gas temperatures. Part of the increase in gas temperature is caused by the increase in compression ratio, as shown in Figure 6. The change in the fuel vapor-air ratio is given in figure 7. As explained earlier, the change in the vapor mol fraction is caused by the increase in (a) vapor produced from the liquid film deposited on the wall, (b) rate of evaporation from the liquid phase due to the higher cylinder gas temperature, (c) recirculated fuel.

The AI calculated from equation (14) is shown in figure 8. It is noticed that AI increases with the cranking period. Autoignition is considered to start in the cycle when AI reaches a critical value. The critical value for the AI index was determined from the cycle when the engine fired in the first cycle. Figure 8 shows that AI reached the critical value in cycle number 3 at an ambient temperature of 283K (10°C). At lower temperatures, AI reached the critical value after a longer cranking period. Figure 9 shows a comparison between the experimental and predicted cranking periods at different ambient temperatures. The model shows the same trend as that of the experimental data. However the model predicted longer cranking periods than the experimental data.

The accuracy of the model predictions can be improved if the orders of the global autoignition reactions are used in equation (14). Unfortunately, these orders are not known, and in the current analysis the reactions were assumed to be of the first order with respect to the fuel and oxygen. The model predictions are slightly better than those predicted in reference [13] when the change in O_2 concentration and fuel penetration with temperature are accounted for in the model.

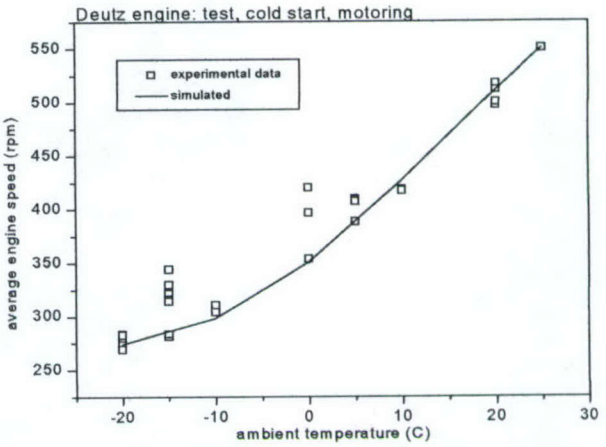

Figure 3 Engine cranking speed at different ambient conditions, Deutz engine, cold start motoring.

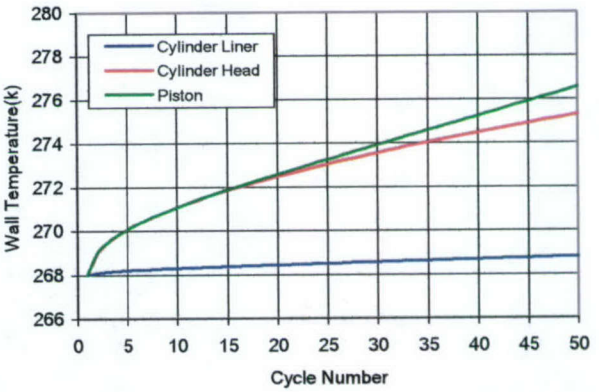

Figure 4 Inner surface temperatures of combustion chamber parts at ambient temperature 268 K

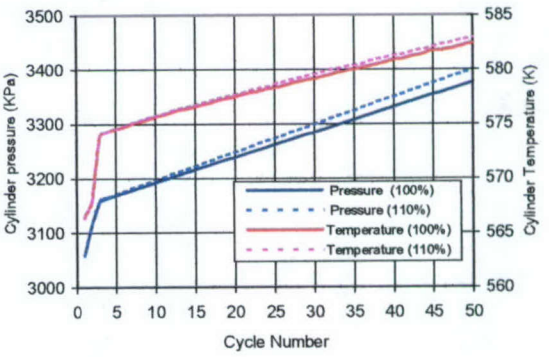

Figure 5 Cylinder pressure and gas temperature at ambient temperature 268 K

Figure 6 Actual compression ratio at 273K ambient temperature

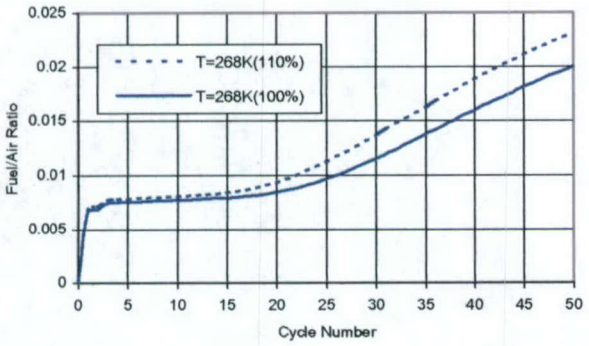

Figure 7 Fuel-air ratio at ambient temperature 268 K

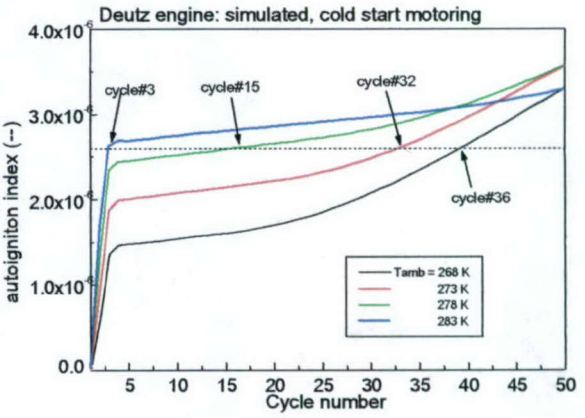

Figure 8 Autoignition index development during cranking at different ambient temperature for a single-cylinder engine.

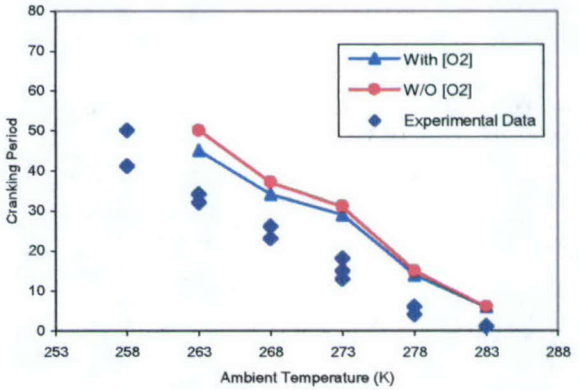

Figure 9 Comparison between predicted and experimental data of number of cranking cycle before first firing, single-cylinder engine

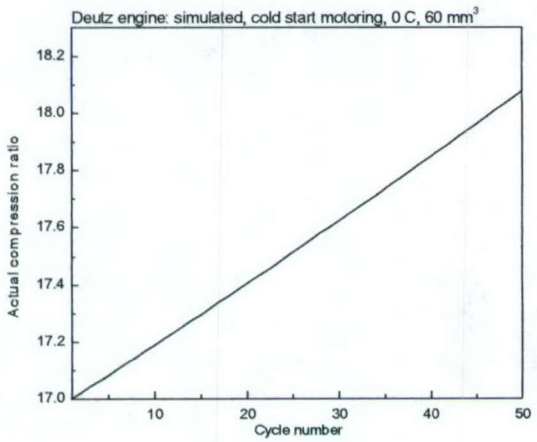

EFFECT OF FUEL PROPERTIES ON CRANKING PERIOD

Equation (14) for AI shows that the cranking period depends on two important fuel properties: (a) fuel volatility which affects [F] and (b) Cetane number which affects E. Diesel fuels are distillates consisting of several hydrocarbons of different structure and carbon atoms. However, the majority of the hydrocarbons are normal paraffins, for which AI and the cranking period will be calculated.

Figure 10 shows the saturation pressure and cetane number for n-paraffins with carbon atom numbers 7 to 19 [23,24]. As the number of carbon atoms decreases, fuel volatility gets higher but CN gets lower. Therefore, AI, or the cranking period should depend on both volatility and CN.

AI and the cranking period are calculated for n-paraffins of different number of carbon atoms.

The activation energy is calculated from [14]

$$E = \frac{618840}{CN+25} \cdot \frac{65}{CN+25} \qquad (15)$$

Where CN is cetane number.

Figure 11 shows the results obtained by applying Equation (14) for the different n-paraffins at different ambient temperatures. The model predicts that autoignition would start in the first cranking cycle for n-paraffins having 7 to 10 carbon atoms. In this work, the engine is considered to fail to start if the cranking period exceeds 90 cycles (180 revolutions).

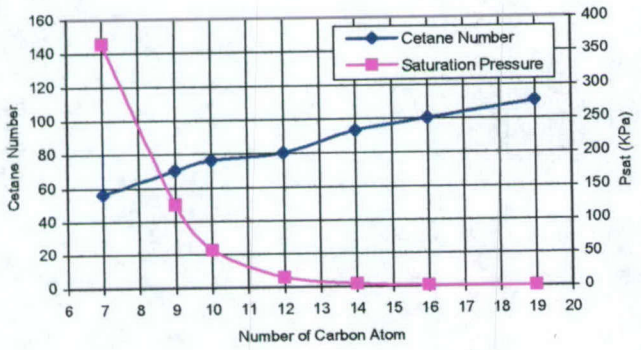

Figure 10 Saturation pressure at 425K and Cetane number

To compare between the model predictions and the experimental results, Equation (14) is applied for two fuels of different volatility and CN. The properties of these two fuels are listed in appendix B. The predicted results shown in figure 12 agree with experimental data that the cranking period in case of fuel A is shorter that in case of fuel D, particularly at the temperature lower than 0 °C,. The difference between two fuels at temperature higher than 0 °C is not significant.

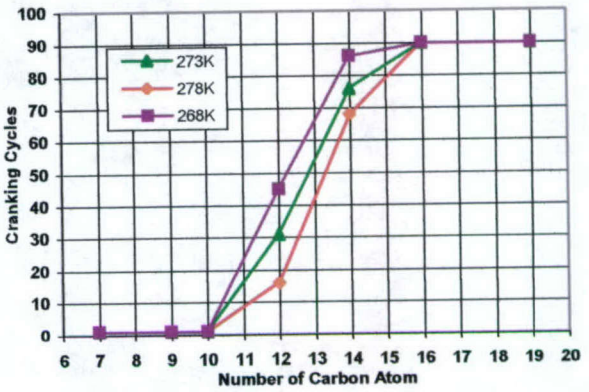

Figure 11 Effect of number of carbon atoms on cranking period.

CONCLUSION

1. A generic mathematical model is developed for the cranking period of direct injection diesel engines at low ambient temperatures. The model includes sub-model for fuel droplet and fuel film evaporation. The model takes into consideration the physical and chemical processes that affect the fuel vapor concentration in the cylinder over the whole cranking period. The model also accounts for the variation in the wall temperature, the fuel accumulated in the cylinder in the liquid and the vapor phases, and the auto-ignition reactions rate.

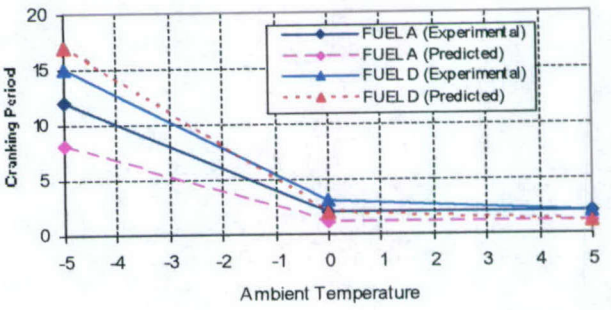

Figure 12 Effect of fuel volatility on engine cold starting

2. The predictions of the model agreed well with the experimental data obtained on a single cylinder diesel engine.

3. An "Auto-ignition Index" (AI) is developed to account for the combined effects of fuel volatility and Cetane Number. Applying the AI to pure N-paraffins shows that the volatility of the fuel plays a major role in shortening cranking period.

ACKNOWLEDGMENTS

The project is supported mainly by ARO under contract No. DAAG55-98-1-O285. The support of the U.S. Army TARDEC and ARC is also acknowledged. The cooperation and help of other members in the Center for Automotive Research at Wayne State University are appreciated.

APPENDIX A ENGINE SPECIFICATION

	DEUTZ 210
Number of Cylinder	1
Bore × Stroke	95 × 95 mm
Radius of Crank Shaft	47.5 mm
Length of Connection Rod	160 mm
Weight of Piston	1.18 kg
Weight of Connection Rod	0.65 kg
Rotating Moment of Inertia (Flywheel, crankshaft, etc.)	0.386 kg·m^2
Compression Ratio	17:1
Displacement	673 ml
Fire Order	
Valve Timing: IVO	23^0 BTDC
IVC	63^0 ABDC
EVO	63^0 BBDC
EVC	23^0 ATDC

APPENDIX B TEST FUEL PROPERTIES

The following table is extracted from reference [5].

Test Fuels	Fuel A	Fuel D
Cetane Number	49.2	48.6
Cetane Index	50.4	48.5
Cetane improver (vol. ppm)	0.0	5500
Density at 15°C (g/cm3)	0.8066	0.8223
Viscosity at 30°C (mm2/s)	1.916	1.667
Distillation, IBP (°C)	142.5	144.5
5%	163.5	167.0
10%	170.0	172.5
20%	179.5	180.5
30%	191.0	187.5
40%	205.5	195.5
50%	221.0	205.0
60%	238.0	218.5
70%	257.0	237.5
80%	280.0	265.5
90%	313.5	304.0
95%	336.5	330.5
FBP	350.0	344.0
Residue (vol %)	2.0	2.0
Loss (vol %)	0.0	0.0
Sulfur (mass %)	0.014	0.011
Hydrocarbon Type (vol %)		
Saturates	78.7	63.8
Olefins	0.0	0.0
Total Aromatics	21.3	36.2
Mono-Aromatics	20.6	34.8
Di-Aromatics	0.7	1.4
Poly-Aromatics	0.0	0.0

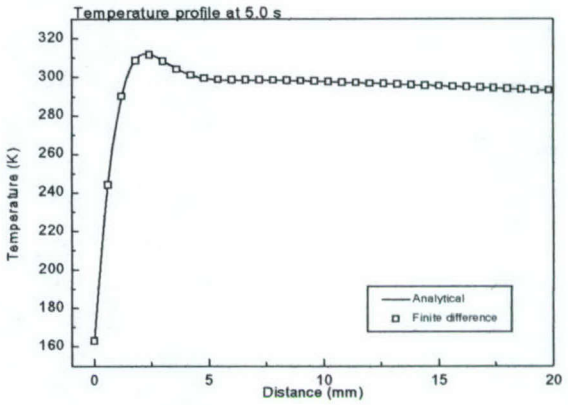

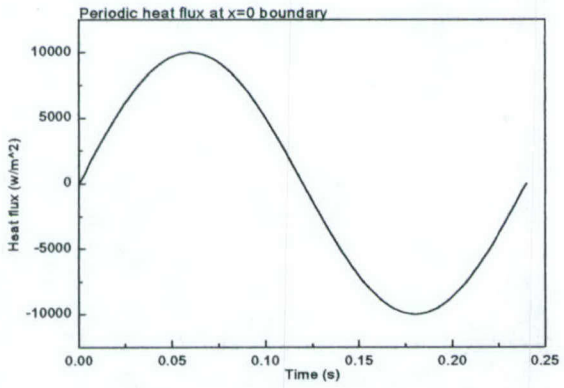

APPENDIX C VALIDATION OF HEAT TRANSFER MODEL

The method was applied to calculate the temperature distribution in a flat slab subject to a given, harmonically varying heat flux at x=0 (figure 1), and a constant ambient temperature at x=L. The exact solution was also obtained analytically for each case. Figures 2~4 show the comparisons of temperature profiles between exact and numerical solutions, for a 20 mm steel layer with ambient temperature 293K, thermal conductivity of 54 W/m·K, density of 7800 kg/m^3 and specific heat of 450 J/kg·K. The results, which are representative of all the cases that we studied, show that the numerical solutions are in excellent agreement with the exact solutions.

Figure 1 Periodic heat flux at boundary x = 0

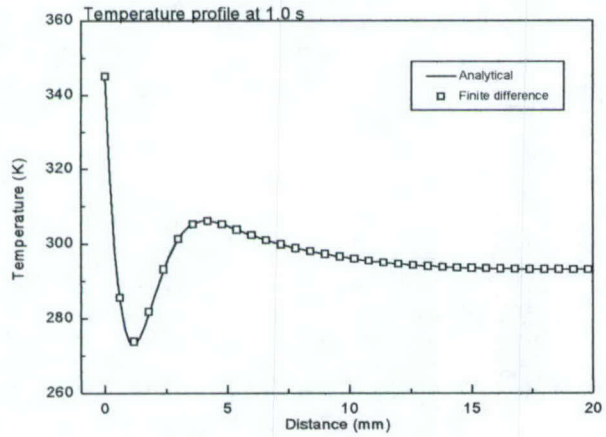

Figure 2 Calculated temperature profile at 1.0 second

Figure 3 Calculated temperature profile at 5.0 second

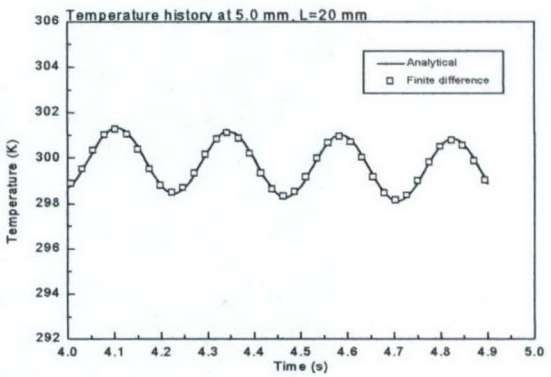

Figure 4 Calculated temperature History of Plate at X = 5.0 mm

REFERENCES

[1]Han, Z.P., Henein, N.A., Nitu, B., Bryzik, W., " Diesel Engine Cold Start Combustion Instability and Control Strategy", SAE Paper 2001-01-1237, 2001.

[2] Liu, Z. and Karim, G. A., "An examination of the role of residual gases in the combustion processes of motored engines fuelled with gaseous fuels", SAE Paper 961087, 1996.

[3] Hardenberg, H. O. and Hase, F. W., "An Empirical Formula for Computing the Pressure Rise Delay of a Fuel From its Cetane Number and from Relevant Parameters of Direct-Injection Diesel Engines", SAE Paper 790493, 1979.

[4] Clerc, J. C., "Cetane number requirements of light-duty diesel engines at low temperatures", SAE Paper 861525, 1986.

[5] Hara, H., Itoh, Y., Henein, N. A. and Bryzik, W., "effect of cetane number with and without additive on cold startability and white smoke emissions in a diesel engine", SAE Paper 1999-01-1476, 1999.

[6] Austen, W. and Lyn, W. T., "Some investigations on cold starting phenomena in diesel engines", SAE Paper no. 5, 1959-60.

[7] Phatak, R. E. and Nakamura, T., " Cold startability of open-chamber direct-injection diesel engines – part I Measurement technique and effects of compression ratio", SAE Paper 831335, 1983.

[8] Osuka, I. and Nishimura, M., "Benefits of new fuel injection system technology on cold startability of diesel engines – improvement of cold startability and white smoke reduction by means of multi injection with common rail fuel system (ECD-U2)", SAE Paper 940586, 1994.

[9] Tsunemoto, H., Yamada, T. and Ishitani, H., "Behavior of adhering fuel on cold combustion chamber wall in direct injection diesel engines", SAE Paper 861235, 1986.

[10] Biddulph, T. W. Lyn, W. T., "Unaided starting of diesel engines", Proc. Inst. Mech. Engrs. , Vol. 181, 1966-67.

[11] Gardner, T. P., "Optimization of compression ratio in compression ignition engines", Ph.D. dissertation, 1986.

[12] Liu, Hengqing, Chalhoub, N. and Henein, N. A., "Simulation of a single cylinder diesel engine under cold start conditions using Simulink", Advanced Engine Simulations vol. 1, ICE-Vol. 28-1, 1997.

[13] Liu, H.Q., Henein, N.A., Bryzik, W., " Simulation of Diesel Engine Cold Start", SAE Paper 2003-01-0080, 2003

[14] Lippert, A.M., Stanton, D.W., Reitz, R.D., Rutland,C.J., and Hallett, W.L.H.," Investigating the Effect of Spray Targeting and Impingement on Diesel Engine Cold Start", SAE Paper 2000-01-0269, 2000.

[15]Hiroyasu, H. and Arai, M., " Fuel Spray Penetration and Spray Angle in Diesel Engines," Trans. Of SAE of Japan, Vol. 21, pp.5-11, 1980.

[16] Henein, N. A. "Starting of diesel engines: Uncontrolled fuel injection problems", SAE Paper 860253, 1986.

[17] Gonzalez, M. A., "A computational study of in-cylinder cold starting processes in a diesel engine", Master thesis, University of Wisconsin-Madison, 1990

[18] Hiroyasu, H. and Kadota, T., "Fuel droplet size distribution in diesel combustion chamber", SAE Paper 740715, 1974.

[19] Stanton, D. W., Rutland, C., J., "Multi-dimensional modeling of heat and mass transfer of fuel films resulting from impinging sprays", SAE Paper 980132, 1998.

[20] Borman, G. L. and Johnson, J. H., "Unsteady vaporization histories and trajectories of fuel drops injected into swirling air", SAE Paper 598C, 1962

[21]Yassine, M.K., Tagomori, M.K., Henein, N.A., Bryzik, W., " White Smoke Emission Under Cold Starting of Diesel Engines", SAE 960249, 1996

[22] Gonzalez, M.A., " A Computational Study of In-Cylinder Cold Starting Processes in a Diesel Engine", Master of Science, University of Wisconsin-Madison, 1990.

[23] Rose, J.W., and Cooper, J.R., " Technical Data of Fuel ", 7th edition, The British National Committee, World Energy Conference, 1977.

[24] Maxwell, J.B., " Data Book on Hydrocarbons", D. VAN Nostrand Company, Inc., 1968.

APPENDIX B

2003-01-0261

New Integrated "O.P.E.R.A.S." Strategies for Low Emissions in HSDI Diesel Engines

N. A. Henein, I.P. Singh, L. Zhong, and M-C. Lai.
Wayne State University

W. Bryzik
US ARMY TARDEC

ABSTRACT

Integrated control strategies for the O.P.E.R.A.S. (**O**ptimization of injection **P**ressure, **E**GR ratio, injection **R**etard or **A**dvance and **S**wirl ratio) are demonstrated. The strategies are based on an investigation of combustion and emissions in a small bore, high speed, direct injection diesel engine. The engine is equipped with a common rail injection system and is tested under simulated turbocharged engine conditions at two loads and speeds that represent two key operating points in a medium size HEV vehicle. A new phenomenological model is developed for the fuel distribution in the combustion chamber and the fractions that are injected prior to the development of the flame, injected in the flame or deposited on the walls. The investigation covered the effect of the different operating parameters on the fuel distribution, combustion and engine-out emissions. Illustrations of integrated strategies for O.P.E.R.A.S., that take into consideration the needs of the after-treatment devices, are given.

INTRODUCTION

Direct injection diesel engines power most of the heavy-duty vehicles. Due to their superior fuel economy, high power density and low carbon dioxide emissions, turbocharged, small bore, high speed, direct injection diesel engines are being considered to power light duty vehicles (1-2). Such vehicles have to meet the future 2007 emission standards. However, it is difficult to meet these standards by modifying the in-cylinder thermodynamic and combustion processes to reduce engine-out emissions (3-5). After-treatment devices will be needed to achieve even lower emission targets required in the production engines to account for the anticipated deterioration after long periods of operation in the field. Such devices include CRT (Continuously Reacting Traps), DPF (Diesel Particulate Filters), NO_x absorber systems and (SCR) Selective Catalytic Reduction devices.

To reduce the size, mass and cost of the after-treatment devices, there is a need to optimize both the engine and the after-treatment devices as one integrated system. For example, the trade-off between engine-out NOx and PM, suggests that one of these species can be minimized in the engine, with a penalty in the other, which can be addressed efficiently in the after-treatment devices.

Controlling the engine-out emissions can be achieved by optimizing many engine designing and operating parameters. The design parameters include, but are not limited to, the type of injection system: (CRS) Common Rail System, (HEUI) Hydraulically Actuated and Electronically controlled Unit Injector, or (EUI) Electronic Unit Injector; engine compression ratio, combustion chamber design (bowl design, reentrance geometry, squish area (3) and intake and exhaust ports design. With four-valve engines, the swirl ratio depends on the design of both the tangential and helical ports and their relative locations.

For any specific engine design, the operating variables need also to be optimized. These include injection pressure (6-8,13), injection rate, injection duration and timing (pilot, main, and post injection), EGR ratio (9-12), and swirl ratio (14).

This paper introduces a phenomenological model for the fuel distribution and combustion, and emissions formation in the small bore, high speed, direct injection diesel engine. This will be followed by an analysis of the effect of each of the key operating parameters, and their combinations on engine-out emissions. Finally, some strategies for the

Optimization of the injection **P**ressure, **E**GR, injection timing, **R**etard or **A**dvance, and **S**wirl ratio **(O.P.E.R.A.S),** will be presented.

The work described in this paper is a part of an on-going program on the combustion and emission characteristics of small-bore high-speed diesel engines and is a follow up to the work published earlier (15,16,35).

EXPERIMENTAL SET-UP

Experiments were conducted on a single-cylinder, 4-valve, direct-injection, four-stroke-cycle, water-cooled, diesel engine equipped with a common rail fuel injection system. AMOCO Premium diesel fuel was used in all the experiments reported in this paper. Engine specifications are given in Appendix-A.

The engine is supercharged with heated shop air, and the exhaust backpressure is adjusted to simulate actual turbo-charged diesel engine conditions. The engine has four valves. Closing the intake tangential port to different degrees, by using a gate valve, increased the swirl ratio. Position 90° is for the valve in the full open position. The relationship between the swirl ratio and the position of the gate valve is given in Appendix B. The data is recorded in terms of valve position, rather than the swirl ratio, in order to be able to reproduce the same swirl ratio and valve opening in different runs.

Experiments were conducted on the engine under different fuel injection pressures, EGR ratios, main injection retarded and advanced timings, pilot injection, post injection, and swirl ratios. The test matrix is given in Appendix C. The details of the setup and experimental procedure are given in reference (16). The particulate matter was measured by using a mini dilution tunnel, filtration and microbalance. Also soot was measured by using Bosch Smoke meter and the results are in Bosch Smoke Units (BSU). In this paper the data is in BSU.

A PHENOMENOLOGICAL MODEL FOR COMBUSTION AND EMISSION FORMATION IN SMALL BORE DIESEL ENGINES

Combustion and emission formation in diesel engines has been the subject of several investigations. Such investigations include imaging in optically accessible engines (19) and mathematical modeling (37). More recently, a model has been developed at Sandia National Laboratory, for combustion and emission formation in heavy-duty diesel engines. The model is based on images taken in an optically accessible single-cylinder diesel engine, and laser-based measurements of the concentration of different autoignition and combustion intermediate species (20, 21). The model explained the role of the fuel distribution in the spray plays in the autoignition, combustion and the formation of the engine-out emissions, particularly NOx and soot.

In small-bore diesel engines, the conditions are different from those in heavy-duty diesel engines in many aspects. The first is the shorter spray travel before the fuel reaches the wall in the small bore engine. Here, the fuel impingement and the liquid film formed on the wall play a major role in the combustion process. The second is the relatively strong swirling motion needed in the small bore engine to mix the fuel and air. The third difference is the smaller piston bowl diameter as a fraction of the cylinder diameter in the small bore engine and the resulting squish component, which might be absent in the large bore engine.

In the study of engine-out emissions in small-bore direct injection diesel engines, particularly those using high-pressure injection systems, it is important to follow the spray as if moves into the combustion chamber and determine the time it reaches the wall, the time the flame is established in the chamber, and whether the fuel is injected in the flame or reaches the wall as a vapor or liquid. Further more, it is important to find out the effect of the different operating parameters on the fuel distribution in the combustion chamber and its subsequent effect on combustion and engine-out emissions.

FUEL DISTRIBUTION IN THE COMBUSTION CHAMBER

Figure 1 shows a line sketch of the combustion chamber used in this investigation. Before describing the fuel distribution in the combustion chamber, reference is made to the images taken by Paul Miles (14) on an optically accessible version of the engine used in the current investigation. These images taken every crank angle degree showed clearly that a sizeable flame was developed in the combustion chamber at the peak of the ARHR. Based on these observations, we can divide the fuel delivered in the combustion chamber into two major parts, each of which undergoes different processes and contributes in the engine-out emissions in a different way.

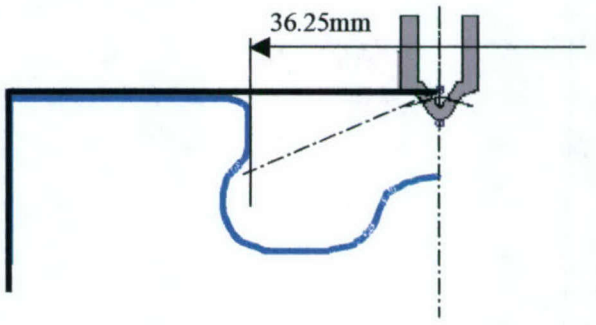

Figure 1. Combustion Chamber of HSDI Engine

The first part is the fuel that is injected prior to the time when the flame is established in the combustion chamber, [F_{pf}]. Here, the lighter components, [F_{pfv}], evaporate, mix with the air, autoignite and burn in the premixed combustion mode. The heavier components deposit on the wall [F_{pfw}], and burn in the mixing-controlled, or diffusion-controlled combustion mode. The difference between [F_{pf}] and [F_{pfw}] represents the fuel in the combustion chamber that does not reach the wall and is referred to as [F_{trans}].

The second part is the fresh fuel injected in the flame [F_{if}] that is exposed to fairly high gas temperatures. Here the fuel may decompose forming soot, or in the presence of air, burns in the mixing-controlled combustion mode or the diffusion-controlled combustion mode.

The third part is the fuel delivered near the very end of the injection process, as the needle is about to close [F_t]. This is a very small amount that is poorly atomized and may decompose, or burn in a diffusion-controlled combustion mode.

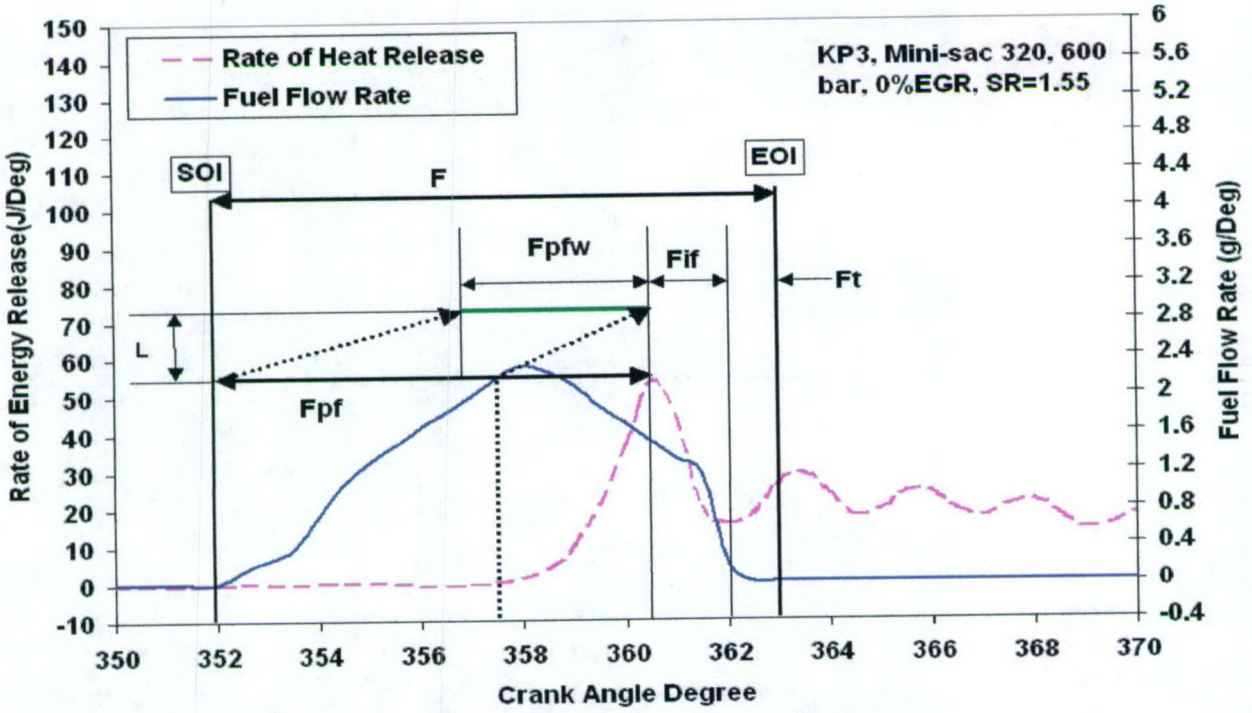

Figure 2. Fuel distribution in the combustion chamber related to the rate of fuel delivery and rate of energy (Heat) release

Reference is made to figure 2, to illustrate the effect of fuel distribution in the combustion chamber on combustion and emission formation. For this figure, the engine test conditions are as follows: nozzle: 320 mini sac; fuel injection pressure = 600 bar; IMEP = 5 bar; engine speed = 2000 rpm; swirl ratio= 1.55; EGR = 0 and LPP (Location of the peak cylinder pressure): (6° - 7°) aTDC. The rate of fuel delivery was computed from the needle lift and the pressure drop across the nozzle holes. The rate of energy release (RER) from the combustion reactions is computed from the cylinder pressure, accounting for the heat transfer and blow by losses. (RER) is usually referred to as Gross Rate of Heat-Release Rate (17). In the following sections RER or ARHR will be used and refer to the energy releases from the combustion reaction.

The fuel distribution in the combustion chamber, under the operating conditions of Figure 2 can be described as follows:

<u>Fuel injected prior to the flame, evaporated and burned [F_{pfv}]</u>

The fuel delivery [F] starts at 352.0° and continues for 11°. As the spray travels into the combustion chamber, the light components [F_{pfv}] evaporate and mix with the surrounding air and deflect along the wall. This is the early stage of combustion where autoignition nuclei are formed at different sites in the spray envelope and produce flamelets that burn the surrounding combustible mixture. Figure 2 shows the energy release due to premixed combustion starts at 358° and takes 2.4 CAD (0.264 ms) to reach an energy release rate of 54 J/CAD, due to the combustion of

35.14% of the fuel. As discussed earlier, the flame is established in the combustion chamber at 360.4°.

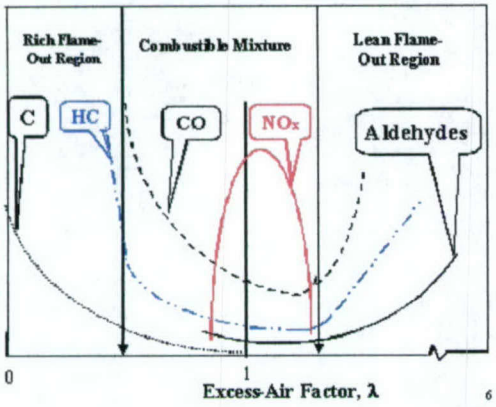

Figure 3. Illustration of the variation in the emissions with the change in the quality of the premixed combustion zone of the spray.

The total period of the premixed combustion is about 4.3 CAD (0.47 ms). The local quality of the fuel vapor-air mixture determines the emissions formed during this early stage of combustion. The premixed combustion fraction will have a local air/fuel ratio that ranges from zero to infinity. The mole fractions of the different gaseous emission species at different excess air factors would be close to those in the spark ignition engines, as illustrated in Figure 3. Previous investigations on diesel combustion, without EGR, showed that the dominant emission in the premixed charge is NO_x (18). The mass of the emissions formed at the end of this stage depends on the mass of the charge that burns in the premixed mode.

Fuel injected prior to the flame and deposited on the walls [F_{pfw}]

Previous investigations on heavy duty diesel engines showed that during the early stages of diesel combustion, the core of the spray remains in the liquid phase and its length from the nozzle is known as the liquid length (22, 23). In the current small bore engine, under similar operating conditions, the liquid core was found to reach the wall (24). The spread of the liquid film on the wall depends mainly on the speed of the spray, which in turn depends on the injection pressure.

In order to determine [F_{pfw}] in this investigation, the spray penetration during the injection period is calculated from the pressure drop across the nozzle holes and the flow area, calculated at different values of the needle lift. Figure (2) shows that the first element of the spray arrives at the wall at 356.5°. The heavier parts of the fuel continue to be deposit on the wall up to 360.4°, before the flame is established in the combustion chamber. It is noticed that the period of time the spray takes to arrive at the wall varies during the injection process, due to the changes in the injection pressure, cylinder gas density and needle opening area.

The rate of evaporation of the fuel deposited on the wall depends on the relative velocity between the gas phase and the liquid fuel film, the gas temperature as well as the wall temperature. The gas motion in the combustion chamber depends on the interaction between the swirl and squish components.

The wall temperature plays an important role in the rate of liquid fuel evaporation. At light loads, the wall temperatures are relatively low, allowing the heavier fuel components to remain on the wall and evaporate late in the expansion stroke. Upon evaporation, the heavier molecules may evaporate and appear as exhaust hydrocarbons, or they may be partially oxidized and produce aldehydes if the gas temperature is low, or they may incompletely burn at higher temperatures and produce CO and soot.

Fresh Fuel injected into the flame [F_{if}]

The fresh fuel injected after the peak of energy release rate evaporates and burns at a fast rate as it mixes with the hot combustion products in the presence of the flame. This is the part of the fuel that has the least chance to penetrate into the combustion chamber and be exposed to the high velocity swirling air near the periphery of the piston bowl before it burns.

The emission species formed in this mode of combustion varies with the load. At light loads there is a chance that the evaporated fuel will be completely oxidized and thus contribute in NO_x formation. However, at higher loads, the chances for the complete oxidation of this part of the fuel decrease, and the result is the formation of incomplete combustion products including carbon.

Fuel delivered near the very end of the injection process, [F_t]

During the closing of the injector needle, the flow area decreases, and the flow coefficient drops to a point where the fuel is not well atomized. This part of the fuel will be referred to as the spray tail. Microscopic images taken very close to the nozzle hole, showed the fuel flowing out of the nozzle hole forming ligaments (25) that would have a small chance to evaporate, mix with the cylinder gases and completely burn. This part of the fuel is believed to be a source of unburned hydrocarbons and soot emissions.

ENGINE-OUT EMISSIONS IN SMALL BORE HIGH SPEED DIRECT INJECTION DIESEL ENGINES

The following analysis is based on the above discussions of the fuel distribution in the combustion chamber, and is aimed at identifying the different

parameters that control the engine out emissions. The experimental results will identify the controlling parameter(s) (CP).

NO_x Emissions

Many expressions have been developed to calculate NO_x formation during engine combustion, based on both the formation and decomposition reactions in the extended Zeldovitch mechanism. Assumptions, usually made to arrive at an expression for NO concentration, include the equilibrium concentration or the steady state approximation for the nitrogen and/or oxygen atoms. In this paper, in order to simplify the discussions, NO decomposition reactions will not be considered and the steady state approximation for N will be assumed. Under these conditions, the NO formed over the period of time from the start of combustion to the opening of the exhaust valve can be given by:

$$NO = \int_{SOI}^{EVO} \int_{0}^{V} A\omega K_{O_2} \exp\left(\frac{-E}{RT}\right)[F]^a[O_2]^b \, dV dt \quad (1)$$

where
A, a and b: Constants
ω: Engine instantaneous angular velocity
K_{O2}: Equilibrium constant for O_2 , which is a function of temperature.
E: Activation energy
T: Local gas temperature
[F] : Fuel vapor concentration
$[O_2]$: Oxygen concentration.
V: Volume of the reacting gases
t: time

Equation (1) shows that engine-out NO_x concentration is a function of the following controlling parameters: oxygen concentration, fuel vapor concentration and residence time, in addition to the combustion products temperature. All these parameters change with the engine load, injection pressure P, EGR, Retarding or Advancing injection timing, and Swirl.

Soot Emissions

Engine-out soot emission is the result of its formation and oxidation.

$$\frac{d[S]}{dt} = \frac{d[S_f]}{dt} - \frac{d[S_o]}{dt} \quad (2)$$

Equation (2) is integrated over the whole period from the start of combustion to the time the exhaust valve opens.

The following are the sources of soot formation:
1.Liquid fuel injected in the flame [F_{if}].
2.Fuel injected, evaporated and premixed with air and formed a rich mixture.
3.Fuel injected and premixed with air diluted with EGR.
4. Fuel film on the wall [F_{pfw}].
5. Fuel in the spray tail [F_t].
The rate of soot formation can be given by (26)

$$\frac{d[S_f]}{dt} = K_f[F_v]P^{0.5} \exp\{-\frac{E_f}{RT}\} \quad (3)$$

E_f = 12,500 cal/mole
where $[F_v]$ is the vapor concentration

The rate of soot oxidation can be given by (26)

$$\frac{d[S_o]}{dt} = K_o[S]X_{O_2}P^{1.8} \exp\{-\frac{E_o}{RT}\} \quad (4)$$

E_o= 14,000 cal /mole
where [S] is the soot concentration

The extent of soot oxidation depends on the following controlling parameters: oxygen concentration, charge temperature, mixing rate and a certain period of time. During the expansion stroke, the gas temperature drops and there is a window during which the mass average gas temperature is high enough to render effective soot oxidation reactions. As will be explained later, many operating variables affect the residence time within this window.
Note, the activation energy for the oxidation reactions is higher than that for the formation reactions. Accordingly, in the presence of enough oxygen, the oxidation reactions are favored as the temperature increases.

Hydrocarbon Emissions

The hydrocarbons in diesel exhaust are originated from the following (27):

1. The very lean and rich flameout regions of the premixed charge in the spray.
2. The liquid fuel film deposited on the wall.
3. Spray tail, where the fuel in not well atomized.

Similar to soot, HC can be oxidized later in the expansion stroke, if they have enough time to mix with the oxidants, at a temperature high enough to render effective oxidation reactions.

CO Emissions

CO is related to the incomplete oxidation of the hydrocarbons. This occurs wherever there is a rich mixture. Also, CO can be formed from the incomplete oxidation of the HC late in the expansion stroke.

EFFECT OF INJECTION PRESSURE (P) ON ENGINE-OUT EMISSIONS

EFFECT OF INJECTION PRESSURE ON NO_X EMISSIONS AT 0% EGR

Figures 4(a) and 4(b) show a trend for EI-NO to increase at higher injection pressures at 0% EGR. This increase can be explained by examining the effect of injection pressure on the several parameters given in Equation (1).

Higher injection pressures increase the volume of the premixed charge (V) and fuel vapor concentration [F]

The volume (V) and concentration [F] are related to the spray penetration, spray angle, spray atomization and evaporation. Higher injection pressures produce faster sprays at the nozzle exit, and increase spray penetration in proportion to the square root of the pressure differential across the nozzle holes. This can be made clear by examining the different correlations for spray penetration, given in the Appendix D.

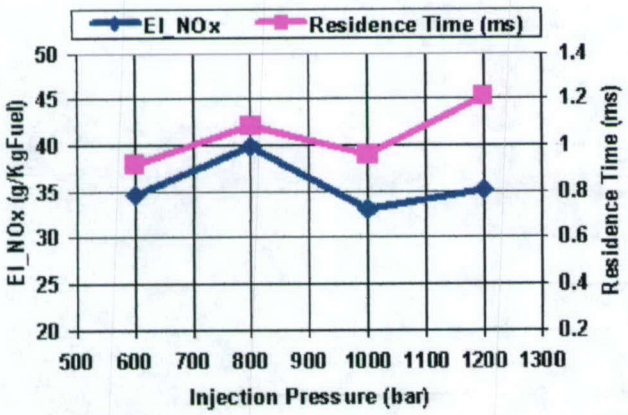

Figure 4(a) Effect of injection pressure on NOx emission (Mini sac 320 nozzle, kp3).

In addition, higher injection pressures affect the spray angle. The far-from-the-nozzle spray angle was found to increases with injection pressure (28). Meanwhile, the spray becomes puffier at higher injection pressures (29). Further more, higher injection pressures improve atomization and produce sprays of smaller SMD. In addition, higher injection pressures produce more turbulence and better mixing due to the faster sprays.

A comparison between Figure 5, for 1200 bars and Figure 2 for 600 bars, will be made to explain the effect of fuel injection pressure on the distribution of the fuel in the combustion chamber and emission formation. Both figures are at the same load and speed.

At the higher pressure the spray reaches the wall faster in 4° compared to 4.7° at 600 bars, both the vapor phase and liquid phase are expected to spread more on the surface at the higher injection pressures. In addition, at higher injection pressures, the spray moves further along the wall toward the bottom of the bowl and radically inward toward the center of the bowl. This improves the mixing of the fuel with the bulk of the air in the bowl.

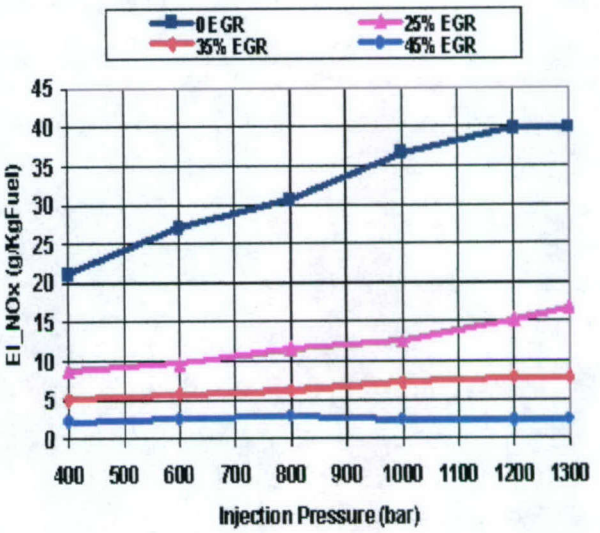

Figure 4(b) Effect of injection pressure on NOx emission (mini sac 320, KP2).

All the above physical processes contribute to the production of larger amounts of the autoignitable mixture (V), cause an increase in the population of the autoignition nuclei in the spray, and reduce the ignition delay period. Figures 2 and 5 show that ID occupied 5.7 CAD at 600 bars, compared to 4.3 CAD at 1200 bar.

Higher injection pressures increase the combustion products temperature (T)

Higher injection pressures improve the chemical autoignition processes due to the following: (i) an increase in the concentration of the fuel vapor [F], and its effect on enhancing the reaction rates and (ii) an increase in the specific reaction rate of the autoignition reactions, under the conditions of the current experiments. In the current investigation, the injection timing was retarded at the higher injection pressures, in order to keep the cycle peak pressure location (PPL) constant with respect to TDC. Figure (5) shows that at 1200 bars injection started at 357 CAD, compared to 352 CAD at 600 bars, and the period of injection occupied 8.5 CAD at 1200 compared to 10.5 CAD at 600 bar.

With late injection timing, the fuel was injected in the cylinder when the gases were at a higher compression pressure and temperature. It should be noted that all the injection timings were earlier than 2 degrees before TDC where the compression temperature reaches its maximum value.

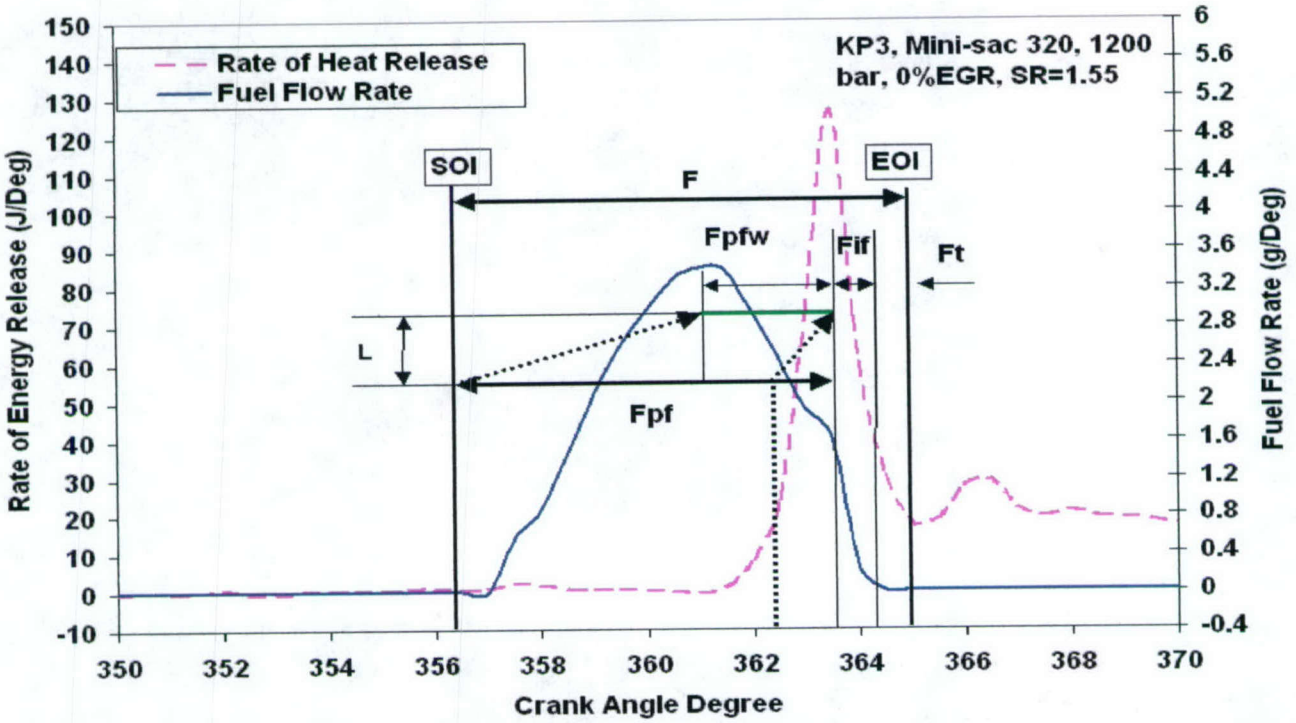

Figure 5 Fuel distributions in the combustion chamber related to rate of fuel delivery and rate of energy (Heat) release.

In spite of the shorter ID at the higher injection pressure, more fuel vapor was accumulated in the combustion chamber before the end of ID, and burned in the premixed combustion mode causing the RER to reach 126 J/CAD, compared to 53.57 J/CAD at 600 bars.

Higher injection pressures produce locally higher combustion gas temperatures

The local combustion gas temperature was calculated from the energy release rate and rate of injection (17). It is important to notice that the peak combustion products temperature is higher than the mass average gas temperature computed from the cylinder gas pressure. The local combustion gas temperatures for the two pressures are plotted in Figure 6. At 1200 bars, the peak combustion gas temperature reached 2155K, compared to 2045 K at 600 bars.

Higher injection pressures increase the residence time the combustion products spend in the critical temperature window for NO formation

The NO chemical kinetics indicate that, in the presence of oxygen, under the engine operating conditions, any significant formation of NO occurs in a temperature window above about 1700K. At lower temperatures, the rate of NO formation is so low that it can be neglected. Figure 6 shows that the residence time at 1200 bars was equivalent to 15 CAD, compared to 11CAD at the lower pressure.

The above four factors played a major role in increasing the premixed combustion fraction, which, in the presence of enough oxygen, increases NO engine-out emissions at the higher pressures.

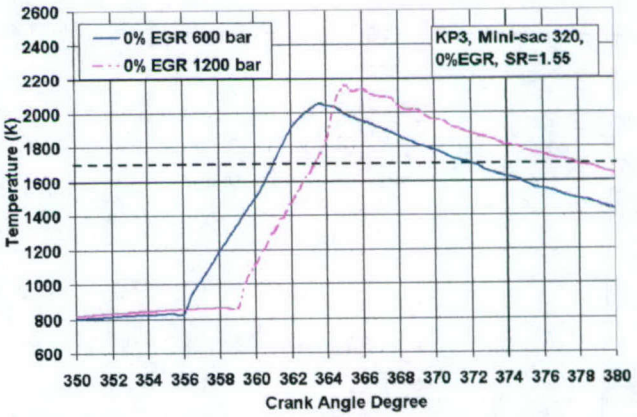

Figure 6. Comparison between the combution gas temperature at 600 bars and 1200 bars.

EFFECT OF INJECTION PRESSURE ON ENGINE-OUT SOOT EMISSION (BSU) AT 0% EGR

Figure 7 shows the effect of increasing the injection pressure on reducing BSU for mini sac 320 nozzle, at KP2. Many factors cause the drop in BSU at higher injection pressures.

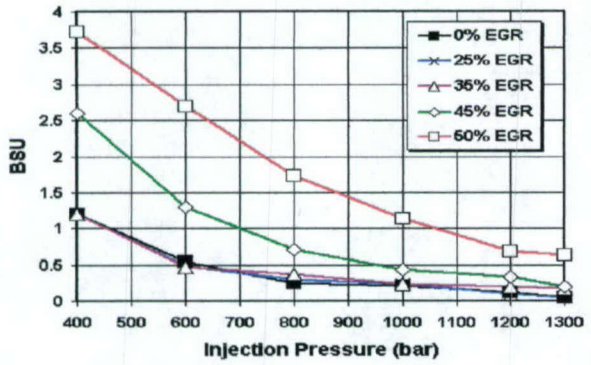

Figure 7 Effect of injection pressure on BSU at different EGR ratios (mini sac 320).

(a) The smaller fraction of the fuel that is injected in the flame [F_{if}] at the higher pressures. Figure 8 shows that an increase in injection pressure from 600 bars to 1200 bars reduced the fuel injection in the flame from 12% to 2%.

(b) The higher mass average gas temperature that is effective in soot oxidation, as shown in Figure 8.

(c) The increase in the premixed combustion fraction (Fpp) at higher injection pressure for KP3 and mini-sac 320 nozzle as shown in figure 9.

(d) The more effective oxidation reactions caused by the presence of enough oxygen at zero EGR.

(e) The better mixing and increased turbulence caused by the high spray velocity at the high injection pressure.

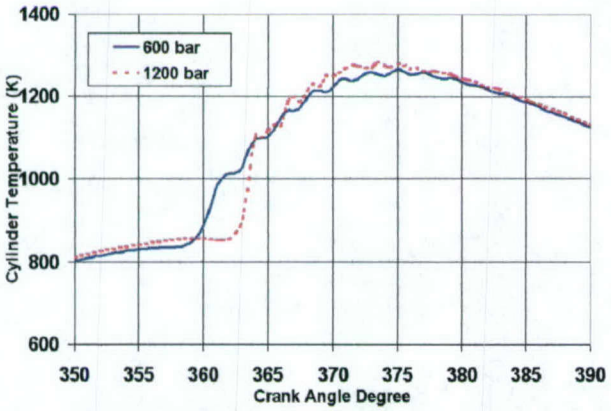

Figure 8 Effect of injection pressure on mass average gas temperature (KP3, 0%EGR, mini sac 320 nozzle).

EFFECT OF INJECTION PRESSURE ON ENGINE-OUT SOOT EMISSION (BSU) AT HIGHER EGR RATIOS

An increase in injection pressure at high EGR ratios causes more fuel to be delivered in the combustion chamber before the flame is established in the combustion chamber, as illustrated in Figure 10. This reduces the fuel injection in the flame [F_{if}], improves the chances of fuel evaporation and mixing, increases the premixed combustion fraction and ultimately reduces soot emissions.

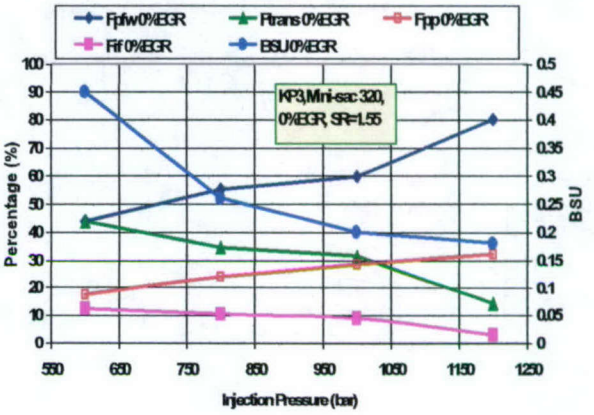

Figure 9 Effect of injection pressure on the fuel distribution in the combustion chamber.

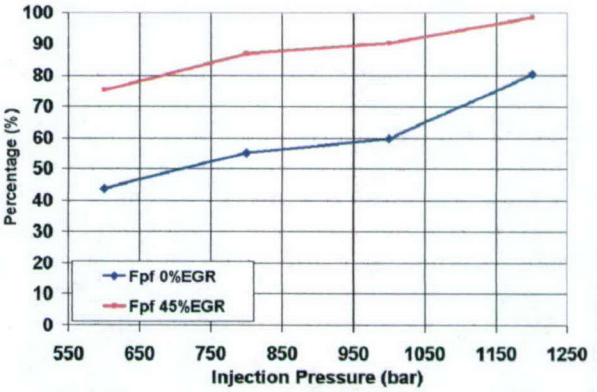

Figure 10. Effect of injection pressure on fuel injected prior to the establishment of the flame (KP3, mini sac 320 nozzle).

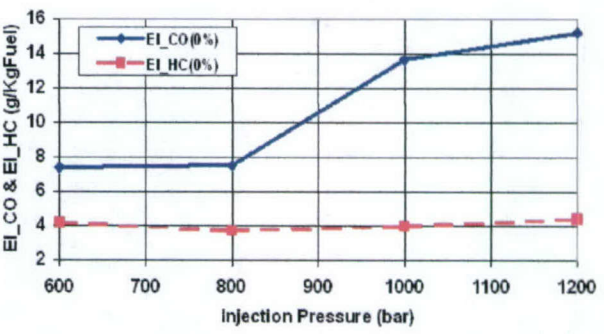

Figure 11 Effect of injection pressure on EI_HC and EI_CO (KP3, 0%EGR, mini sac 320 nozzle).

EFFECT OF INJECTION PRESSURE ON ENGINE-OUT HC AND CO EMISSIONS AT ZERO EGR

Figure 11 shows that the engine-out HC and CO emissions followed the same pattern, they almost remained constant as the pressure increased from 600 bars to 800 bars, after which they increased again. Many factors might have contributed to this pattern. The increase in pressure from 600 bars to 800 bars caused more fuel to be deposited on the wall, shown in Figure 9. But the increase in turbulence at the higher injection pressure enhanced mixing and the oxidation of HC and CO that might have increased from the fuel deposited on the wall. At pressures higher than 800 bars, the improvement in oxidation reactions of the hydrocarbons and co could not match the increase of their formation due to the larger amount of the heavy fuel components that was deposited on the wall and could not achieve complete combustion.

EFFECT OF EGR (E)

EFFECT OF EGR RATIO ON NO_X

Figures 12 and 4(b) show the impact of EGR on reducing NO_x over a wide range of injection pressures of KP2 and KP3. To find out the factors that contributed in the reduction of NO_x, a comparison is made between the fuel distribution in the combustion chamber at two different injection pressures, without EGR and with 45% EGR at KP3.

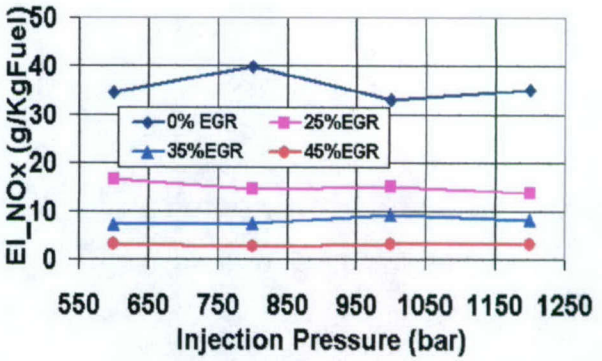

Figure 12 Effect of EGR on reducing NOx (kp3, mini sac 320 nozzle).

Figures 13 is for 600 bar and 45% EGR, and Figure 2 is for the same running conditions but without EGR. A close examination of these figures reveals the effects that would enhance or hinder NO_x formation. This would point out to the principal controlling parameter responsible for the drop in NO_x at higher EGR ratios. The parameters that enhance NO formation are: (a) ID delay increased from 5.7 ° at zero EGR to 7.0° at 45% EGR. The increase in ID is due to the drop in the oxygen concentration, in addition to the drop in the compression temperature caused by the higher thermal capacity of the charge. (b) The premixed combustion fraction increased at the higher EGR ratio. The increase in ID allowed more fuel to be injected, evaporated and mixed prior to the start of combustion.

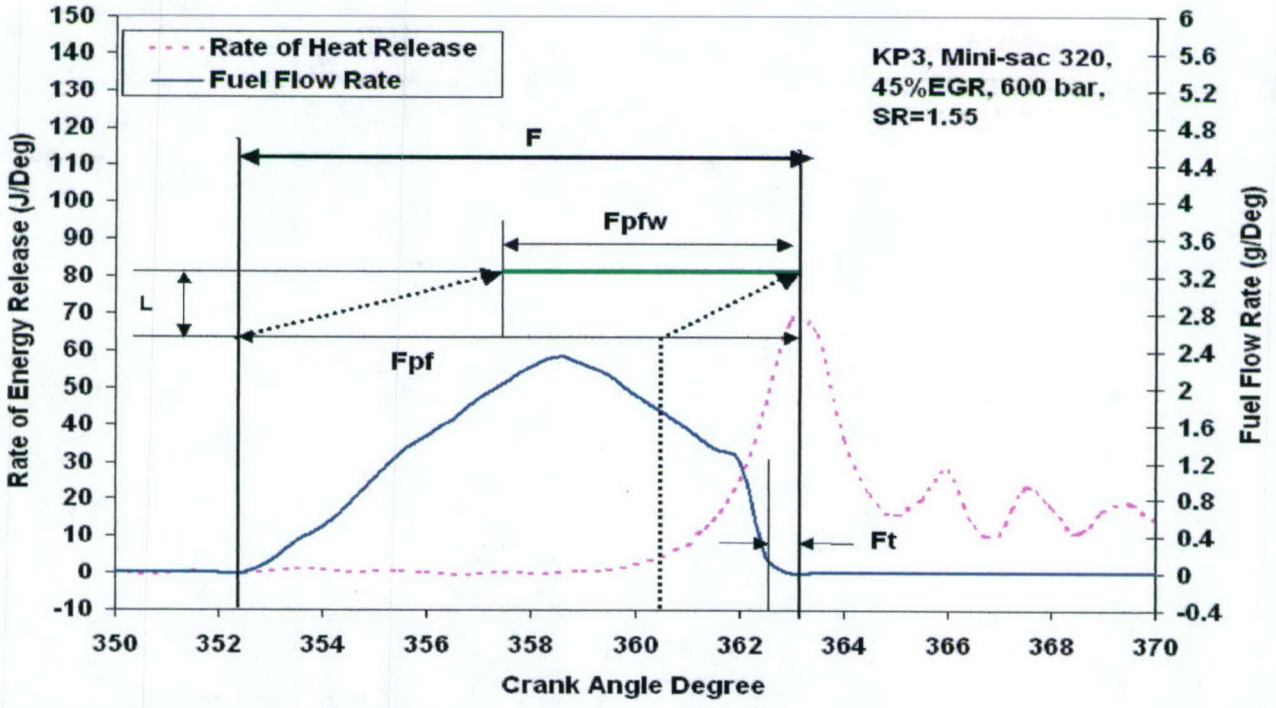

Figure 13 Fuel distribution in the combustion chamber related to rate of fuel delivery and rate of energy (Heat) release (KP3, mini-sac 320 nozzle, 600 bar and 45% EGR).

(c) The magnitude of the RER at its peak increased from 54 J/degree at 0% EGR to 70 J/CAD at 45% EGR. (d) In addition, the high concentration of the fuel that burned in the premixed combustion mode caused the peak temperature to increase from 2156.2 K at 0% EGR to 2544.5 at 45% EGR, as shown in Figure 14. All these changes would increase NO_x at 45% EGR. However, NO_x dropped with EGR.

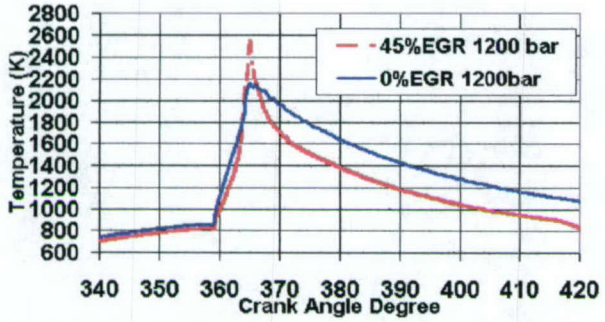

Figure 14 Effect of EGR on combustion gas temperature at 1200 bar injection pressure.

Therefore, controlling parameters other than the premixed combustion fraction and the peak temperature of the combustion products are responsible for the drop in NO_x with EGR. By examining equation (1), the only other parameters that affect NOx emissions are the oxygen concentration and residence time in the critical temperature window. Figure 15 shows the in-cylinder A/F ratio as a function of EGR ratio, and Figure 16 shows the effect of the in-cylinder A/F ratio on NO. This makes it clear that the drop in oxygen concentration is a principal controlling parameter (PCP) in NO_x emissions. The second major parameter is the shorter residence time of the combustion products in the temperature window above 1700K, as shown in Figure 14. At the higher EGR ratio, the residence time is only 27% of that at the lower EGR ratio.

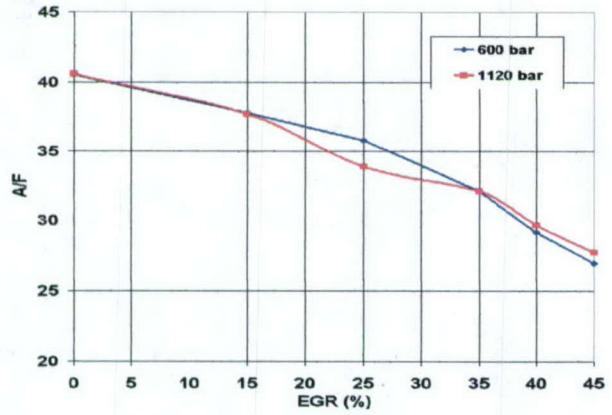

Figure 15 Relation between percentage of EGR and in-cylinder A/F ratio (KP3, VCO 430).

This discussion indicates that PCPs for NO formation at higher EGR ratios are O_2 concentration and residence time at temperatures above a critical temperature.

EFFECT OF EGR RATIO ON ENGINE-OUT SOOT EMISSIONS

Engine-out soot increases with EGR, in spite of the lower fraction of the fuel injected in the flame and the reduction in the mixing-controlled and diffusion-controlled combustion fractions. Figure 17, for 1200 bar injection pressure and mini-sac 320 nozzle, shows that all the fuel was delivered in the combustion chamber before the peak of RER was reached. Accordingly, the fuel has a chance to evaporate, mix with the other gases and reduce the mixing-controlled and diffusion controlled combustion fractions.

From this analysis, other parameters contributed to the increase of soot . Figure 18 shows the impact of reducing the in-cylinder air fuel-air ratio on engine-out BSN.

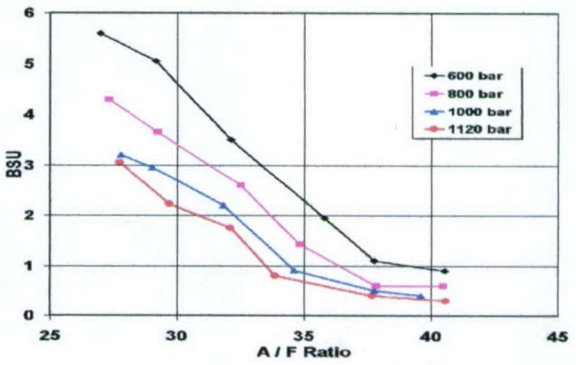

Figure 16 Relation between A/F ratio and EI_NOx (KP3, VCO 430).

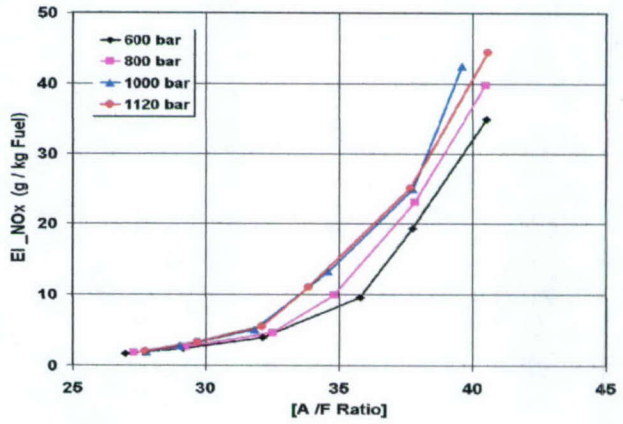

Figure 18 Relation between A/F ratio and BSU, (KP3, VCO 430).

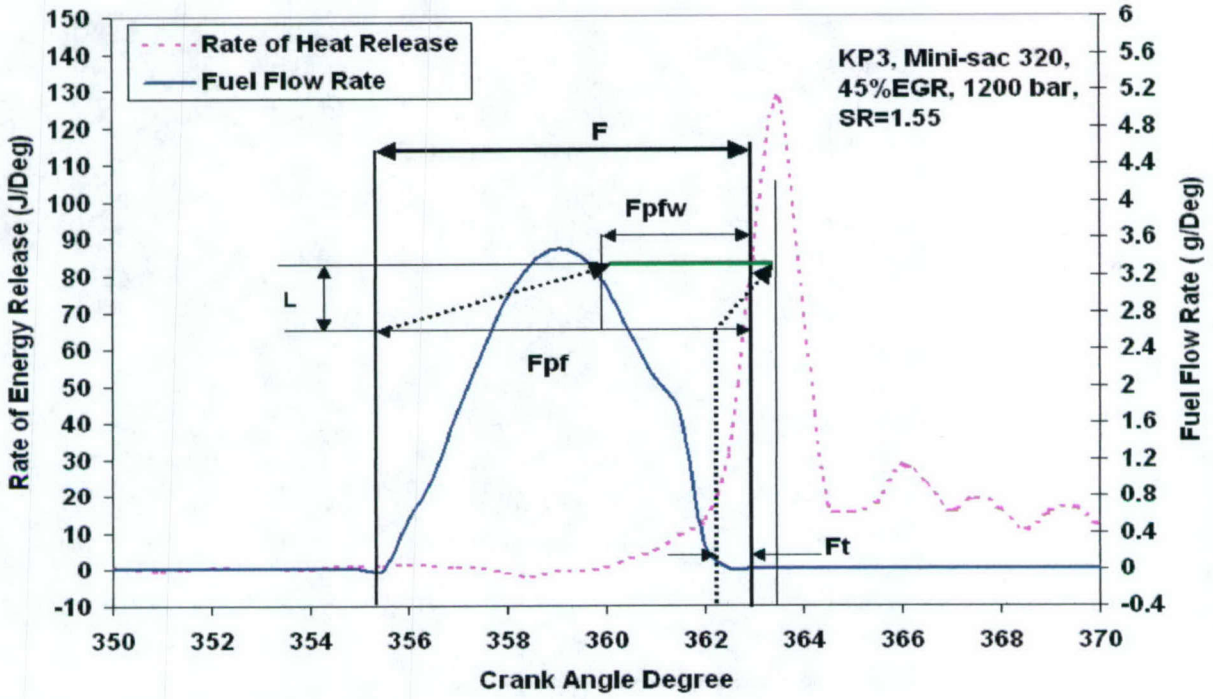

Figure 17. Fuel distribution in the combustion chamber related to rate of fuel delivery and rate of energy (Heat) release (KP3, mini-sac 320 nozzle, 1200 bar and 45% EGR)

It is clear that the oxygen concentration is a principal controlling parameter in soot emissions, since it improves the oxidation reactions. Another factor that might have contributed in the increase in soot formation is the higher percentage of the liquid fuel deposited on the wall during the long ignition delay period as shown in Figure 19. The heavy fuel components evaporate at a fast rate due the high gas temperatures, but have no chance to burn completely and end up forming soot.

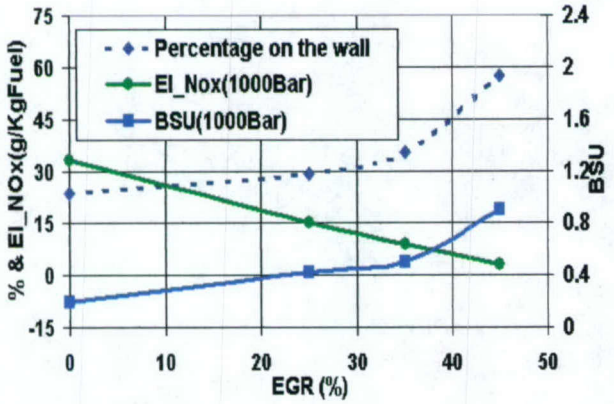

Figure 19 Effect of EGR on fuel injected on the wall, BSU and EI_NOx (KP3, mini sac 320, 1000bar injection pressure).

EFFECT OF EGR RATIO ON ENGINE-OUT CO

Figure 20 shows that at injection pressures of 600 bars and 800 bars, CO increased at the higher EGR ratios. But at 1000 bar and 1200 bar, CO dropped as EGR increased to 25%, after which it increased at higher EGR ratios. The drop in CO at the higher pressures can be attributed to the increase in premixed combustion fraction. The increase in CO at higher EGR ratios can be attributed to (a) the drop in oxygen concentration and the corresponding deterioration of the oxidation reactions and (b) the shorter residence time of the products at temperatures high enough to enhance the oxidation of CO, and (c) the incomplete combustion of the heavy hydrocarbon compounds deposited on the walls.

EFFECT OF EGR ON ENGINE-OUT HC EMISSIONS

Figure 21 shows a general trend for the drop in HC emissions at the higher EGR ratios at all the injection pressures. This drop is accompanied by an increase in CO. This suggests that, while the fuel deposited on the wall increased at higher EGR ratios, more of it evaporated and burned incompletely to CO.

OPTIMIZATION OF THE INJECTION PRESSURE AND EGR: (O.P.E.)

O.P.E. is achieved by developing trade-off maps for NO_x and BSU at three different operating points. Two

trade-off maps for two different nozzles are given in Figures 22.a and 22.b for KP 2 and KP3 respectively.

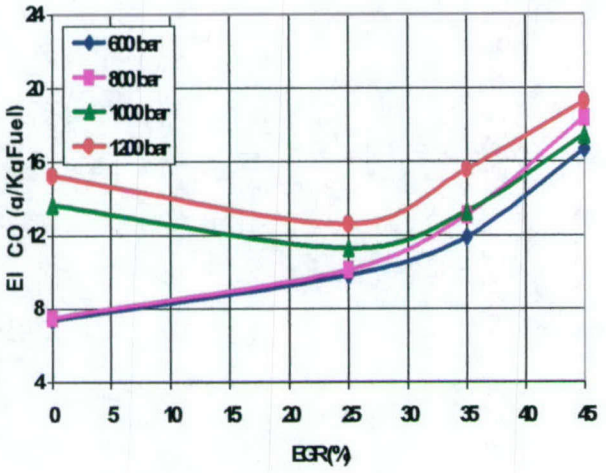

Figure 20 Effect of EGR ratios on engine out CO (KP3, mini sac 320)

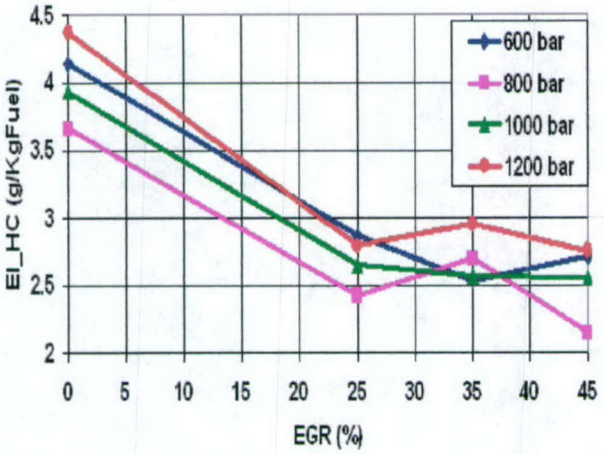

Figure 21 Effect of EGR ratio on engine out HC (KP3, mini sac 320).

For KP2, figure 22.a shows the ISO-EGR lines as well as the ISO-BAR injection pressure lines. The strong effect of EGR on reducing EI_NO_x is very clear at all the injection pressures. The figure also shows the strong effect of increasing the injection pressure on reducing BSU at all EGR ratios.

Notice that the reduction in EI_NO_x by EGR was associated with an increase in BSU. The smaller nozzle showed no increase in BSU at all the injection pressures with the increase in EGR up to 35%. The larger hole nozzle showed the same trend at the high injection pressures. But at low injection pressures BSU increased continuously with EGR. Also For the large nozzle, there is a penalty in BSU by raising the injection pressure above 800 bar at the high EGR ratios. At EGR ratios of 45% and 50% BSU increases at an accelerating rate.

The slopes of the ISOEGR lines gives the penalty in EI_NO_x caused by the increase in the injection pressure. Figure 22.a indicates that the penalty in EI_NO_x depends on the EGR ratio. At zero EGR the penalty is severe. However, the penalty is reduced at the higher EGR ratios. It is interesting to notice that there is no penalty in EI_NO_x at the EGR ratios higher than 45%. Notice that 50%EGR reduced EI_NOx by 96%. The smaller nozzle reduced BSU to much lower levels at the higher EGR ratios, than the larger hole nozzle. This is expected because of the better atomization of the spray. However, for KP3, figure 22.b shows the similarity of the trade-off maps with KP2 maps, except for the following: (a) The two nozzles produce higher BSU at KP3 than that at KP2. (b) the smaller hole nozzle produces higher EI_NO_x at KP3 than that at KP2.

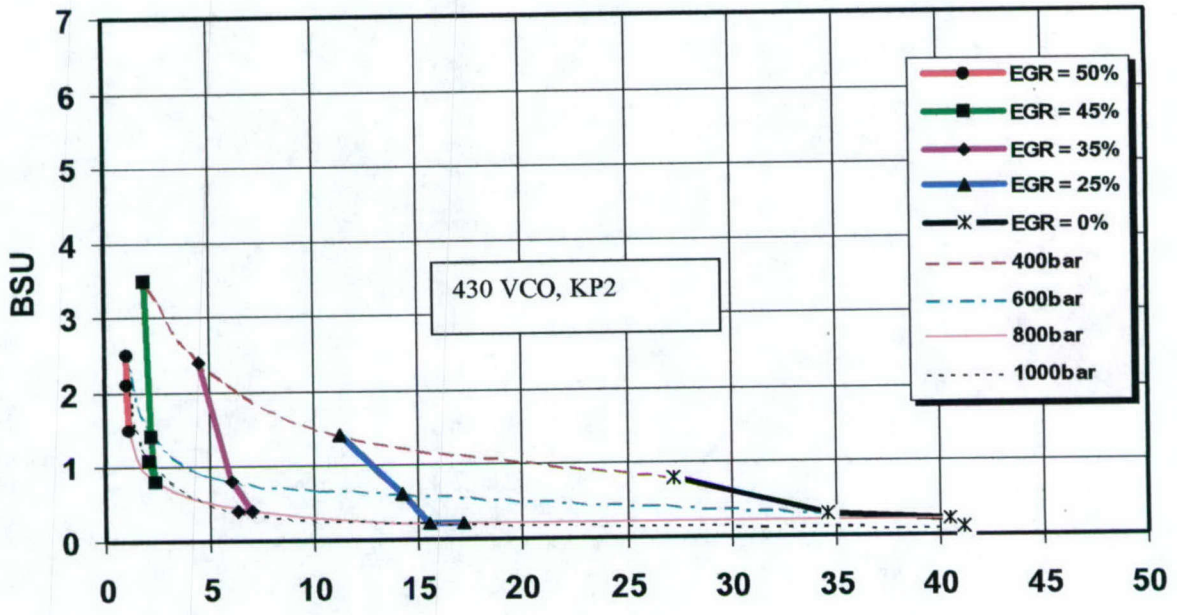

RPM = 1500, IMEP = 300kPa, Tin = 350k, Pin = 1.2bar, Pexh = 1.5bar, Angle of Ppeak:6-7ATDC VCO 430 Nozzle

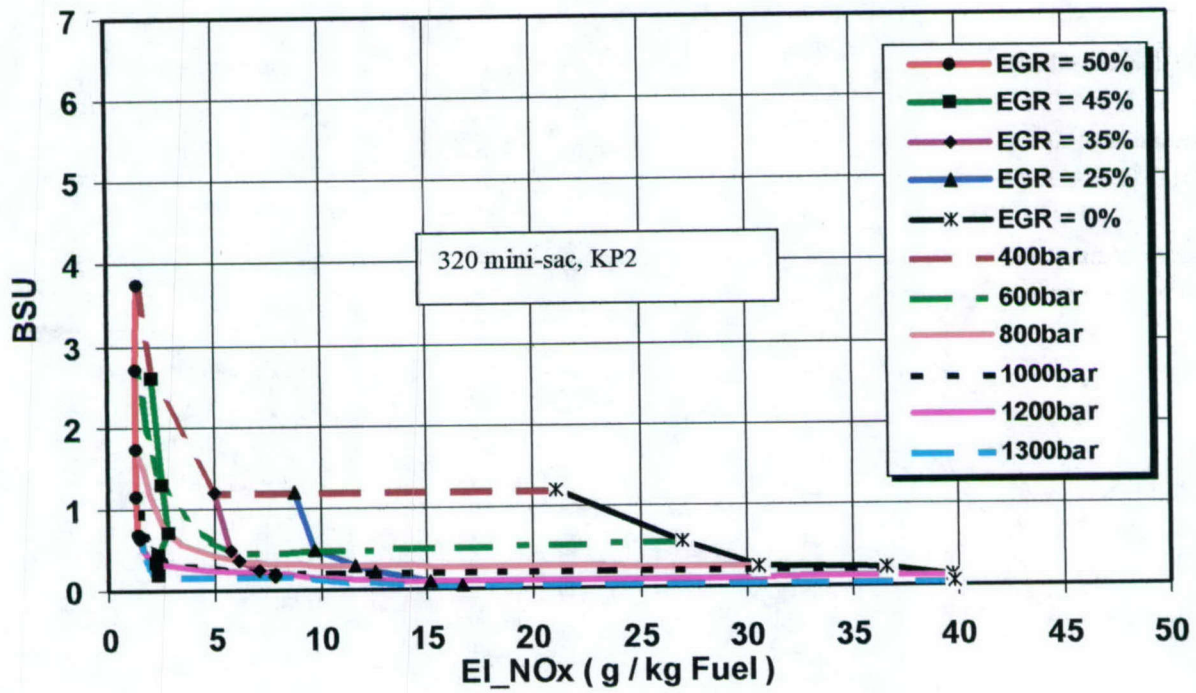

Figure 22(a) Trade off maps at KP2 and two different nozzles

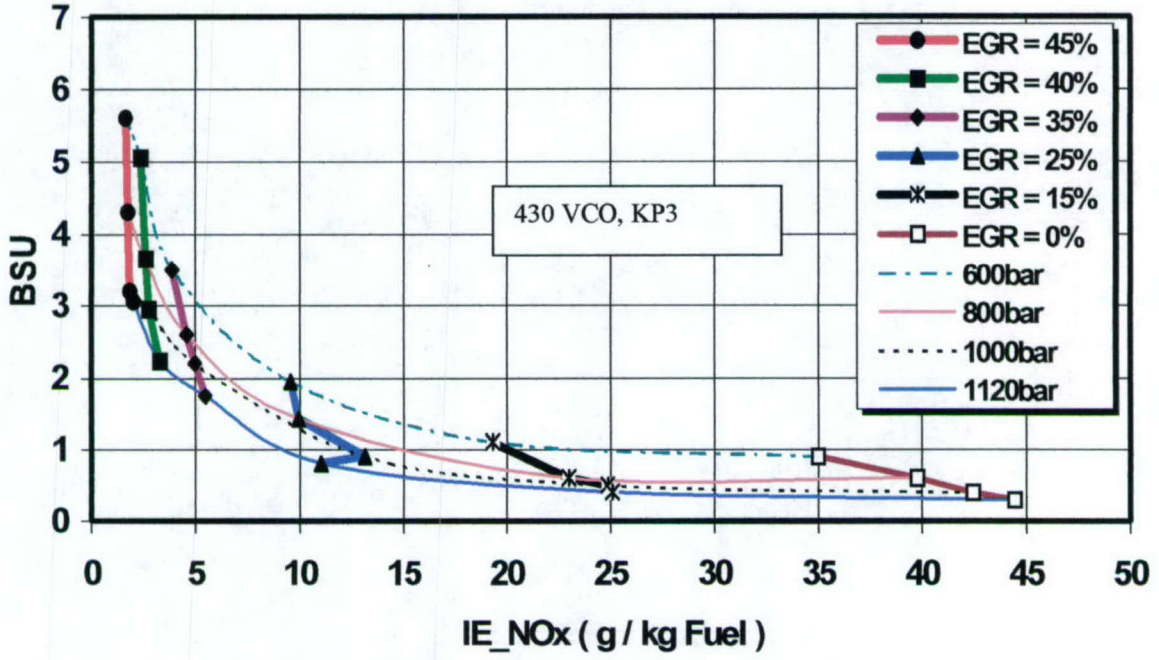

RPM = 2000, IMEP = 500kPa, Tin = 350k, Pin = 1.4bar, Pexh = 1.8bar, Angle of Ppeak:6-7ATDC, VCO 430 Nozzle

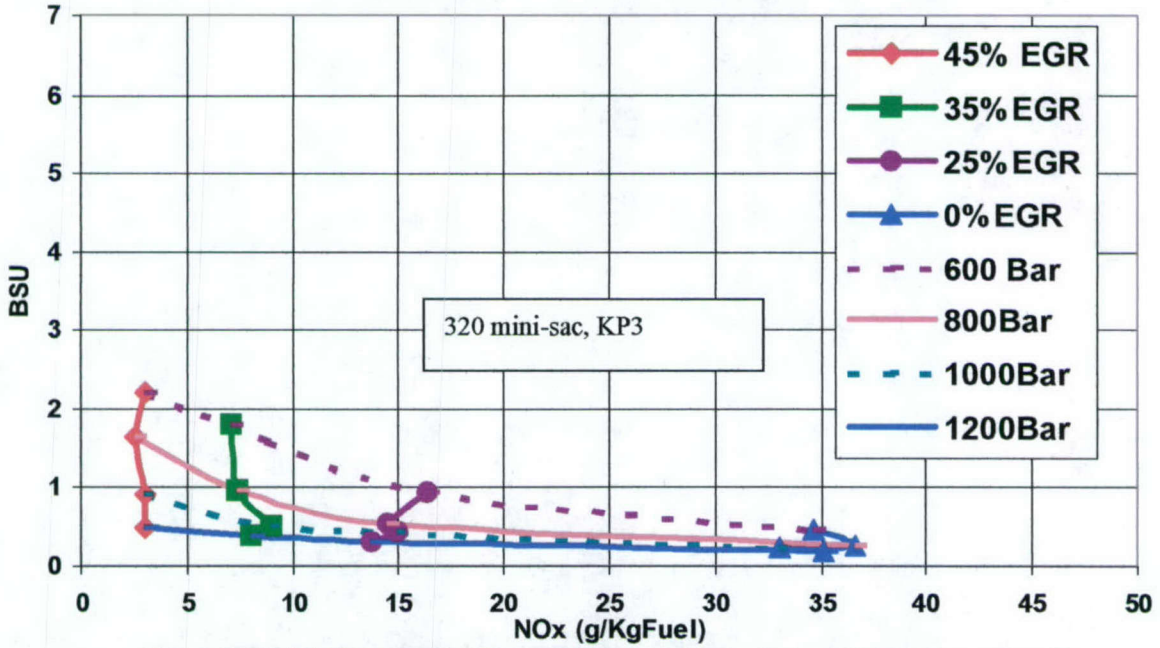

RPM=2000,IMEP=500KPa, Tin=350K,Pin=1.40Bar,Pex=1.80Bar,Ppeak=6~7 ATDC, Mini-sac 320 Nozzle

Figure 22(b) Trade off maps at KP2 and two different nozzles

EFFECT OF NJECTION RETARD AND ADVANCE: (R.A.)

The main, pilot and post injections may be retarded or advanced to achieve certain performance and emission reduction goals. Pilot injection is utilized to reduce ignition delay and the premixed combustion fraction in order to reduce engine noise and NOx_EI. Split or post injection is used to improve the effectiveness of the post combustion oxidation reactions and reduce the emission of the incomplete combustion products, such as soot, HC and CO emissions. Also, retarded post injection is used to increase the hydrocarbon emissions, to meet the needs of the after treatment device.

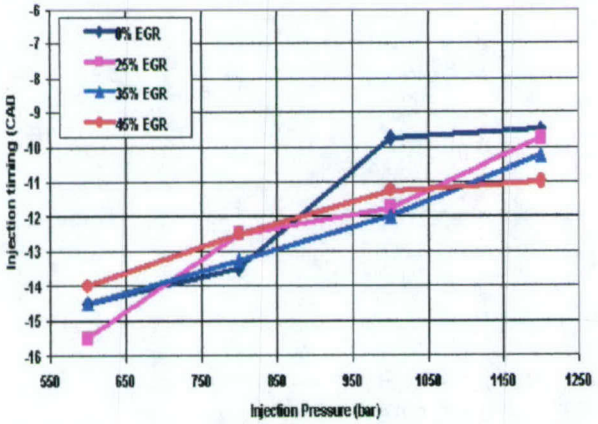

Figure 23 Effect of injection pressure and EGR on injection timing

EFFECT OF TIMING OF MAIN INJECTION

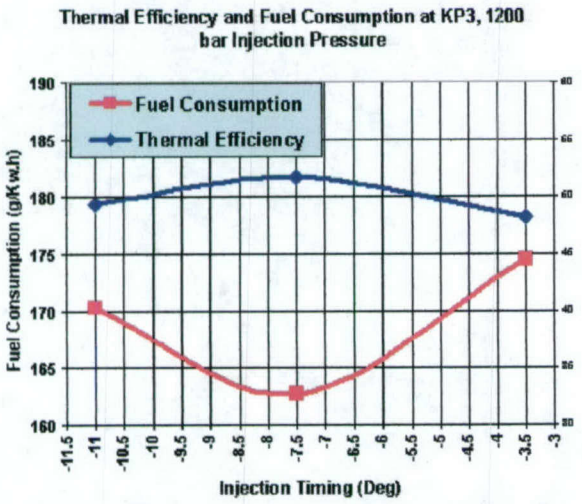

Figure 24 Effect of injection timing retarding on fuel economy

Note that in all the runs covered earlier in this paper, the timing was adjusted to have the peak cylinder gas pressure location at 6-7 degrees after TDC. To achieve this, the injection timing was retarded at the higher injection pressures, and advanced at the higher EGR ratios, as shown in Figure 23.

Figure 24 shows an improvement in ISFC by retarding the timing to 7.5 °bTDC. Any more retard caused deterioration in fuel economy. The gain in fuel economy with the injection retard from 11.0 °to 7.5 °bTDC, is caused by the improved spray evaporation and mixing, as indicated from the higher peak of the energy release from the premixed combustion fraction, as shown in figure 25. The effect of timing on CO and HC is shown in Figure 26(a). The effect of timing on soot and NO is shown in Figure 26(b).

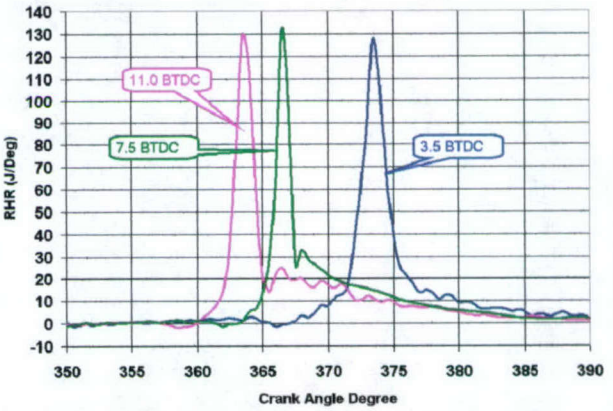

Figue 25 Rate of energy release at different injection timing(KP3, 1200 bar, 45% EGR)

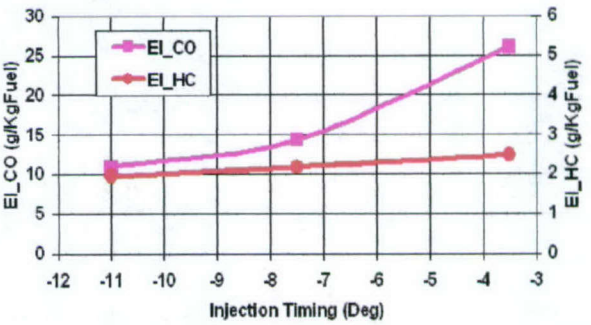

Figure 26(a) Effect of retarding injection timing on engine out emissions (KP3,1200 bar, 45%EGR)

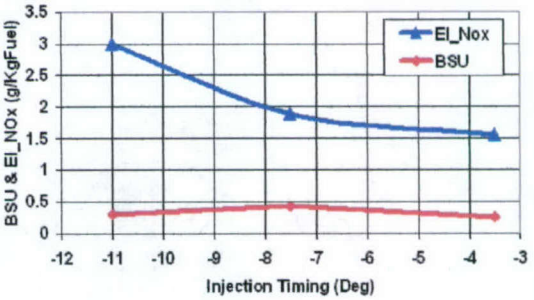

Figure 26(b) Effect of retarding injection timing on engine out emissions (KP3,1200 bar, 45%EGR)

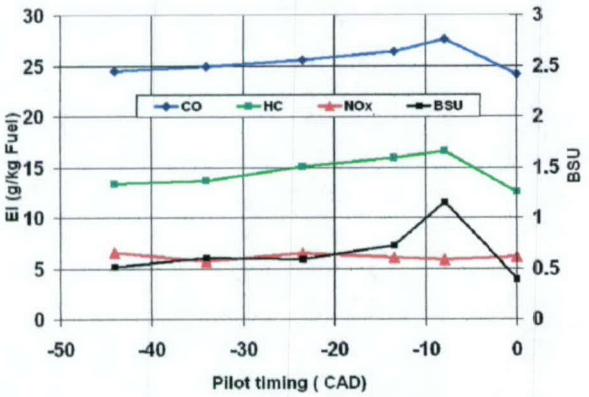

Figure 27 Effect of pilot injection timing on engine out emissions

EFFECT OF PILOT INJECTION

The experiments to investigate the effect of the pilot and post injection timing were conducted on a mini sac 390 nozzle with hole diameter 0.141 mm. The effect of pilot injection timing on engine-out emissions is shown in Figure 27. Figure 28 shows the effect on ID delay and the fuel economy.

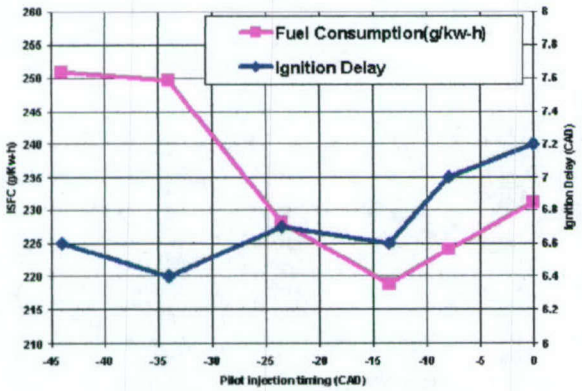

Figure 28 Effect of pilot injection timing on ISFC (KP2, mini-sac 390 nozzle)

For OPERAS, it is clear that there is a timing for the pilot injection that is appropriate to meet the goal of reducing the emissions without a penalty in fuel economy.

EFFECT OF POST INJECTION

The effect of the timing of post injection on engine-out emissions is given in Figure 29, at KP2 and shows no effect on NO_x. However there is a general trend of increasing the incomplete combustion products (HC, CO and BSU) to a point after which these products were reduced. This is clear from Figure 29, except at a post injection timing of 15 CAD after the main injection. The factors that led to this effect are discussed in reference (35). It is noticed that, even with the drop in the complete combustion products at the late post injection timing, their levels were higher than the original level without post injection.

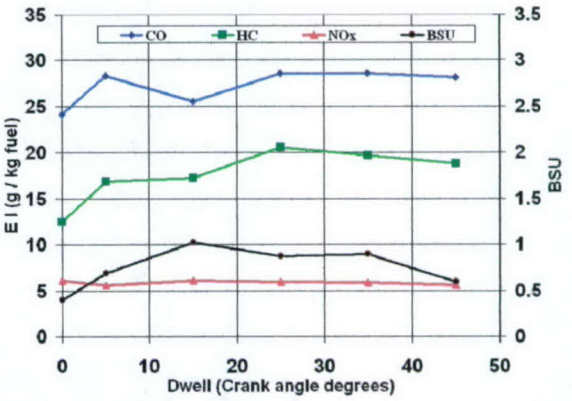

Figure 29 Effect of post injection on engine out emissions, KP2, 390 minisac.

Retarding post injection affects the engine-out HC speciation. Speciation depends on the cylinder gas temperature and the residence time prior to the exhaust valve opening, both of which affect the decomposition of the hydrocarbons and the formation of the partial oxidation products. The closer the post injection to the exhaust valve opening, the closer the

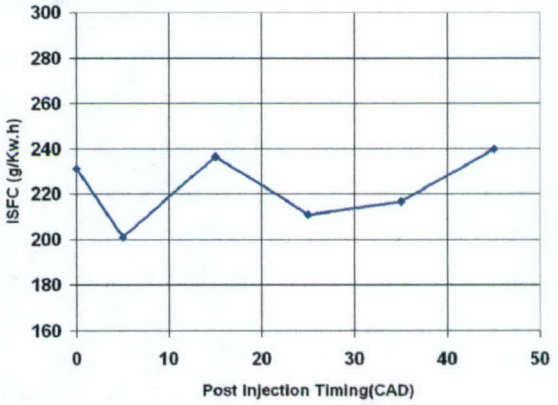

speciation to the original composition of the fuel.

Figure 30 Effect of post injection timing on ISFC (Kp2, mini-sac 390 nozzle)

For OPERAS, if SCR is used, post injection can be a useful tool to produce higher levels of the HC species needed to promote the NO reduction reactions.

The effect of post injection on fuel economy, given in figure 30, shows that there is an optimal timing for best fuel economy.

EFFECT OF SWIRL (S)

The swirl ratio affects the flow field in the combustion chamber, as it interacts with the fuel spray and the squish component. A recent study, using a combination of laser imaging and numerical simulation, reported that the swirl motion, combined with the squish components produce a coil-like motion (38). At low swirl ratios, the coil-like motion allows the fuel to

flow into the piston bowl and utilize the air. At higher swirl ratios the coil-like motion prevents the fuel from flowing into the bowl and enhances it spilling into the squish area. Under these conditions, the utilization of the air in the bowl is poor and results in an increase in soot emissions. In a recent investigation, Miles (24) reported the location and intensity of the gas expansion associated with the premixed burn that influence the large scale flow structures, thereby modifying both mixing rates and bulk transport of unburned fuel during the mixing-controlled burning.

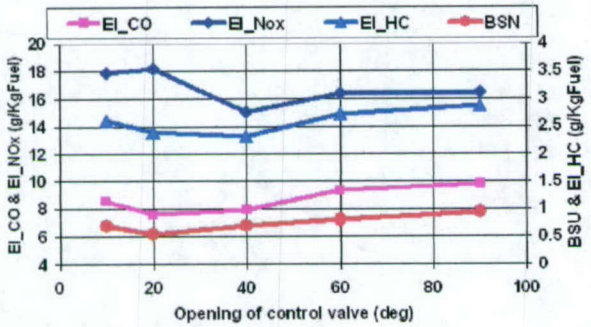

Figure 31 Effect of swirl ratio on engine out emissions (KP3, 25%EGR,1200 bar, mini sac 320)

Figure 31 shows the effect of swirl ratio on engine-out emissions. As the valve was closed from 90°-fully open position- to 60°, there is no change in the engine out emissions because the swirl ratio did not vary, as shown in the Appendix B. When the valve was closed from 60° to 40°, the swirl ratio is almost doubled and this caused better mixing and a reduction in the HC and CO emissions. The associated reduction in NOx suggests that the increase in turbulence occurs late in the expansion stroke, as reported by Miles (24). By closing the valve from 40° to 10°, the swirl ratio increases by 180%, causing an increase in the premixed combustion fraction and the other parameters that enhance NOx formation.

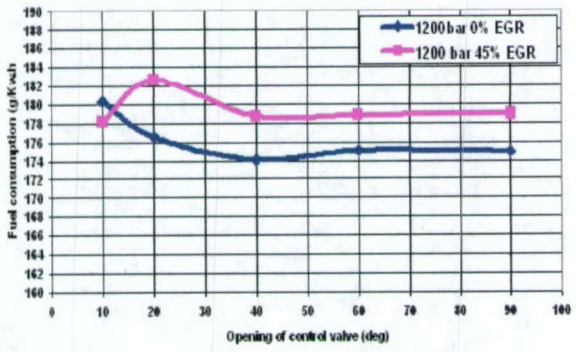

Figure 32 Effect of swirl ratio on fuel consumption at KP3.

The effect of swirl ratio on fuel economy is given in Figure 32 at zero and 45% EGR. The SR at the valve opening position of 40 degrees gives the best fuel economy and lowest NO_x EI, without any penalty in soot emissions. Higher SR, up to a valve opening of 20 degrees improve the oxidation reactions, with a penalty in NO_x and fuel economy. A further increase in SR at smaller valve openings had a negative effect except at high EGR ratios.

Figure 33, a blown up figure of the lower left corner of figure 22.b, gives in some details the effect of the swirl ratio on the gains and penalties in the trade-off between NO_x and BSU, at KP3, using the 320 mini sac nozzle. The dotted arrows show the drop in BSU by increasing the swirl ratio from the base value of 1.55 to its optimized value. The optimized swirl ratio was found to be 2.7, except otherwise indicated on the figure. It can be noticed that at the same EGR%, the swirl is more effective in reducing BSU at the low injection pressures than it is at the higher pressure. Also, at the same injection pressure, the penalty in NO_x is less at the higher EGR ratio.

Figure 33 shows, also, the effect of the optimized retard on reducing NO_x, with a slight reduction in BSU. The main injection was retarded from 11° bTDC (for LPP at 6° - 7° aTDC to 3.5° bTDC.

STRATEGIES TO OPTIMIZE INJECTION PRESSURE, EGR, INJECTION TIMING RETARD or ADVANCE and SWIRL RATIO (O.P.E.R.A.S.)

The main goals of the control strategy for the HSDI small-bore turbocharged diesel engine are: (a) to meet the basic performance, fuel economy and NVH targets, (b) to meet the emissions goals with minimum penalty in fuel economy and power and (c) to meet the goals of affordability, reliability, durability and serviceability with limited increase in life-cycle cost.

Since the HSDI engine cannot meet these goals without the after treatment devices, there is a need for the integrated controls of the in-cylinder processes together with the after treatment techniques. The following after treatment devices are considered: diesel particulate filters, selective catalytic reduction and NOx absorbers.

The control of the in-cylinder processes can be achieved via advances in the design of engine components and by optimizing the different operating variables. Advances in engine design include variable geometry turbocharging or dual turbo charging, cam less valve operation for variable valve timing, intake port designs for variable swirl, high pressure injection systems, matching the combustion chamber design with the characteristics of the injection systems.

This discussion is focused on the approaches that can be taken to meet the tail pipe emissions goals by controlling the in-cylinder processes by optimizing the

following parameters: injection Pressure, EGR, injection timing Retard or Advance, and Swirl ratio.

Based on the analysis conducted in this investigation, a directional map has been developed to show the effect of the above operating parameters on the trade-off between engine-out NO_x and soot emissions expressed as BSU. Figure (34) shows the general directions for O.P.E.R.A.S. in order to reduce NO_x and BSU and the resulting penalties. The directions and magnitudes might change depending on the initial conditions. The map shows the iso-EGR lines and the iso-bar lines from which the gain and penalties can be realized.

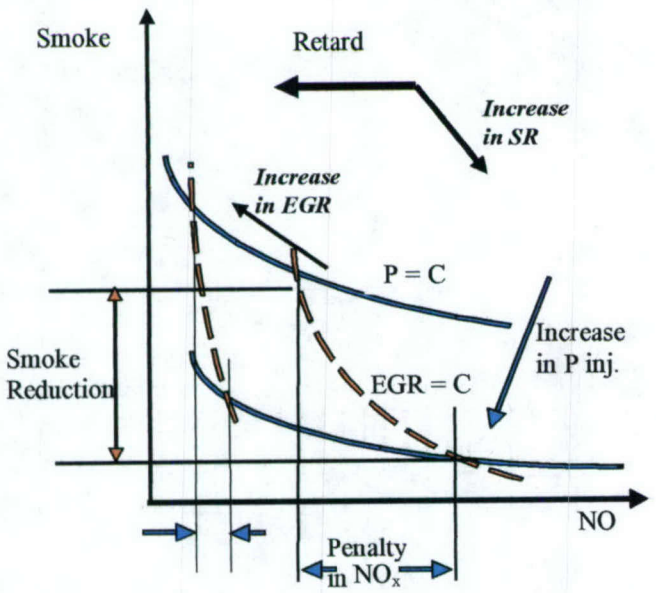

Figure 34 Directional map for the control of engine-out NOx and smoke emissions

It is important to match the engine-out emissions to the needs of the after treatment devices in the feed gas composition. In some cases, in-cylinder processes can achieve these. In other cases, the composition of engine-out gases need to be modified to meet the needs of the after treatment devices. Such Devices include:

(1) Diesel Particulate Filters that require regeneration and might have an impact on fuel economy. In thermal regeneration, the loss in fuel economy is due to fuel consumed in a burner, or in driving the alternator for electric heating. In such a case, the policy would be to reduce the engine-out NO_x by using large amounts of EGR, and burning the soot in the after treatment filter. In this case the demand on NO_x after treatment device is reduced.

(2) Catalytic regeneration that lowers the ignition temperature of the accumulated particulate that burn with oxygen. In such a case EGR would be limited to allow enough oxygen for the oxidation reactions to be completed within the residence time in the filter. Here also, there is a space limit for the filter size, depending on the vehicle.

(3) Catalytic regeneration by oxidation of the PM with NO_2 in the continuously regenerating trap (CRT) (39). Here, the effectiveness of the catalyst in oxidizing the particulates depends on the ratio of engine-out carbon and NO_2.

$$NO_2 + C \longrightarrow NO + CO \qquad (5)$$

There are two avenues for NO_2 formation:

(a) At low space velocity

$$NO + 0.5\,O_2 \longrightarrow NO_2 \qquad (6)$$

(b) At high space velocity

$$2\,NO \longrightarrow NO_2 + CO \qquad (7)$$

Equation 5 shows that the stoichiometric ratio for NO_2 and carbon is 3.83. (40) From Equations 6 and 7 the ratio [NO] / [C] is between 3.83 and 7.66. Recent investigations pointed out to an appropriate ratio that varies between 8:1 and 16:1 (41). This implies that an engine-out emission levels that produce such a ratio would optimize the operation of the engine and after treatment devices as one integrated system.

An illustration of O.P.E.R.A.S. in the experimental engine used in this investigation while running at KP3 is given in Figure 35. The engine is assumed to have a CRT after treatment device. An arbitrary scale is used for NO_x and Carbon, and the zone where the ratio of NO_x to carbon is between 8:1 and 16:1 is identified and referred to as" Optimum Zone for CRT Feed". Based on this figure, there are alternate combinations for O.P.E.R.A.S.

The first strategy is based on limiting EGR to 35%. Here, the choice is for low injection pressure and high swirl or a high injection pressure and low swirl ratio. The following are the different combinations of O.P.E.R.A.S. : (a) Injection pressure (600 bar), combined with a Swirl ratio of 2.7 and LPP at 6°-7° aTDC. This is referred to as [600, 35%, 6°-7° a , 2.7]. (b) [800, 35%, 6°-7° a, 2.7], (c) [1000, 35%, 6°-7° a, 1.55].

B. The second strategy is based on the use of a higher EGR ratio, such as 45%. Here, the choices are limited to a high injection pressure of 1200 bars, and a swirl ratio of 2.7 and an injection retard from 11° bTDC to 3.5° bTDC.

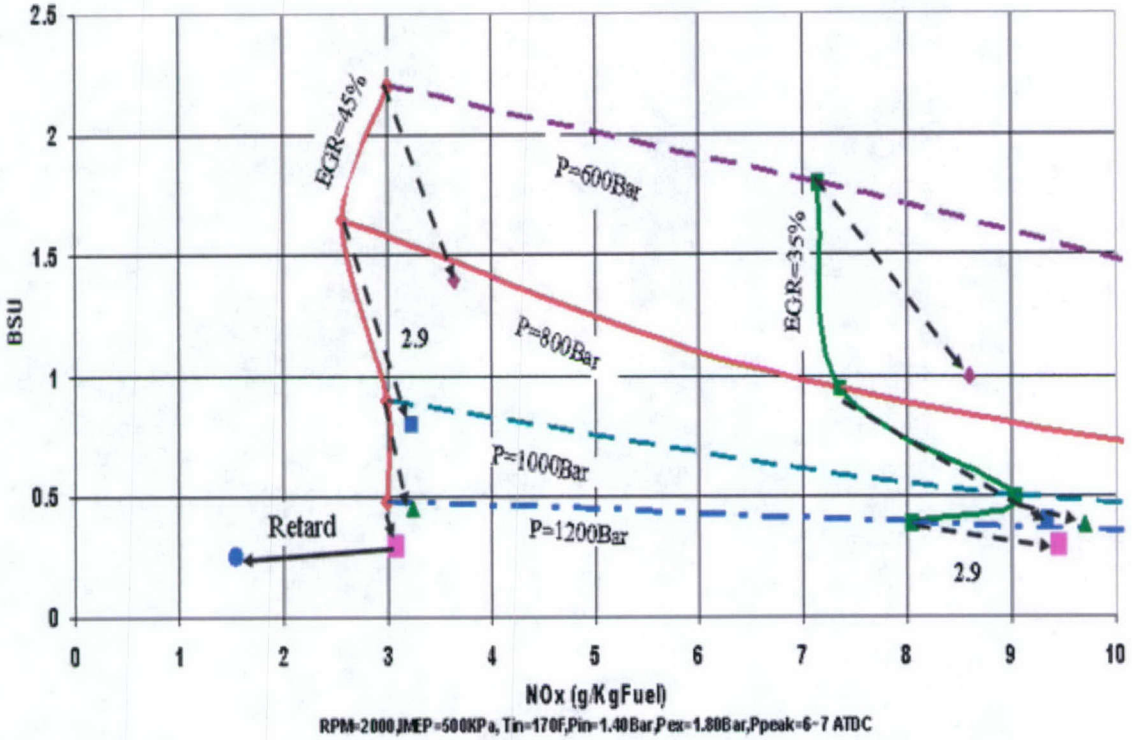

Figure 33. Effect of different operating parameters on the Trade-off between NO_x and BSU, (KP3, 320 mini sac)

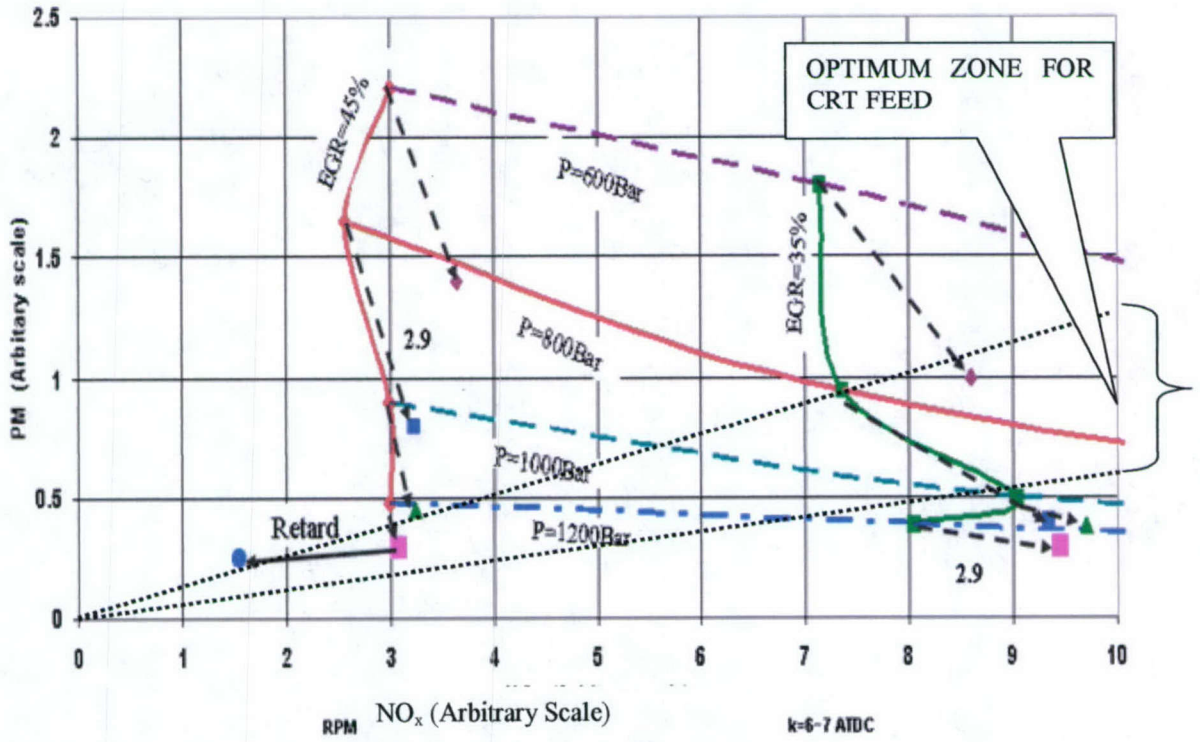

Figure 35. An illustration of O.P.E.R.A.S for an engine fitted with a CRT after treatment device. (KP3, mini sac 320 nozzle)

It should be made clear that the above analysis is just an illustration on how to develop O.P.E.R.A.S. In an actual engine, other factors, such as the exhaust gas temperature plays a major role in the development of the strategy.

In another after treatment device, (SCR), HC is used for the NO reduction reaction. In such a case, late post injection would be appropriate. Also, the amount of post injection can be adjusted to give the proper [HC] / [NO_x] load-dependent ratio.

CONCLUSIONS

These conclusions are based on an investigation conducted on a single-cylinder, small bore, high-speed, direct-injection diesel engine, equipped with a common rail fuel injection system. Tests were conducted under simulated turbocharged conditions at two sets of loads and speeds that represent two major key points in the operation of a medium size HEV. The tests were conducted using two types of nozzles: a VCO and a mini-sac, and covered a wide range of injetion pressures, EGR ratios, injection timings and swirl ratios.

1. A new phenomenal model is developed for the fuel distribution in the chamber of the HSDI engine and its effect on combustion and engine-out emissions, particularly, NO_x and BSU. The model accounts for the fractions of the fuel injected prior to the establishment of the flame, the fresh fuel injected in the flame and the fuel deposited on the walls.
2. New trade-Off maps are developed for each key point to show the interdependency of NOx and BSU on the different operating parameters. The ISO-EGR and ISO-BAR lines plotted on the maps can identify the different strategies needed to achieve a certain engine-out emissions goal.
3. Increasing EGR ratio proved to be a very effective strategy to progressively reduce NOx. Applying an EGR ratio of 45% reduced NO_x EI by 96% at the two key points. However, BSU increased at a rate that is slow at low EGR ratios, but accelerates at EGR ratios above 35%.
4. Increasing the injection pressure is a very effective strategy to reduce BSU at all EGR ratios. The resulting penalty in NO_x decreases at the higher EGR ratios and disappears at 45% EGR.
5. Increasing the swirl ratio is effective in reducing BSU at all injection pressures and EGR ratios. The resulting penalty in NO_x, depends on the combinations of injection pressure and EGR ratios used.
6. Advancing the pilot injection timing improved fuel economy to a point beyond which it had an opposite effect, had a moderate effect on increasing NO_x, and reducing BSU, HC and CO. Retarding the post injection timing had no effect on NO_x, but increased BSU, CO and HC and reduced fuel economy.
7. Control strategies can be developed to integrate between the properties of the engine-out emissions and the needs of the after-treatment devices. To control engine-out emissions, some strategies for the **"O.P.E.R.A.S."** (**O**ptimization of the injection **P**ressure, **E**GR ratio, injection **R**etard or **A**dvance and **S**wirl ratio) are presented.

ACKNOWLEDGEMENT

The U S Department of Energy, Office of Transportation Technologies, Office of Advanced Automotive Technologies, supports this program. This is a part of the PNGV program, conducted under the technical sponsorship of Sandia National Laboratories. The continuous technical support and help of Dr. Paul Miles, in running this program and supplying engine parts and instruments are gratefully acknowledged and appreciated.

Also, the support of the U.S. Army TARDEC, ARO and ARC are acknowledged. The cooperation and help of Lydia Nedeltcheva, Bogdan Nitu, the other members of the Automotive Research Center and the machine shop at Wayne State University are appreciated.

APPENDIX A: ENGINE SPECIFIATIONS

Specification	Units	Description
Combustion System		Direct Injection
Total Piston Displacement	(cm^3)	421.932
Working Cycle		Four-stroke Diesel
Bore	(mm)	79.5
Stroke	(mm)	85
Direction of Rotation		Counterclockwise
No. Of Cylinders		1
Rated Speed (max)	(rev/min)	4000
Compression Ratio		20:1
Valve System		2 IN./ 2Exh
Combustion Chamber		Bowl-in-piston sign, Flat head, Central located Nozzle
Cooling System		External Water Pump
Lubricating System		External Oil Pump
Injection system		Bosch Common Rail (Max. Pressure 1350 Bars)
Injection Controller		Fiat CPU controller
Connecting Rod Length	(mm)	179
Varying Swirling Ratio		1.5 to 3.5

APPENDIX B: SWIRL RATIOS VERSUS GATE-VALVE POSITION

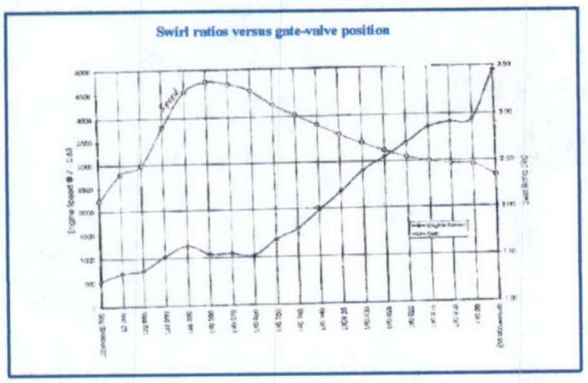

APPENDIX C:TESTS MATRIX

Nozzles : 430 VCO, 390 Mini-Sac, 320 Mini-Sac

Test Points:	RPM	IMEP(Bar)	MAP(Bar)
KP1	900	1.2	1.0
KP2	1500	3.0	1.2
KP3	2000	5.0	1.4

Injection Pressures: 400, 600, 800, 1000, 1200 Bar

Injection Modes: Main, Pilot-Main, Main-Post

EGR ratios: 0%, 25%, 35%, 40%, 45%, 50%, 55%

Swirl Ratios: 1.5 – 3.00

APPENDIX D: Spray correlations

Correlations developed for spray penetration X, agree on the following format:

$$X = (\Delta P)^a (\rho_F)^b (\sigma_F)^g (\rho a)^c (d)^e (t)^m$$

where
(ΔP): pressure drop across the nozzle hole
ρ_F : fuel density
σ_F : fuel surface tension
ρa: air density
d : diameter of the nozzle hole
t : time
a = 0.25 to 0.6, b = 0.25 to 0.65 ,
c = -0.5 to - 0.25, e = 0.18 to 0.82,
g = -0.20 to - 0.30, m = 0.48 to 0.64.

REFERENCES

1. Krieger, R. B., Siewert, R. M., Pinson, J. A., Nicholas, E., Gallopoulos, 1997, "Diesel Engine: One Option to Power Future Personal Transportation Vehicle " SAE 972683.
2. Needham, J. R., and Whelan, S., 1994, "Meeting the Challenge of Low emissions and Fuel Economy with the Ricardo 4-Vlave high-Speed Direct Injection Engine," J. Automobile, Engineering, Vol. 208, pp. 181-190.
3. Nehmer, D. A. and Reitz, R. D., 1994, "Measurement of the Effect of Injection Rate and Split Injections on Diesel Engine Soot and NOx Emissions," SAE 940668.
4. Pierpont, D. A. and Reitz, R. D. , 1995, "Effects of Injection Pressure and Nozzle Geometry on DI Diesel Emissions and Performance" SAE 950604.
5. Montgomery, D. T. and Reitz, R. D., 1996, "Six-Model Evaluation of the Effect of EGR and multiple Injections on Particulate and NOx Emissions from a D. I. Diesel Engine," SAE 960316.
6. Shundoh, S., Kakegawa, T., Tsuiimura, K., 1991, "The Effect of Injection Parameters and Swirl on Diesel Combustion with High Pressure Fuel Injection," SAE 910489.
7. Shundoh, S., Komori, M., Tsujimura, K., and Kobayashi, S., 1992, "NOx Reduction from Diesel Combustion Using Pilot Injection with High Pressure Fuel Injec1ion," SAE No. 920461.
8. Bower, G. R., Foster, D. E., 1993, "The Effect of Split Injection on Fuel Distribution in an Engine-Fed Combustion Chamber," SAE 930864.
9. Needham, J., Doyle, D., and Nicol, A., 1991, "The Low NOx Truck Engine", SAE 910731.
10. Herzog, P. Burgler, L., Winklhofer, E., Zelenka, P., and Cartellieri, W., 1992, "NOx Reduction Strategies for DI Engines", SAE 920470.
11. Dürnhoz, M., Eifler, G. and Endres, H. 1992, "Exhaust Gas Recirculation - a Measure to Reduce Exhaust Emissions of DI Diesel Engines", SAE 920725.
12. Kakegawa, T., Suzuki, T., Tsujimura, K., Shimoda, M., 1988, "A study on combustion of high pressure fuel injection for direct injection diesel engine," SAE 880422.
13. Shimada, T., Shoji, T., and Takeda, Y., 1989, "Effect of Fuel Injection Pressure on Diesel Engine Performance", SAE 891919.
14. Miles, P., 2000, "The Influence of Swirl on HSDI Diesel Combustion at Moderate Speed and Load, SAE 2000- 01-1829.
15. Henein, N. A., Lai, M.-C., Wang, D., Liu, L. and Miles, P., 2000 "Combustion and Emission Characteristics of a Single-Cylinder HSDI Diesel Engine," Proceedings of the 2000 Technical Meeting of Central State Combustion Institute, pp. 157-162, Indianapolis, April 16-18, 2000.
16. Henein, N. A., Lai, M-C., Singh, I., Wang, D., and Lui, L., "Emission Trade-Off and Combustion Characteristics of a High-Speed Direct Injection Diesel Engine," SAE paper 2001-01-097, SP-1592, 2001.
17. Heywood, J. B., " Internal Combustion Engine Fundamentals", McGraw-Hill Inc., 1988.
18. Henein, N, A.," Combustion and Emission Formation in fuel Sprays injected in Swirling Air," SAE 710220, 1971
19. Dec, J.E., " A Conceptual Model of D. I. Diesel Combustion Based on Lase-Shet Imaging," SAE paper 970873, 1997.
20. Dec, J. E., and Espey, C.,"Ignition and Early Soot Formation in a Diesel Engine Using Multiple 2-D Imaging Diagnostics," SAE Transactions, Vol. 104, Sec 3, pp. 853-875, 1995.
21. Dec, J. E. and Coy, E.B.," OH Radical Imaging in a DI Diesel Engine and the Structure of the Early Diffusion Flame," SAE 960831, 1996.
22. Naber, J. D. and Siebers, D. L.," Effect of Gas Density and Vaporization on Penetration and Dispersion of Diesel Sprays," SAE 960034, 1996.
23. Siebers, D. L.," Scaling Liquid-Phase Fuel Penetration in Diesel Sprays Based on Mixing-Limited Vaporization," SAE 1999-01-0528, 1999.
24. Miles,P., Sick,V.,Megerle,K., Richards, K.,Nagel,Z, Reitz,R., "The Evolution of Flow Structures and Turbulence in a Fired Hsdi Diesel Engine", SAE paper 2001-01-3501, 2001.
25. Wang, T. C. Han, J.-S. Xie, X., Lai, M.-C., and Henein, N. A., 1999, "Direct Visualization of High Pressure Diesel Spray and Engine Combustion," SAE 1999-01-3496.
26. Rakopoulos, C.D. and Hountalas, D.T.,"Development and validation of a 3-D multi-zone combustion model for the prediction of a DI diesel engines performance and pollutants emissions", SAE Transactions, Journal of Engines, Vol. 107, pp. 1413-1429, 1998.
27. Henein, N. A., 1976, "Analysis of Pollutant Formation and Control and Fuel Economy in Diesel Engines," Prog. Energy Combust. Sci., Vol. 11, pp. 165-207.
28. N. Ishikawa and K. Niimura," Analysis of diesel spray structure using magnified photography and PIV", SAE paper 960770, 1996.

29. Han, J-S., Lu, P-H, Xie, X-B., Lai, M-C and Henein, N.A.., "Invstigation of Diesel Spray Primary Break-up and Development for Different Nozzle Geometries," SAE 2002-01-2775, 2002.
30. Stumpp, G., and Ricco, M., 1996 "Common Rail – An Attractive Fuel Injection System for Passenger Car DI Diesel Engines", SAE 960870.
31. Boehner W., and Hummel, K., 1997, "Common rail Injection System for Commercial Diesel Vehicles" SAE 970345.
32. Guerrassi N., and Dupraz, P. 1998, "A Common Rail Injection System for High Speed Direct Injection Diesel Engines" SAE 980803.
33. Badami, M., Trucco, G., Nuccio, P., 1999, "Influence of Injection Pressure on the Performance of a DI Diesel Engine with a Common Rail Fuel Injection System, SAE 1999-1-0193.
34. Schommers, J., Duvinage, F., Stotz, M., Peters, A., Ellwanger, S., Koyanagi K., and Gildein, H., 2000, " Potential of Common Rail Injection System for Passenger Car DI Diesel Engine" SAE 2000-01-0944.
35. Henein, N.A.,Lai, M.C., Singh,I.P.,Zhong, L., Han,J.," Characteristics of a common-rail diesel injection system under pilot and post-injection modes", SAE paper 2002-01-0218, 2002.
36. Plee, S.L., Ahmad, T. and Myers, J.P. 1981, "Flame Temperature Correlation for the Effects of Exhaust Gas Recirculation on Diesel Particulate and NOx Emissions", SAE 811195.
37. Richards,K.,J., Subramaniam,M.N., Reitz,R.D., Lai,M-C., Henein N.A., Miles,P.C.," Modeling The Effects Of EGR And Injection Pressure On Emissions In A High- Speed Direct-Injection Diesel Engine", SAE Paper 2001-01-1004, 2001
38. Hotta,Y., Nakakita, K., Fuyuto,T. Inayoshi,M., Fujiwara, K., and Sakata, I., "Cause Of Exhaust Smoke And Its Reduction Methods In An HSDI Diesel Engine Under High-Speed And High-Load Conditions", SAE Paper 2002-01-1160, 2002.
39. Cooper,B.J.,Thoss,J.E." Role Of NO In Diesel Particulate Emission Control ", SAE Paper 890404, 1989.
40. Zelenka P., Michael P., Wolfgang C. "Ways to meet future emission standards with diesel engine powered sport utility vehicles (SUV)" SAE Paper 2000-01-0181
41. Zelenka,P., Egert,M., and Cartellieri,W., "Cooled EGR- A Key Technology for Future Efficient HD Diesels", SAE Paper 980190, 1998.

LIST OF SYMBOLS

A, a and b: Constants
ARHR: Apparent Rate of Heat of Release
PPL: Peak Pressure Location
SOI: Start of Injection
EOI: END of Injection
RER: Rate of Energy Release
E_f: Global activation energy for soot formation
EI_CO: Emission Index of CO
EI_HC: Emission Index of HC
EI_NOx: Emission Index of NOx
E_0: Global activation energy for soot oxidation
EVO: Exhaust Valve Opening
F: Fuel delivery
[F]: Fuel vapor concentration
F_{if}: Fresh fuel injected into the flame
F_{pf}: Fuel injected prior to the time when the flame is established in the combustion chamber
F_{pfv}: Fuel injected prior to the flame that evaporated and burned
F_{pfw}: Fuel injected prior to the flame and deposited on the walls
F_t: Fuel injected near the very end of the injection process
K_{O2}: Equilibrium constant for O_2 , which is a function of temperature.
$[O_2]$: Oxygen concentration.
O.P.E.R.A.S: Optimization of injection Pressure, EGR, injection timing Retard or Advance and Swirl.
P: Pressure
R: Universal gas constant
S_f: The rate of soot formation
S_0: The rate of soot oxidation
SR: Swirl Ratio
t: time
T: Local gas temperature
V: Volume of the reacting gases
ω: Engine instantaneous angular velocity

APPENDIX C

2003-01-0699

Effect of Cycle-to-Cycle Variation in the Injection Pressure in a Common Rail Diesel Injection System on Engine Performance

L. Zhong, I. P. Singh, J. Han, M-C. Lai, and N. A. Henein
Wayne State University

W. Bryzik
U.S. Army Tank Automotive Command

ABSTRACT

The performance of the Common Rail diesel injection system (CRS) is investigated experimentally in a single cylinder engine and a test rig to determine the cycle-to-cycle variation in the injection pressure and its effects on the needle opening and rate of fuel delivery. The engine used is a single cylinder, simulated-turbocharged diesel engine. Data for the different injection and performance parameters are collected under steady state conditions for 35 consecutive cycles. Furthermore, a mathematical model has been developed to calculate the instantaneous fuel delivery rate at various injection pressures. The experimental results supported with the model computations indicated the presence of cycle-to-cycle variations in the fuel injection pressure and needle lift. The variations in the peak-cylinder gas pressure, rate of heat release, cylinder gas temperature and IMEP are correlated with the variation in the injection rate. The effect of these variations on NOx emission and soot are also discussed in this paper.

INTRODUCTION

The common rail fuel injection system (CRS) is being used in heavy duty as well as light duty diesel engines. The main difference between this system and the traditional ones is that the fuel pressure generation is completely separated from the fuel metering. Also, the injection process is independent of the engine speed and engine load. This allows more flexibility and accuracy in controlling the different injection parameters (such as multiple injections) and the combustion process in order to meet the performance and emissions goals [2, 6, 7].

The CRS applies a common rail to keep the injection pressure constant and at the same level for all the cylinders. However, many researchers reported a drop in the injection pressure [7, 8, 9, 10] and injection-to-injection variations in the split and post injection [1]. In some studies, it was difficult to realize multiple injection strategy because of dwell time between two consecutive injections [9].

One of the objectives of this paper is to find out the effect of cycle-to-cycle variation in the injection pressure on combustion in the consecutive cycles, and its effect on the engine-out emissions, particularly NOx and soot. A mathematic model is developed to calculate the instantaneous fuel injection rate in consecutive cycles.

The causes of the cycle-to-cycle variations are not within the scope of this paper since they are related to the design characteristics of the system and the control strategies applied to adjust the pressure in the common rail.

COMMON RAIL INJECTION SYSTEM

A detailed description of the common rail fuel system and injector used in the experiment is given in references [1,5]. This system is a first generation system. A schematic diagram of the system installed in Bosch Injection Rate Meter is given in Figure 1. A radial piston pump, separately driven by an electric motor, produces the high injection pressure. A pressure-control valve at the pump exit regulates the pressure. The compressed fuel is stored in a common rail (accumulator), fitted with a pressure limiter valve. A short high-pressure line connects the accumulator to the injector. Injection starts when the Engine Control Unit (ECU) triggers a solenoid valve mounted on the injector. The solenoid opens a ball valve to start fuel injection. To end the injection process the ECU triggers the solenoid to shut the ball valve. The period of injection is controlled by the ECU.

EXPERIMENTAL SETUP AND INSTRUMENTATION

The experimental test rig used in this investigation is a single-cylinder, small-bore, high-speed, direct-injection diesel engine equipped with a CRS. The injector is equipped with a mini-sac nozzle, having six holes; each is 0.131 mm in diameter, and a length of 0.6 mm. The flow rate for the nozzle is 320 cm^3/sec. The experiments covered engine speeds of 1500rpm and 2000rpm; and injection pressures of 600bar, 800bar and 1000bar. A Hi-Tech data acquisition system was used to collect data in consecutive cycles for the fuel pressure, needle lift and cylinder pressure. The detailed specification and running conditions of the engine are given in index A.

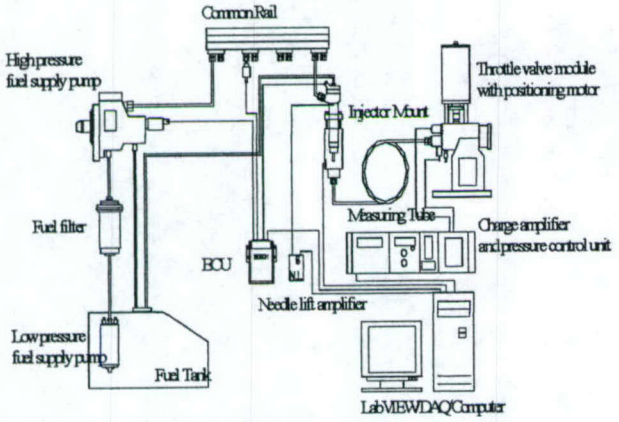

Figure 1. Schematic diagram of the common rail fuel system installed in a Bosch Flow Rate Meter test rig

MATHEMATICAL MODEL FOR THE INSTANTANEOUS FUEL INJECTION RATE

A schematic diagram of fuel flow passages from the high-pressure fuel line to the nozzle tip is given in Figure 2. The instantaneous injection rate can be computed from the difference in the pressures in the mini-sac chamber and the cylinder pressure [13, 15]. The cylinder gas pressure is measured by using a water-cooled quartz crystal pressure transducer. The pressure in the mini-sac chamber varies during the injection process. It is close to the cylinder pressure before the start of injection and after it ends. During injection, the pressure in the mini-sac chamber depends on the net rate of flow into the mini-sac chamber and the flow out of the six holes. Since it is almost impossible to measure the pressure in the mini-sac chamber in a running engine, there is a need to develop a model for its calculation.

The method developed by reference [4] is used in the current work and the following assumptions are made:

1. The fuel flow passages from the pressure sensor to injector nozzle was divided into the following three separate volumes: (a) a high pressure fuel line, (b) the pressure chamber and (c) the mini-sac chamber. The definition of pressure chamber is the volume from the exit of high-pressure fuel line to the middle section of seat passage and the volume from the middle section of the seat passage to the exit of injection nozzle is defined as mini-sac chamber. Each volume has its zero-dimension model.

2. The boundary conditions are the measured fuel pressure in the high-pressure line, the needle lift and the cylinder gas cylinder pressure.

3. The pressure drop in the fuel line between the transducer and the inlet to the injector due friction and speed head loss is small so it can be neglected. However, there is a phase shift of 0.2 millisecond between the pressures in the two locations.

4. The fuel flow from the pressure chamber to the control chamber is negligible

CONTINUITY EQUATION IN THE PRESSURE CHAMBER

According to the continuity equation, the equation in the pressure chamber is

$$\frac{dQin}{dt} = \frac{Vp}{E}\frac{dPp}{dt} + \frac{dVp}{dt} + \frac{dQout}{dt} \qquad (1)$$

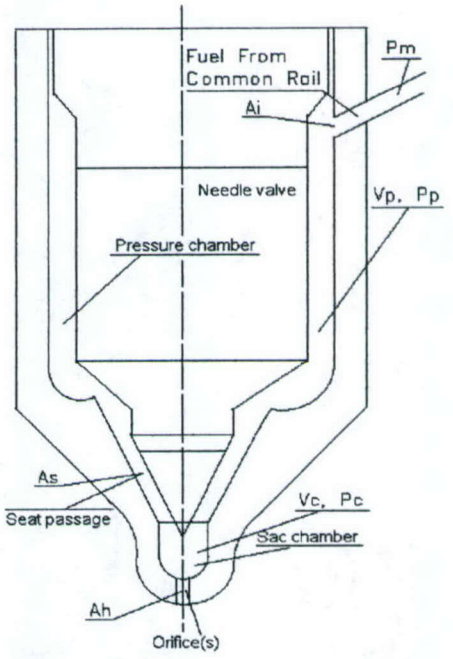

Figure 2 Schematic diagram of fuel flow passages from the high-pressure fuel line to the nozzle tip (Not to scale).

Based on Bernoulli's theory, the volumetric flow rate is

$$\frac{dQ}{dt} = C * A * \sqrt{\frac{2\Delta P}{\rho l}} \qquad (2)$$

The continuity equation in the pressure chamber is written as

$$\frac{dPp}{dt} = \frac{E}{Vp}(Cd * Ai * \sqrt{\frac{2(Pm - Pp)}{\rho l}} - \frac{dVp}{dt} - Cs * As * \sqrt{\frac{2(Pp - Pc)}{\rho l}}) \quad (3)$$

CONTINUITY EQUATION IN THE SAC CHAMBER

The equation of continuity in the sac chamber is in the form

$$\frac{dPc}{dt} = \frac{E}{Vc}(Cs * As * \sqrt{\frac{2(Pp - Pc)}{\rho l}} - \frac{dVc}{dt} - Ch * Ah * \sqrt{\frac{2(Pc - Pa)}{\rho l}}) \quad (4)$$

Since equations (3) and (4) are stiff ordinary differential equations, the Treanor method was applied to solve these two equations. Figure 3 shows a sample of the simulation results for the pressure in the pressure chamber and in the mini-sac chamber. The input to the program was the measured fuel pressure upstream of the injector. The discharge coefficients were determined by using the formulas in reference [4] and validated by the experimental data from the test rig. The method to calculate the flow area and volume was very similar to reference [4], therefore it wasn't detailed in this paper. Notice the phase shift in the pressure chamber. Also, notice the great difference between the pressure in the mini-sac chamber and the measured pressure upstream of the injector.

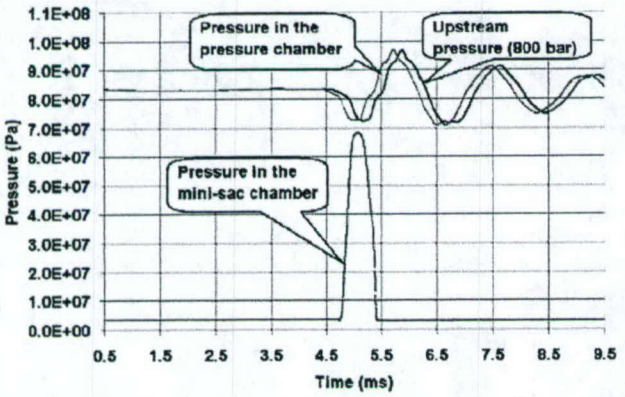

Figure 3 Fuel pressures in the pressure chamber, mini-sac chamber and upstream

VERIFICATION OF MATHEMATIC MODEL

The results of the simulation were compared with the results of experiments conducted on the test rig over a wide range of injection pressures, injection durations, pilot injection and post injection, for a single cycle as well as for several consecutive cycles.

Figures 4 shows a comparison between the results of the simulation and the experimental data for the mass of fuel injected per cycle at three different injection pressures and two injection durations. There is a fair agreement between the two sets of data. Similarly, figure 5 shows a fair agreement between the two sets of data for the instantaneous fuel flow rate over the injection period. It should be mentioned that the oscillations in the measured flow rate after the needle closing is caused by the characteristics of the flow rate meter, which are beyond the scope of this investigation.

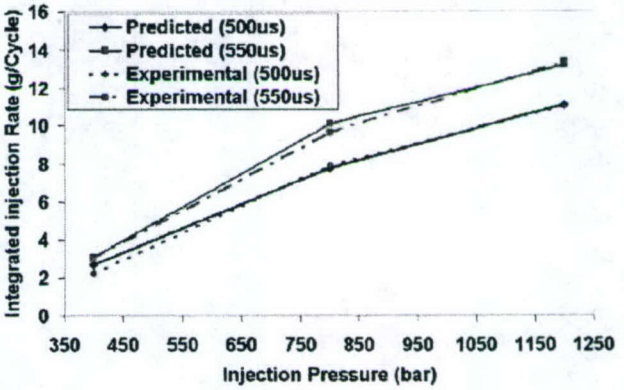

Figure 4 Comparison between calculated and experimental mass of fuel injected.

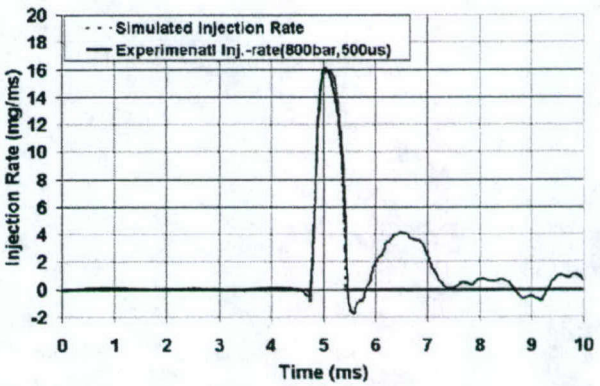

Figure 5 Comparison between simulated and experimental injection rates at 800 bar, 500 us .

Figure 6 shows the agreement between the simulation results and experimental data for pilot and main injection. The injection pressure is 800bar, pilot injection duration is 200us, dwell duration is 1000us and main injection duration is 600us.

Figure 7 shows the agreement between the simulation results and experimental data for the main and post injection. The injection pressure is 800bar, the main injection duration is 390us, the dwell duration is 2778us and the post injection duration is 290us.

The simulation of consecutive cycles indicated the presence of cycle-to-cycle variation in the fuel delivery per cycle. Figure 8 displays the same trend and even shows an agreement between the two sets of data in the frequency of the cyclic variation.

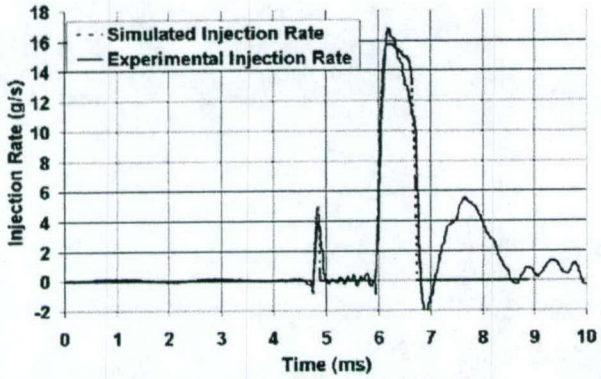

Figure 6 Comparison between injection rates at pilot injection (200us, 1000us, 600us, 800 bar).

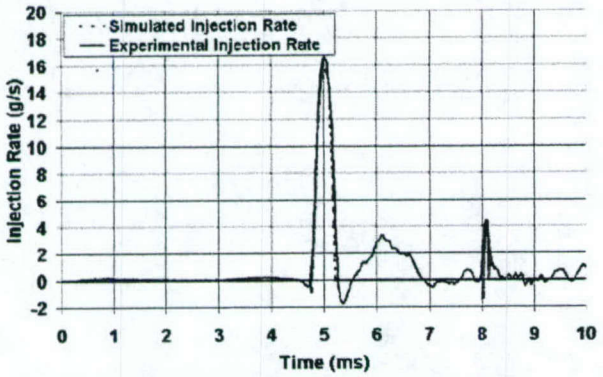

Figure 7 Comparison between injection rates at post injection (390us, 2778us, 290us and 800bar).

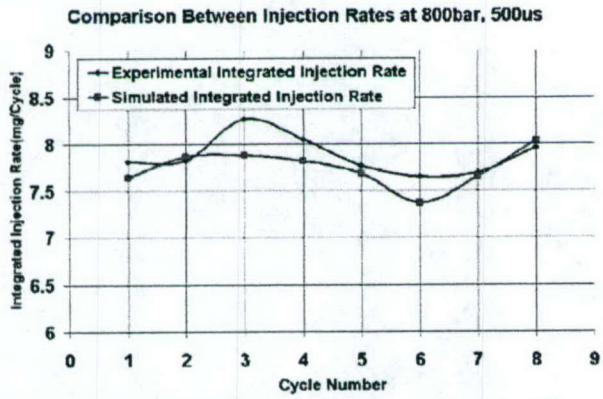

Figure 8 Comparison between simulated and experimental integrated injection rates at 800 bar and 500 us.

The above comparisons between the simulated and experimental data validate the ability of the model in predicting the characteristics of the common rail system. This model will then be utilized to determine the performance of the CRS in the single-cylinder engine. The model will calculate the pressure in the sac chamber, the instantaneous fuel injection rate in consecutive cycles.

CYCLE-TO-CYCLE VARIATION IN FUEL INJECTION AND ITS EFFECT ON ENGINE PERFORMANCE AND EMISSIONS

ANALYSIS OF CYCLE-TO-CYCLE IN THE TEST RIG

Figure 9 shows traces of the fuel pressure measured upstream of the injector for four consecutive cycles. Cycle-to-cycle variations are clear in the pressure waves before the start of injection, during and after the end of injection. The variations occur in both the amplitude and phase shift. The commanded injection pressure in this case is 1000 bar and its duration is 800 μs. The cycle-to-cycle variation in the pressure produced cycle-to-cycle variation in the needle lift, as shown in figure 10. The cycle-to-cycle variation in the integrated injection rate is measured by the Bosch Injection Rate Meter from the test rig, and is shown in Figures 11 and 12. The injection rate varied from 17.92 mg/cycle in cycle number 1 to 15.07 mg/cycle in cycle number 4. This represents a variation of 15.9%.

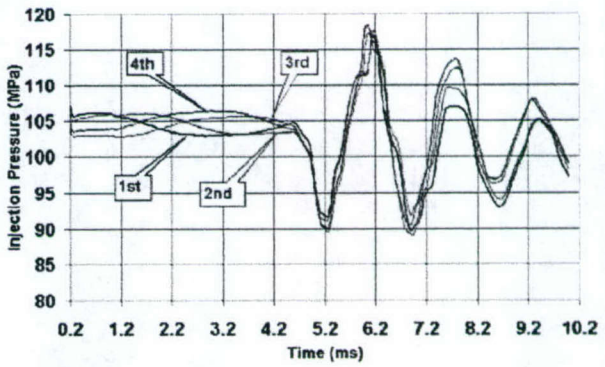

Figure 9 Traces for the injection pressure in four consecutive cycles showing cycle-to-cycle variations. (Test rig data at injection pressure: 1000bar, duration: 800 μs)

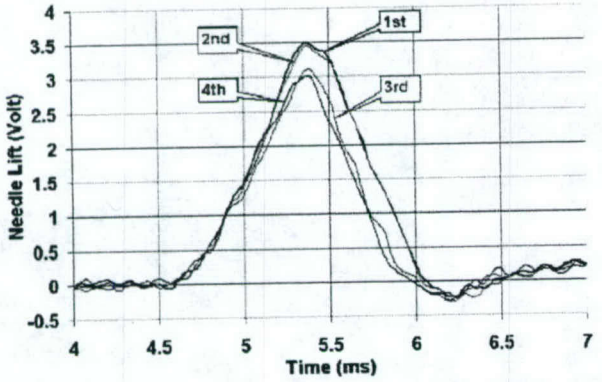

Figure 10 Traces for the needle lift for the four consecutive cycles of Figure 9, showing cycle-to-cycle variations. (Test rig data at Injection pressure: 1000bar, duration: 800 μs)

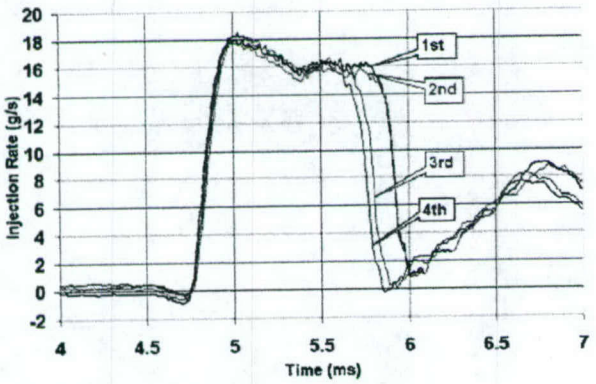

Figure 11 Cycle-to-cycle variations of injection arte at 1000bar measured in the test rig.

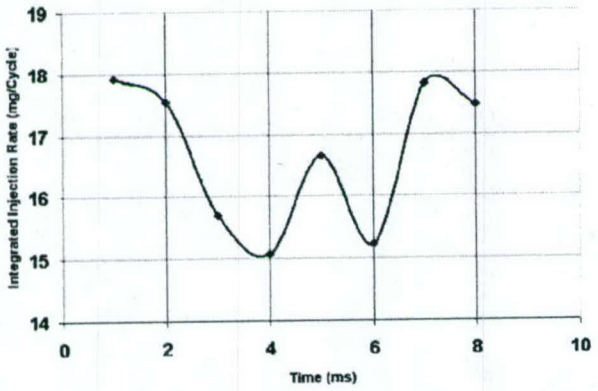

Figure 12 Cycle-to-cycle variations of integrated injection rate at 1000bar measured from test rig

CYCLE-TO-CYCLE ANALYSIS IN A SINGLE-CYLINDER DIESEL RESEARCH ENGINE

The injection system, including the pump, common rail and injector, used in the test rig was used in the single cylinder engine. Figure 13 shows in 3-D plot of the fuel injection pressure measured in 35 consecutive cycles. The engine was running under steady state at 2000 rpm. The command pressure was 1000bar and its duration is 410 μs. The variation in the fuel pressure before the start of injection is shown in table 1 and figure 14. It ranges from 1% to 9%. For the pressure waves after the end of injection, the variation in the amplitude value in each cycle fluctuates from 4.5% (min. valley) to 11.4% or 13% (max. peak) to 22%. Figure 15 shows the cycle-to-cycle variation in the needle lift of typical cycles where the fuel pressure varies from a minimum value of 1010bar to a maximum of 1090bar.

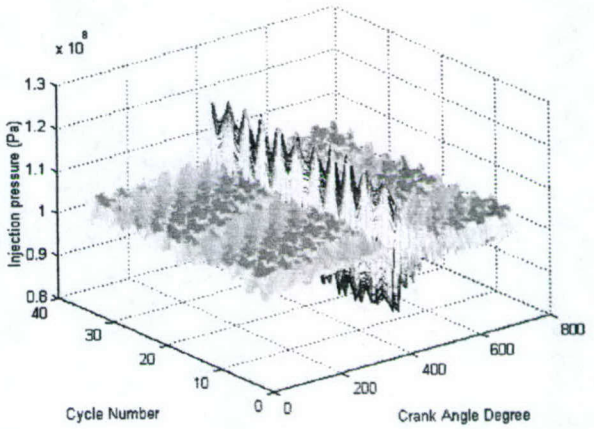

Figure 13 Cycle-to-cycle variations of injection pressure (1000bar)

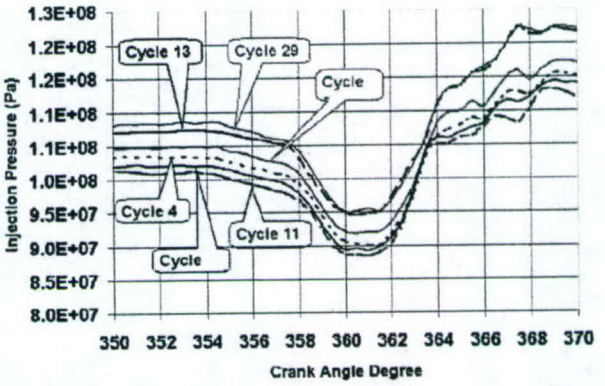

Figure 14 Variations of injection pressure at different cycles (1000 bar)

Increasing the fuel pressure from 1010 bar to 1090 bar caused the needle to reach its maximum opening value. Figure 16 indicates that a pressure of 1050 bar, under the current running conditions, moves the needle to its maximum opening position.

Table 1 Fuel pressure variations (bar)

Cycle		Pmin	Pmax	Paver
11	Value	886	1130	1010
	Deviation	11.4%	13%	1%
29	Value	955	1220	1090
	Deviation	4.5%	22%	9%

The variations in the fuel pressure and the needle valve opening have a great impact on the fuel injection rate. The pressure in the sac chamber and the rate of fuel injection are calculated from the model and the results are given in figures 17&18. The variation of fuel injection rate from cycle to cycle amounts to 23%.

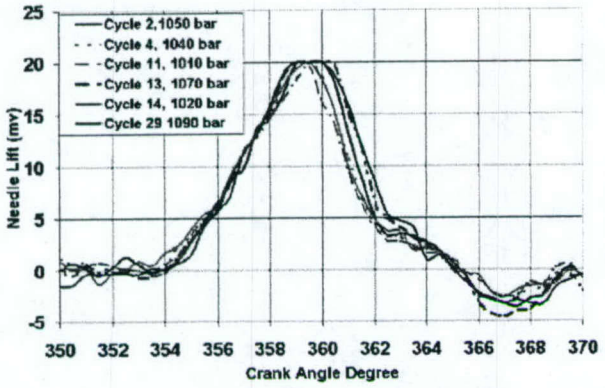

Figure 15 Variations of needle lift at different cycles (1000 bar)

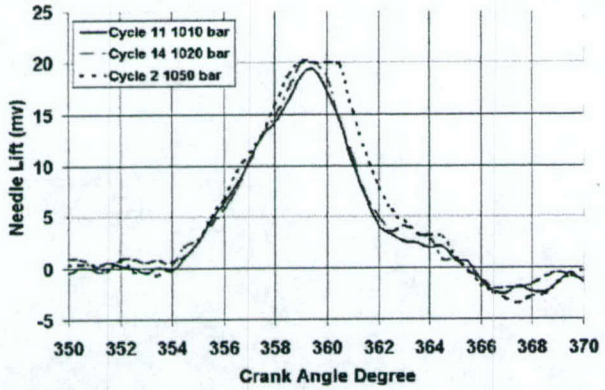

Figure 16 Effect of injection pressure on the needle lift (1000 bar)

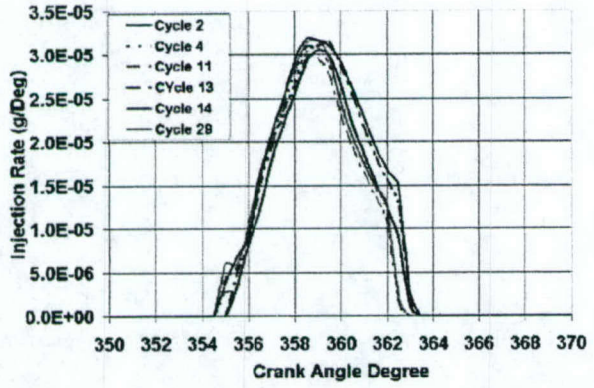

Figure 17 Fuel injection rate at different cycles (1000 bar)

It is clear that the cycle-to-cycle variation in fuel delivery has an effect on combustion and engine-out emissions. Figure 19 shows the indicated mean effective pressure (IMEP) and integrated injection rates (Mf) calculated from rate of heat release of the combustion reactions (RHR), referred to as apparent rate of heat release (ARHR), and the rate of fuel injection computed from the fuel pressure and the mathematical model. It can be noticed that the cycle-to-cycle variation in IMEP follows very closely the cycle-to-cycle variation in the fuel injected. The same pattern has been observed at the other injection pressures covered in this investigation.

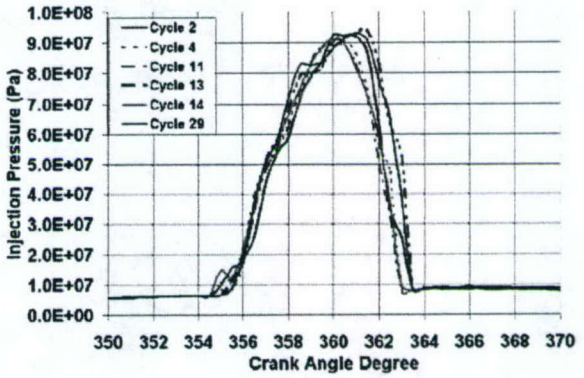

Figure 18 Fuel injection pressure in the sac at different cycles (1000 bar)

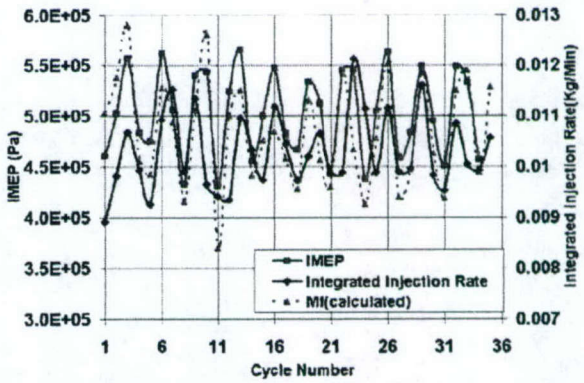

Figure 19 Indicated mean effective pressure (IMEP) and integrated injection rates calculated from rate of heat release and injection pressure &needle lift (1000 bar)

Cycle-by-cycle variations of injection pressure have an impact on the instantaneous engine speed. Figure 20 shows a typical trace for the instantaneous angular velocity of the engine. The velocity drops during the compression stroke and reaches a minimum close to TDC. At the beginning of the expansion stroke the engine accelerates and reaches its maximum velocity at near 385 CAD. Figure 20 shows the engine speeds from cycle 3 to cycle 6 for which the injection pressure traces are shown in figure 21. The peak engine velocity is higher for the cycles with higher injection pressures. The engine speed is governed by an electro-dynamometer and kept constant when motoring.

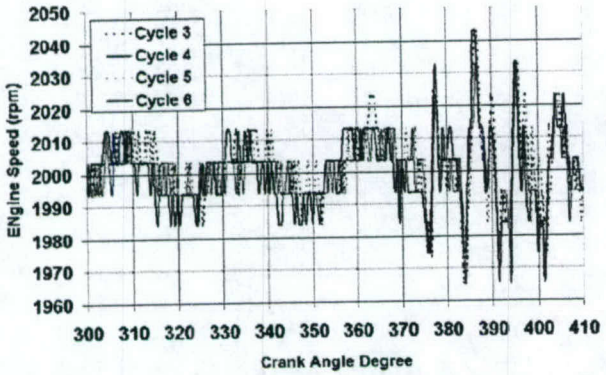

Figure 20 Four consecutive cycles of engine speeds at engine speed 2000 rpm, IMEP=500KPa, injection pressure 1000 bar

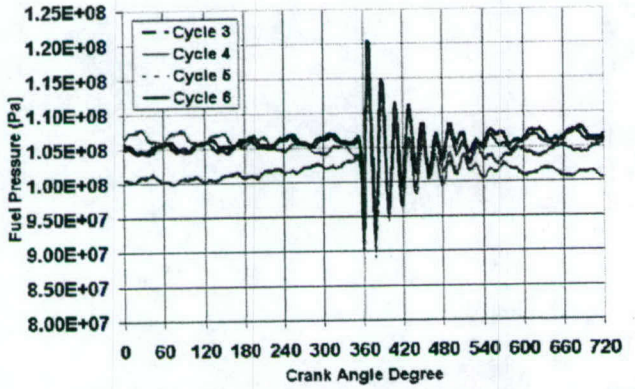

Figure 21 4 consecutive cycles of fuel injection pressure (cycle 3 to cycle 6) at 2000rpm and IMEP=500Kpa (injection pressure 1000 bar)

EFFECT OF CYCLE-TO-CYCLE VARIATION IN INJECTION PRESSURE ON ENGINE-OUT EMISSIONS

The variation of fuel injection rate has significant impact on the combustion process, and in turn on the engine-out emissions. In this analysis we will explain the effect of the cycle-to-cycle variation on NO and soot emissions.

NO formation is very sensitive to the variations in the peak cylinder pressure [11], the peak temperature of the combustion products and residence time [14].

Figure 22 shows the close relationship between the variation frequencies in the injection rate and the peak cylinder pressure for 35 consecutive cycles. Figure 23 shows the pressure traces around TDC for five cycles. The difference between the peak cycle pressures is 6.9 bars. This is an indication of the amount of variation in many combustion parameters, which have a significant influence on the NO formation, such as equivalence ratio [12], cylinder gas temperature [14] and the peak cylinder pressure [11]. Figure 24 shows that the variation in the peak mass average cylinder gas temperature amounts to 190 °C. Figure 25 shows the adiabatic flame temperatures varying with injection pressures. The maximum difference of the peak temperature is 542.6°C. In addition, the residence time of the combustion products increased with the increase in injection pressure or fuel injected. Such difference has a great impact on NO formation [14]. Figure 26 shows the rate of heat release (RHR) for the five cycles. Figure 27 shows the relationship between the heat release of the fuel that burned in the premixed combustion mode and the fuel injection per cycle.

In addition to its effect on NO emissions, the cycle-to-cycle variation in injection pressure can have an impact on engine-out soot concentration. The equivalence ratio increases with the amount of fuel delivery, and the cycles with higher injection pressures are expected to produce more soot in the exhaust gas under the same engine running conditions.

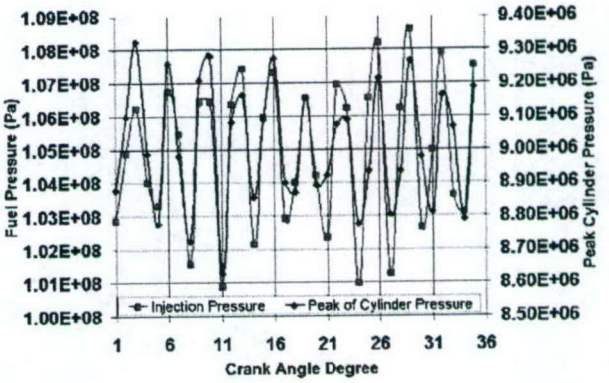

Figure 22 Correlation between injection pressure and peak of cylinder pressure (1000bar)

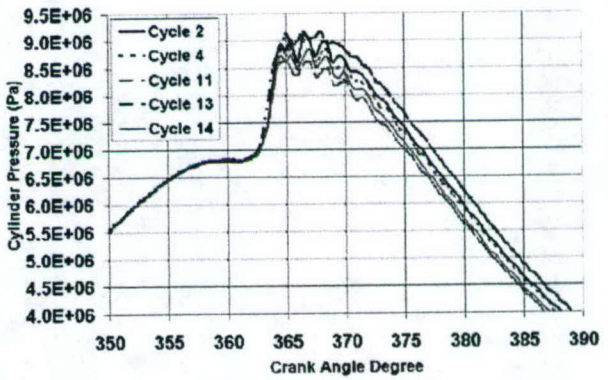

Figure 23 Cylinder pressures at different cycles (1000 bar)

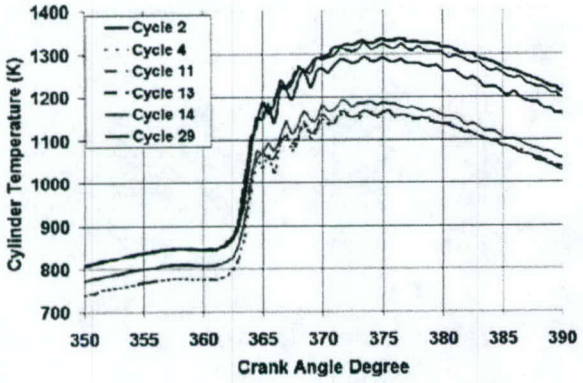

Figure 24 Cylinder temperatures at different cycles (1000 bar)

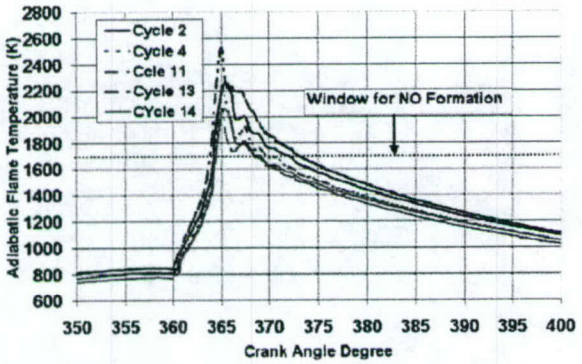

Figure 25 Adiabatic flame temperature at various cycles (1000 bar)

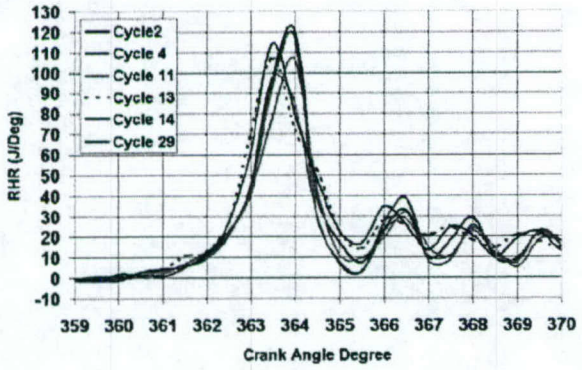

Figure 26 Rate of heat release at various cycles (injection pressure1000bar)

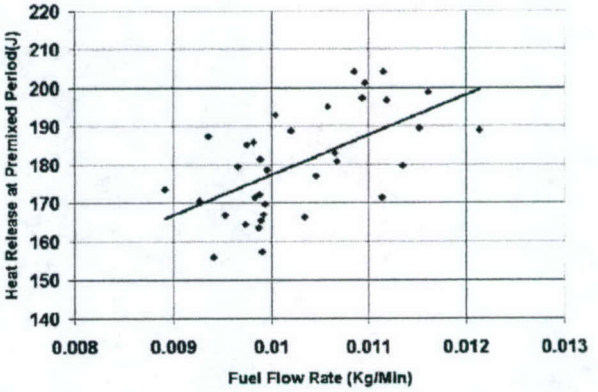

Figure 27 Effect of fuel injection rate on the heat release of fuel burned at premixed combustion mode at identical injection pressure (1000 bar) and injection timing.

CONCLUSIONS

The following conclusions are based on the results of an investigation conducted on a common rail fuel system, using a test rig and a single-cylinder small bore high-speed direct injection research diesel engine. The injector was fitted with a mini-sac nozzle. The engine was run at a load of 5.0 bar IMEP and an engine speed of 2000 rpm.

(1) The results of the simulation model developed in this investigation show a good agreement with experimental data obtained on the test rig. The model can be used to calculate the instantaneous pressure in the mini-sac and fuel delivery under steady and transient engine operating modes.

(2) Cycle-to-cycle variations in the injection pressure at a command pressure of 1000 bar were between 1% and 9%. The resulting variations in the needle lift caused a variation in fuel delivery that reached 23%.

(3) The variations in the fuel delivery were correlated with the corresponding cycle-to-cycle variations in the IMEP and instantaneous angular velocity of the engine.

(4) Theoretical investigations indicated the effect of cycle-to-cycle variations in fuel delivery on the key parameters that control the engine-out NOx and soot emissions. The variations have a negative impact on these emissions since they affect the temperature of the combustion gases, the local equivalence ratio and the residence time in the temperature windows that are critical for NO formation and soot oxidation.

ACKNOWLEDGEMENT

The U S Department of Energy, Office of Transportation Technologies, Office of Advanced Automotive Technologies, support this program. This is a part of the PNGV program, conducted under the technical sponsorship of Sandia National Laboratories. The continuous technical support and help of Dr. Paul Miles, in running this program and supplying engine parts and instruments is gratefully acknowledged and appreciated.

Also, the support of the U.S. Army TARDEC, ARO and ARC is acknowledged. The cooperation and help of Lydia Nedeltcheva, other members of the Center for Automotive Research and the machine shop at Wayne State University is appreciated

LIST OF SYMBOLS

A: Geometrical cross sectional area of the passage
Ah: Total area of orifices of injector nozzle
Ai: Cross-area of fuel inlet
As: Flow area of the seat passage
C: Discharge coefficient
Cd: Discharge coefficient at the inlet of pressure chamber
Ch: Discharge coefficient at orifices of injector nozzle
Cs: Discharge coefficient at the seat passage
$\frac{dPc}{dt}$: Derivative of Pressure Pc
$\frac{dPp}{dt}$: Derivative of pressure Pp
$\frac{dVc}{dt}$: Derivative of volume Vc
$\frac{dVp}{dt}$: Derivative of volume Vp
$\frac{dQin}{dt}$: Fuel flow in the pressure chamber
$\frac{dQout}{dt}$: Fuel flow out of the pressure chamber
E: Bulk modulus of the fuel
Pa: Cylinder pressure
Pc: Fuel pressure in the sac chamber
Pf: Average fuel pressure
Pm: Measured pressure before the inlet of pressure chamber
Pmax: Maximum fuel pressure
Pmin: Minimum fuel pressure
Pp: Fuel pressure in the pressure chamber
Vc: Volume of the sac chamber
Vp: volume of the pressure chamber
ρl : Density of fuel
ΔP : Pressure difference

REFERENCES

1. N.A. Henein, M.C Lai, I.P. Singh,L. Zhong, J. Han,"Characteristics of A Common Rail Diesel Injection System Under Pilot and Post Injection Modes", SAE paper No. 2002-01-0218, 2002
2. T.Fujimura, T.Konomi,"Development of the Toyota 1CD-FTV-type diesel engine with Common-Rail system", SAE paper No.12-01-1999, 1999
3. "Diesel-engine Management", 2nd edition, Robert Bosch GmbH, 1999
4. Min XU, Keiya Nishida, Hiroyuki Hiroyasu," A Practical Calculation Method for Injection Pressure and Spray Penetration in Diesel Engines", SAE paper No. 920624, 1992
5. N.A.Henein, M.C.Lai, I.Singh, D.H.Wang, L.Liu, "Emission trade-off and combustion characteristics of a high-speed direct injection diesel engine", SAE paper No. 2001-01-0197, 2001
6. Noboru Uchida,Kiyohiro Shimokawa,Yugo Kudo and Masatoshi Shimoda,"Combustion Optimization By Means of Common Rail Injection System for Heavy-Duty Diesel engines", SAE paper No. 982679, 1998
7. José M Desantes,Jean Arrègle and Pablo J. Rodríguez," Computational Model for Simulation of Diesel Injection Systems", SAE paper No. 1999-01-0915, 1999
8. Ficarella, D. Laforgia and V. Landriscina,"Evaluation of Instabiblty Phenomena in a Common Rail Injection System for High Speed Diesel Engines", SAE paper No.1999-01-0192, 1999
9. G.M. Bianchi,S.Falfari,P. Pelloni, F.Filicori and M. Milani," A Numerical and Experimental Study Towards Possible Improvement of Common Rail Injectors", SAE paper No. 2002-01-0500, 2002
10. G.M. Bianchi,S.Falfari,P. Pelloni, Song-Chang Kong and R.D. Reitz," Numberical Analysis of High-pressure Fast-Response Common Rail Injector Dynamics", SAE paper No. 2002-01-0213, 2002
11. J.K Ball,C.R. Stone and N Collongs, "Cycle-by-cycle Modeling of NO Formation and Comparison with Experimental Data" ,Proc. Instn Mech Engrs Vol 213 part D,page 175~189, 1999
12. G.H. Abd Alla,H.A. Soliman and M.F. Abd Rabbo,"Effect of Operating Conditions on the NOx Emissions from an Indirect-Injection Diesel Engine Fueled with Gaseous Fuel",SAE paper 2000-01-2790, 2000
13. D.N. Assanis, Z.S. Filipi, S.B. Fiveland and M. Syrimis, " A methodology for cycle-by-cycle transient heat release analysis in a turbocharged direct injection diesel engine", SAE paper 2000-01-1185, 2000.
14. N. A. Henein, I.P. Singh, L. Zhong, M-C. Lai, W. Bryzik, "New Integrated "O.P.E.R.A.S." Strategies for Low Emissions in HSDI Diesel Engines ", SAE Paper 2003-01-0261, 2003
15. I. Koizumi, N. Gyakushi, Y. Takamoto, " Study on the cycle-by-cycle variation in diesel engines", JSME Journal, Vol. 20, No. 145-14, 1977.

APPENDIX A

The tests covered conditions shown in table 2. For all tests, the injection timing was adjusted to ensure that the cycle peak cylinder pressure is located between 6 and 7 crank angle degree after TDC.

Table 2 Test conditions for engine

Specifications	Units		
Engine speed	rpm	1500	2000
IMEP	KPa	300	500
Intake pressure	Bar	1.2	1.4
Exhaust pressure	Bar	1.5	1.8
Intake temperature	°F	170	170
Coolant temperature	°F	180	180
Oil temperature	°F	140	140

Table 3 Specifications of the engine

Specifications	Units	Description
Combustion system	units	Direct injection
Total piston displacement	Cm^3	421.932
Working cycle		4-stroke
Bore	mm	79.5
Stroke	mm	85
Direction of rotation		Counterclockwise
No. of cylinder		1
Rated speed (max)	rpm	4000
Compression ratio		20:1
Valve system		2 In./ 2 Exh.
Cooling system		External water pump
Lubricating system		External oil pump
Injection system		Bosch common rail (Max. injection pressure 1350bar)
Length of connecting rod	mm	179
Swirl ratio		1.5 to 3.5

2004-01-0931

APPENDIX D

Effect of Smoothing the Pressure Trace on the Interpretation of Experimental Data for Combustion in Diesel Engines

Lurun Zhong and N.A. Henein
Wayne State University

W. Bryzik
U.S. Army Tank Automotive Command

Abstract

The disturbances in the cylinder gas pressure trace caused by combustion in internal combustion engines have an impact on the shape of the rate of heat (energy) release (RHR). It is necessary to smooth the pressure trace before carrying out the RHR calculations and making any interpretations for the combustion process. Different smoothing methods are analyzed and their features compared. Furthermore, the selection of the smoothing starting point and its effect on the smoothing quality of pressure data are described. The Fast Fourier Transform (FFT) analysis is applied to determine the frequency of the disturbances in power spectrum and obtain the optimal specified smoothing parameter (SSP). The experimental data was obtained on a single-cylinder research diesel engine, running under simulated turbocharged steady state conditions. The experiments covered a wide range of engine operating parameters such as injection pressures, injection timing, and EGR ratios. The spline function was found to be the most effective method for smoothing both the steady state pressure trace and the transient state pressure trace.

INTRODUCTION

The increasingly stringent regulations aimed at reducing the particulate matter (PM), NOx ,CO and HC emissions and the drive to improve fuel economy in DI diesel engines have been the force behind the efforts to improve the combustion process. This can be achieved by many measures, including applying high injection pressures by using advanced fuel injection systems, precisely controlling the injection timing and mode by using advanced electronic devices, utilizing EGR and increasing turbulence by the swirl and squish motions. All of these parameters affect the combustion process and the rate of burning as indicated from the rate of heat release (RHR) traces [1,13,15,18,22].

The rate of heat release is computed from the cylinder pressure measured by a quartz crystal pressure transducer. Pressure waves caused by fuel injection or the rapid rate of premixed combustion are measured by the transducer and can cause errors in computing the rate of heat release. To reduce such errors, many researchers [3,5,9~12] suggested averaging many cycles. Such averaging can only remove the random noise in pressure trace. It cannot eliminate the systematic errors. Also, averaging many cycles is not suitable when the engine runs under transient operating modes. Other smoothing methods have been used. References [3,4,9~12] applied the 3-point, 5-point and 7-point polynomial least-square smoothing algorithms to smooth cylinder pressure traces. In order to get further reduction in noise, reference [3] used overlapped-smoothing routine by combining 7-point third-order polynomial least-square algorithm. Harndorf et al [6] adopted "weighted smoothing" method to smooth pressure trace to low systematic error. Miles [1] applied digital filter to smooth pressure trace.

In this paper, the power spectrum is applied to analyze the characteristics of pressure waves at various running conditions. The different smoothing methods such as digital filter, least square polynomial approximation (LPA) and Spline function, are introduced, compared, and their features discussed. Then, the effect of the point in the pressure trace at which the smoothing starts is explained. The smoothing by the Spline function is described. This will be followed by a discussion of the effects of injection pressures and EGR on the pressure trace disturbances. Finally the Spline function is applied to smooth the pressure traces under steady state and on cycle-to-cycle basis.

EXPERIMENTAL SETUP AND INSTRUMENTATION

The experimental test rig used in this investigation is a single-cylinder, small-bore, high-speed, direct-injection diesel engine equipped with a common rail fuel injection

system (CRS). The injector is equipped with a mini-sac nozzle, having six holes; each is 0.131 mm in diameter, and a length of 0.6 mm. The flow rate for the nozzle is 320 cm^3/sec in thirty seconds with a pressure drop of 100 bars. The experiments covered engine speeds of 1500rpm and 2000rpm; injection pressures of 400 bar, 600bar, 800bar, 1000bar, 1200 bar and 1300 bar; and EGR ratios of 0%, 25%, 35%, 45% and 50%. A Hi-Tech data acquisition system was used to collect the data in consecutive cycles for the fuel pressure, needle lift and cylinder gas pressure. The trigger signal interval, from the encoder installed at the free end of the engine, is 0.5 ° CAD. This means that the calculations over the cycles are made every 0.5 CAD. The detailed specification and running conditions of the engine are given in index A and reference [13].

Figure 1 shows a line sketch of the combustion chamber used in this investigation and the position of cylinder pressure transducer. The pressure transducer used is KISTLER 6061B pressure transducer whose natural frequency is 90 KHz, is flush mounted in the cylinder head without any coating.

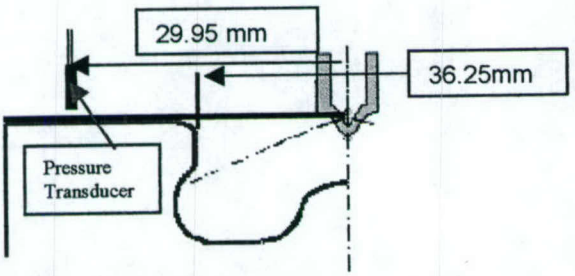

Figure 1. Position of pressure transducer in the cylinder head of the HSDI diesel engine

RATE OF HEAT RELEASE

The first law of thermodynamics is commonly used to calculate the heat release rate [1,3,4,9~16]. The ratio of specific heats is calculated accounting for the change in temperature. The effects of heat transfer and blow-by are partially corrected for by subtracting the corresponding gross rate of heat release for the cycle-averaged motored pressure trace. Because the engine runs at identical conditions when motored and fired, the heat transfer and blow-by losses are expected to be nearly identical, up to the time of significant heat release. The details of the rate of heat release calculations are given in reference [1].

CHARACTERISTICS OF PRESSURE TRACE OSCILLATIONS

THE ORIGIIN OF PRESSURE TRACE OSCILLATIONS

The oscillations in the cylinder gas pressure trace obtained in internal combustion engines can originate from different sources at different frequencies and amplitudes. Some oscillations can be generated from the pressure waves caused by the flow of the fresh charge during the intake stroke. It should be noted here that some oscillations might appear in the pressure trace that can be caused by the closing and opening of the inlet and exhaust valves. These are not caused by changes in cylinder gas pressure, but rather by the oscillations cause by the impact of the valve on its seat.

These pressure waves having different frequencies will be picked up by the pressure transducer and will cause measured cylinder pressure oscillations. As shown in figure 2, at two data acquisition frequencies or resolutions, at engine speed 1500 rpm and under identical motoring pressure wave, the data acquired would be different. The oscillation of pressure trace at lower resolution is less than that at higher resolution.

The oscillations in the rate of heat release are of much higher amplitude than those in the pressure trace, because the RHR is related to the slope rather than the absolute value of the cylinder pressure. This is illustrated in the motoring pressure trace and its rate of heat release, shown in Figure 3. The Frequencies of these oscillations are in low frequency bands (less than 2000Hz for the engine studied), which are close to the natural frequency related to engine speed in pressure traces. These cannot be removed by using various filters.

The oscillations in the pressure trace during the compression stroke are fairly small compared to those originating from the combustion process. This is illustrated in Figure 4 for a single cylinder engine. However, these oscillations in the curve of RHR during the compression stroke can be cancelled mostly by computing the apparent rate of heat release from pressure trace obtained under motored condition as described in reference [1].

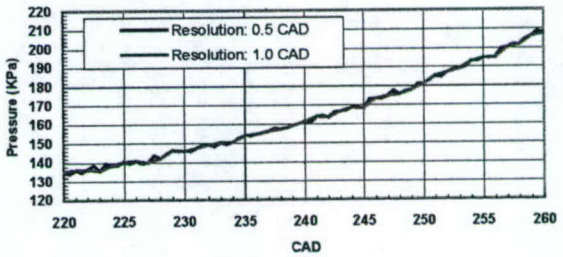

Figure 2. Effect of data acquisition frequencies or resolutions on oscillations of pressure trace acquired

Figure 4 shows the high rate of pressure rise caused by the premixed combustion and its effect on the RHR. The timing, amplitude and frequency of pressure oscillations depend on the location of the pressure transducer, the gas properties, the combustion chamber geometry and the cylinder diameter. For a proper interpretation of the combustion process, it is necessary to remove the oscillations from the pressure trace near TDC at the start of power stroke.

The natural frequency of the pressure oscillations can be roughly given in equation (1) according to the theory of a standing wave in a pipe.

$$fn = \frac{a}{Cl} \qquad (1)$$

Where

fn is natural frequency, a is local acoustic velocity and l is the length of duct, C=4 when one end of the pipe is closed [8, 27], C=2 when two ends are opened [28].

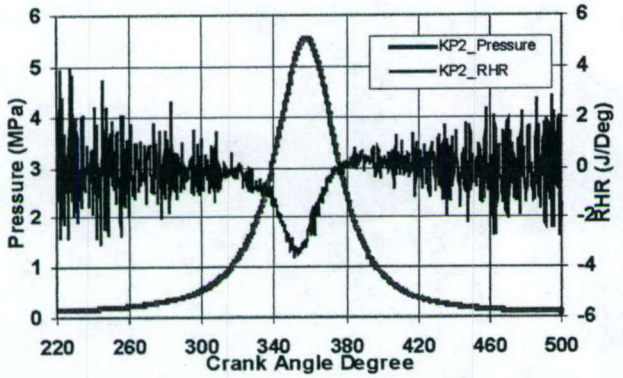

Figure 3. Pressure trace and its RHR at motoring engine speed 1500 rpm

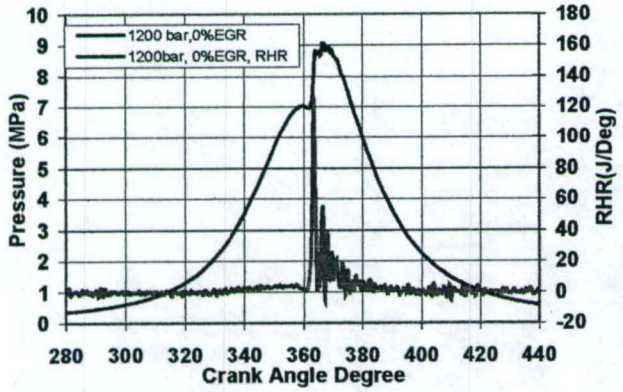

Figure 4. Cylinder pressure and its RHR at engine speed 2000 rpm, 0%EGR, IMEP=500KPa and injection pressure 1200 bar

For small bore engine, when piston is around TDC position, the clearance between piston crown and cylinder head is very small. The clearance can be taken as a duct. So equation (1) is also suitable for calculating natural frequency of pressure wave in cylinder. Here C is a new constant and l is the length from center of piston crown to the pressure transducer.

A BRIEF DESCRIPTION OF POWER SPECTRUM ANALYSIS

The power spectrum analysis is used to analyze the oscillations in the pressure trace in frequency domain by using the MATLAB. Figure 5(a) shows a sample of power spectrum for the pressure traces of 35 consecutive cycles at 2000 rpm (natural frequency is 16.67 Hertz). Theoretically, the power spectrum attenuates exponentially with the increase in frequency and reaches zero at high frequency (here in this study assuming 2000 Hz is a critical frequency between low and high frequencies). However, the existence of pressure waves (more than 2000 Hertz[8]) caused by injection process or premixed combustion will not make the power spectrum tend to zero. Figure 5(b) shows the power spectrum of figure 5(a) at frequency larger than 2000 Hertz.

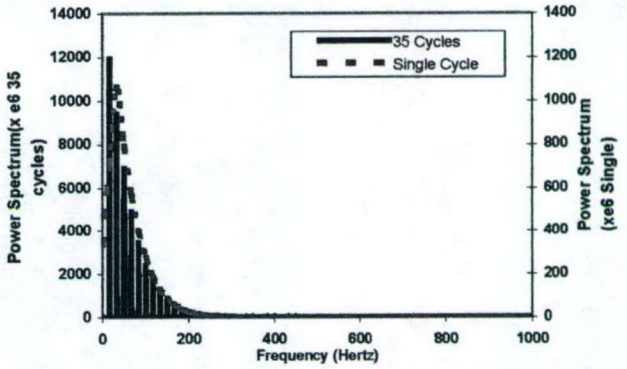

Figure 5(a). Power spectrum of pressure trace at engine speed 2000 rpm, 0%EGR, IMEP 500 KPa and 1200 bar injection pressure

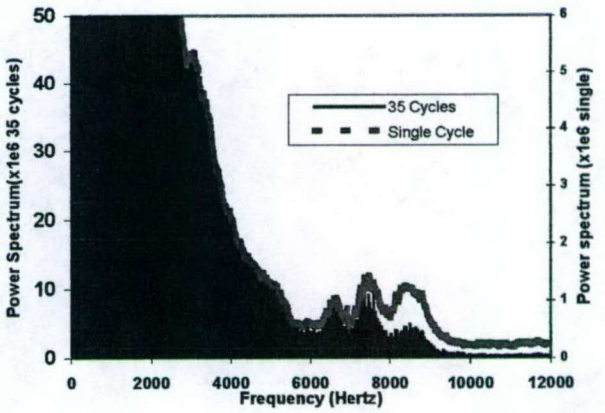

Figure 5(b). Power spectrum of pressure trace at engine speed 2000 rpm, 0%EGR, IMEP 500 KPa and 1200 bar injection pressure

Since the frequencies of the oscillations are distributed in higher frequency domain, the difference in power spectrum distribution at higher frequency domain will be very small while reading multi-cycle data or single-cycle data as input for power spectrum analysis. Figure 5(a) also shows the difference in power spectrum at low frequency and the identical tendency at higher frequency (figure 5(b)) between multi-cycle and single cycle inputs. Because the frequency of pressure wave caused by fuel injection or premixed combustion is in the higher frequency domain, the average of 35 cycles is used as input signal in power spectrum analysis.

Table 1(a) Engine speed 1500 rpm, IMEP 300 KPa, mini-sac 320 injection nozzle

Injection Pressure (bar)	DF1* (Hz)		DF2 (Hz)		DF3(Hz)	
	0%EGR	45%EGR	0%EGR	45%EGR	0%EHR	45%EGR
600	2975.0	2937.5	5900	5800	N/A**	N/A
800	3037.5	3012.5	5937.5	5850	7775	N/A
1000	3087.5	2925	5700	5700	N/A	8650
1200	3012.5	2912.5	5700	5712.5	7712.5	8312.5
1300	3012.5	2987.5	5650	5687.5	7687.5	8325

Table 1(b) Engine speed 2000 rpm, IMEP 500 KPa, mini-sac 320 injection nozzle

Injection Pressure (bar)	DF1* (Hz)		DF2(Hz)		DF3(Hz)	
	0%EGR	45%EGR	0%EGR	45%EGR	0%EHR	45%EGR
600	3000	N/A	5383.33	N/A	N/A	N/A
800	3200	3083.33	6766.66	7650	7666.67	8650
1000	3150	3166.67	7600	7466.67	8516.67	8433.33
1200	3133.67	3083.33	7616.67	7550.	8593.33	8433.33

Table 1(c) Engine speed 1500 rpm, IMEP 300 KPa, VCO 430 injection nozzle***

Injection Pressure (bar)	DF1* (Hz)		DF2(Hz)		DF3(Hz)	
	0%EGR	45%EGR	0%EGR	45%EGR	0%EHR	45%EGR
400	N/A	3037.5	N/A	N/A	N/A	N/A
600	N/A	2962.5	6137.5	N/A	7700	N/A
800	N/A	3025	5412.5	5487.5	7312.5	N/A
1000	3037.5	3050	5487.5	6212.5	7700	N/A

Table 1(d) Engine speed 2000 rpm, IMEP 700 KPa, 0%EGR, Injection pressure 1200 bar, mini-sac 320 injection nozzle

Injection timing (CAD)****	DF1(Hz)	DF2(Hz)	DF3(Hz)
-12.5	3066.67	6933.33	7800
-3.5	3083.33	740	8866.67
2.5	N/A	6766.67	8783.33
4.0	N/A	N/A	N/A

* DF1, DF2 and DF3 mean disturbance frequency 1, 2 and 3

** N/A means the disturbance in power spectrum value is so small that it can be neglected.

*** For the specification of the nozzle see references [15,26]

**** Without specification, the injection timing is determined by fixing the peak of cylinder pressure at 6~7 CAD after TDC

Figures 6(a) and 6(b) show motoring pressure traces and their power spectrum at various engine speeds. Without combustion, the power spectrum of these pressure traces at frequency more than 1000 Hertz tends to zero.

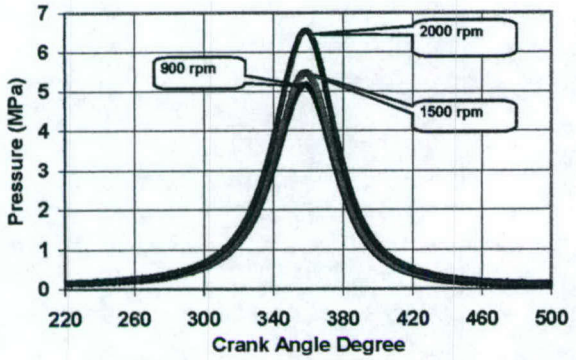

Figure 6(a). Cylinder pressures at various motoring engine speeds

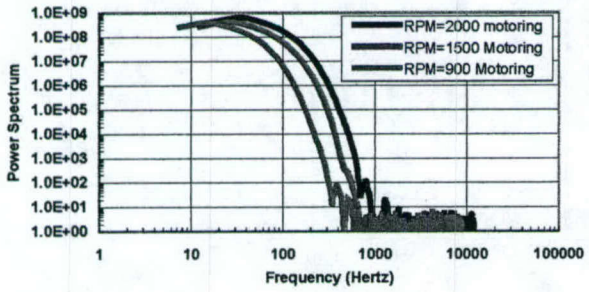

Figure 6(b). Power spectrum of pressure trace of motoring at various engine speeds

FREQUENCY DISTRIBUTION OF THE PRESSURE OSCILLATIONS

The frequency distribution of the pressure oscillations caused by combustion or injection pressure is shown in Table 1(a), (b), (c) and (d) at various running conditions and injection timings.

The frequency (natural frequency) around 3000 hertz doesn't change with engine running conditions and the type of injector nozzle, and it only relates to engine combustion chamber configurations and acoustic velocity, which relates to gas properties i.e. gas temperature and gas density (the composition of gases). The constant C in equation (1) for this engine is 7.50.

Other frequencies in these tables are different at various engine speeds or EGR ratios. These frequencies may be caused by system errors, multiple frequencies of combustion and random noise. The reasons are (a) The pressure trace is only averaged in 35 cycles. Handorf et al [6] suggested that a maximum of 128 cycles had proved to be sufficient. (b) The frequency of the data acquisition system is not high enough to fully pick up the noise caused by combustion flame that has frequencies higher than 4 KHz.

THE EFFECT OF DIFFERENT PARAMETERS ON PRESSURE TRACE OSCILLATIONS

In order to reduce engine-out emissions and improve fuel economy, high injection pressure, injection timing retarding and proper percent of EGR technologies are applied in advanced diesel engines. In this section, the effect of injection pressures, EGR ratios and injection timing on pressure trace oscillations will be discussed.

EFFECT OF INJECTION PRESSURES ON PRESSURE TRACE OSCILLATIONS

Figure 7 shows the cylinder pressure traces averaged for 35 cycles at 1500 rpm, 300Kpa IMEP, 0% EGR and three injection pressures: 400 bar, 800 bar & 1200 bar. Almost the same amount of fuel is injected in the three cases. Notice the increase in the amplitude of the pressure waves at higher injection pressure.

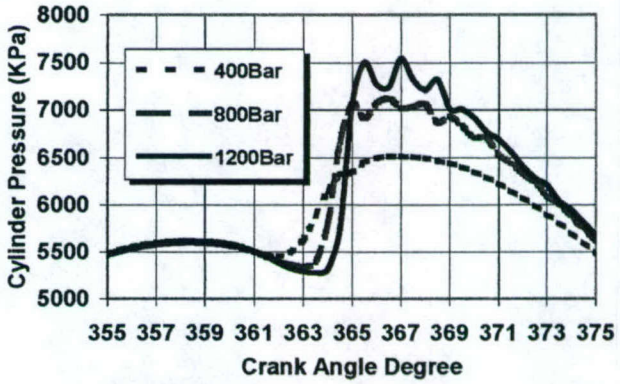

Figure 7. Effect of injection pressures on cylinder pressure trace disturbance at engine speed 1500 rpm, 0% EGR, IMEP 300 KPa

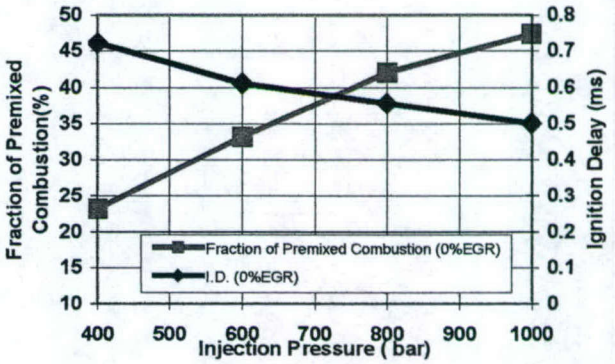

Figure 8. Effect of injection pressure on ignition delay and fraction of premixed combustion at engine speed 1500 rpm, IMEP 300 KPa and 0% EGR

Higher injection pressures increase the premixed combustion due to better atomization and the higher rate of fuel delivery, in spite of its effect on shortening the ignition delay (ID). This is shown in Figure 8 for the engine running at engine speed 1500 rpm, 300 KPa, IMEP and 0%EGR.

In addition to the oscillations caused by the premixed combustion fraction, some oscillation may result from the fuel jet as the fuel moves in the combustion chamber at a high velocity. It is estimated that at an air temperature of 800K and density of 25 Kg/m^3 the pressure wave due to fuel injection propagates at 1000 m/s or so. The pressure transducer should detect this wave at less than 1.0 CAD after the start of injection. When analyzing the power spectrum of pressure trace before combustion starts, however, the authors found that injection pressure has little direct effect on pressure roughness in combustion process shown in figure 9.

EFFECT OF EGR ratios ON PRESSURE TRACE DISTURBANCE

Increasing EGR ratio makes ignition delay longer and more fuel injected will be burned in the premixed combustion period. Figure 10 gives the variations of ignition delay and the fraction of premixed combustion with the increase of EGR ratios.

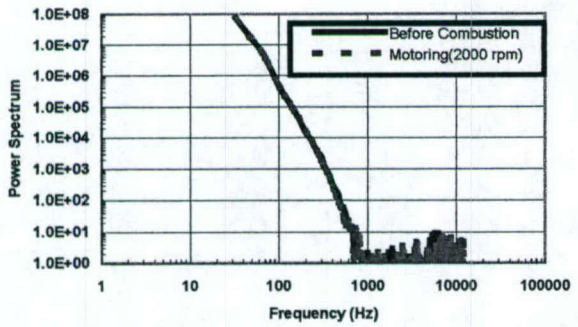

Figure 9. Power spectrum of cylinder pressure at engine speed 2000 rpm, 0% EGR and injection pressure 1200 bar before combustion starts

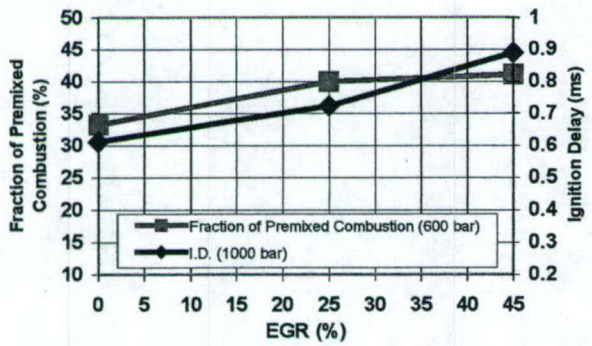

Figure 10. Effect of EGR ratios on ignition delay and fraction of premixed combustion at engine speed 1500 rpm and injection pressure 600 bar

Figure 11 shows the rate of heat release and pressure data at engine speed 1500 rpm, injection pressure 400 bar and 0% & 45% EGR ratios. The peak of RHR is higher at 45% EGR than that at 0% EGR. The oscillation in diffusion period of rate of heat release is bigger at 45% EGR than that at 0%EGR although this oscillation cannot be distinguished in the pressure data.

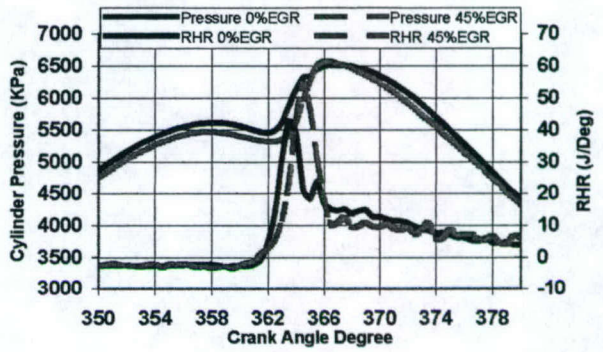

Figure 11. Effect of EGR ratios on pressure trace disturbance at 1500 rpm engine speed and 400 bar injection pressure.

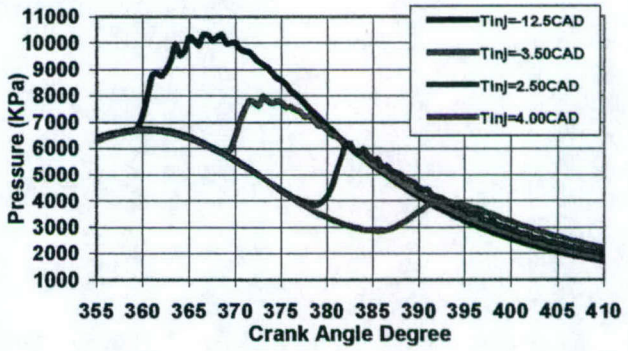

Figure 12. Effect of injection timing on pressure trace disturbance at 2000 rpm engine speed, IMEP 700KPa and 1200 bar injection pressure

EFFECT OF INJECTION TIMING ON PRESSURE TRACE DISTURBANCE

Injection timing has a significant influence on engine performance and emissions, Henein et al[15], Kimura[25], Akihama [23] and Sasaki[24] applied injection timing retarding to reduce NOx and engine noise emissions. The fraction of premixed combustion decreases while the injection timing retarding is reduced. Therefore, the pressure trace disturbance is reduced either. Figure 12 shows the effect of injection timing on pressure trace oscillations at 2000-rpm, IMEP 700KPa, 0%EGR and 1200 bar injection pressure.

NECESSITY FOR SMOOTHING PRESSURE TRACE

As described above, injection pressure, injection timing and EGR ratios have a great effect on the oscillations in the cylinder pressure trace. At higher injection pressure, longer injection timing retarding or higher EGR ratio, this oscillation with identical natural frequency is larger in amplitude. The RHR data shown in figure 4 indicates that the RHR data in diffusion period varies between negative and positive values, which are impractical in the engine. Therefore, it is necessary to smooth the pressure trace before studying the pressure data and analyzing RHR.

METHODS APPLIED IN SMOOTHING PRESSURE TRACE

The cycle-averaged records are digitally used to remove the random noise and the high frequency components associated with acoustic oscillations in the cylinder. However, the pressure trace still need be filtered or smoothed after the premixed burn spike and the early pressure rise because of the effect of pressure waves initiated by combustion flame. Different smoothing methods will be applied to smooth the pressure data in this section and the most suitable method will be determined for smoothing cylinder pressure data in diesel engines.

DIGITAL FILTERS

There are two types of digital filters applied for filtering noise from acquired data, finite impulse response (FIR) and infinite impulse response (IIR). Here a low-pass digital filter is designed to smooth pressure trace according to the performance of data acquisition system and engine speed with MATLAB functions [2], which can handle both FIR and IIR filters. The natural frequencies of the pressure traces at engine speeds 1500 rpm and 2000 rpm are 12.5HZ and 16.67 HZ

There exists phase delay between the smoothed pressure trace and the original one shown in figure 13 since filtering at excessively low frequency may attenuate and phase shift the pressure data [4]. It is well known that the phase in measured pressure data has significant influence on the analysis of combustion and fuel economy. Ullrich et al [5] found that mean indicated pressure (MIP) error lies between 2.5% and 7.5% per degree of crank angle in the TDC adjustment error investigated on two different SI engines. In order to compute the RHR, the smoothed pressure trace must be shifted (here is 1.0 CAD) as shown in figure 13. The difference in phase between original pressure data and smoothed one is dependent on the resolution of crank encoder.

Furthermore, figure 13 shows a significant difference in the slope of pressure trace between shifted pressure trace and original pressure trace, for the period between 363.0 crank angle degree (CAD) to 365.0 CAD. Investigating the power spectrum of the difference of these two pressure traces shown in figure 14, the authors found that part of low frequency signal (less than 200 Hz) in cylinder pressure data was filtered. As will be described in the following sessions, this part is not noise but available signal. The RHR curves are shown in figure 15.

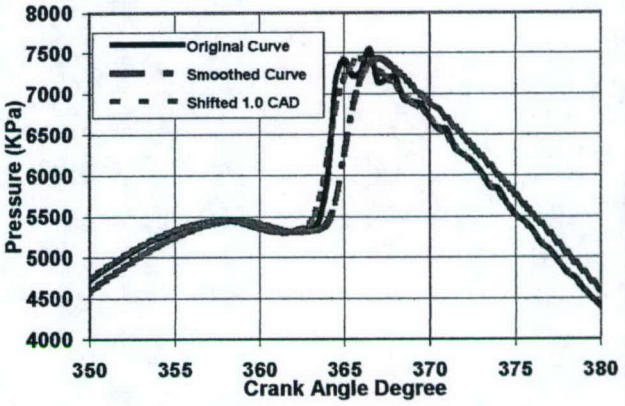

Figure 13. Pressure trace smoothed by digital filter at engine speed 1500 rpm, injection pressure 1200Bar, IMEP 300 KPa and 45%EGR

The peak of RHR is reduced greatly because of the smoothing, which decreases from 135 J/CAD to 87 J/CAD although the oscillation of the curve is cut completely. Furthermore, because of the loss of available low frequency signal, cool flame, ignition delay and diffusion combustion information were changed in the smoothed and shifted curve. Except for these, another disadvantage of digital filter is deformation of the first several points that will effect the selection of starting smoothing point, which will be discussed in later section.

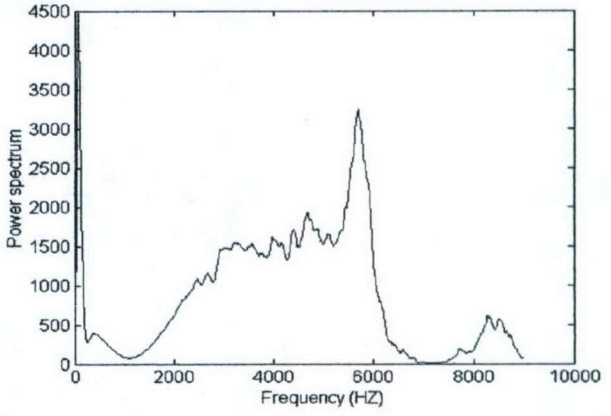

Figure 14. Power spectrum of the pressure data difference at engine speed 1500rpm, 45% EGR and injection pressure 1200 bar.

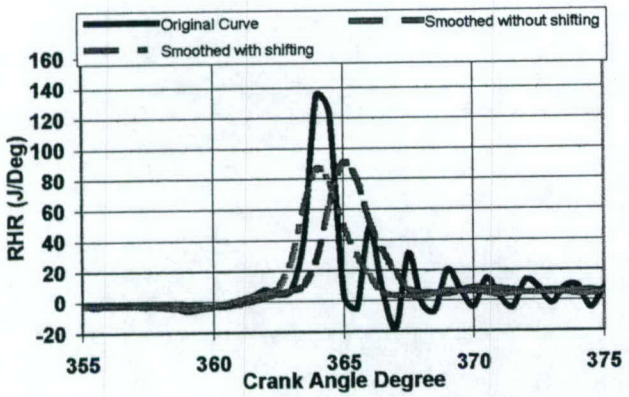

Figure 15. The RHR smoothed by digital filter at engine speed 1500 rpm, injection pressure 1200Bar, 45%EGR and IMEP 300 KPa

LEAST-SQUARES POLYNOMIAL APPROXIMATION (LPA)

Least-square polynomial approximation over a set of points is given by Granino Korn [20]. Here Gram-polynomial approximation was applied to smooth the pressure trace.

Figure 16 shows the pressure traces non-smoothed and smoothed by LPA under engine speed 1500 rpm, 50% EGR, 400Bar injection pressure and their corresponding rates of heat release.

Although after smoothed by LPA, there still exists data oscillation (noise) in pressure trace, the peak of RHR only decreases very little from 135.6 J/CAD to 131.9 J/CAD and the RHR curve becomes smoother.

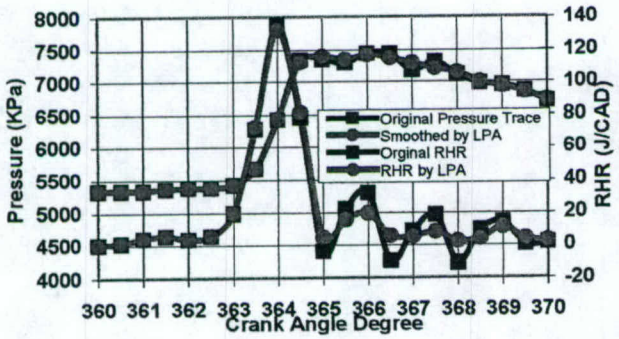

Figure 16. Comparison between non- smoothed and smoothed pressure traces and RHRs

Harndorft et al [7] also applied simple arithmetic smoothing and weighted smoothing methods to smooth the pressure data. As will be explained later in Spline function section, the Spline function in MTALAB possesses all the features of the methods detailed in this section. Therefore, their effect on signal attenuation will be discussed in that section.

SPLINE FUNCTION

Polynomials are the approximating functions of choice when a smooth function is to be approximated locally. For example, the LPA can provide a satisfactory approximation for a function. But if a function is to be approximated on a larger interval, the degree of the approximation polynomial may have to be chosen unacceptably large. The alternative is to subdivide the interval of approximation into sufficiently small intervals so that, on each such interval, a polynomial of relatively low degree can provide a good approximation to the function. This can be done in such a way that the polynomial pieces blend smoothly, i.e., so that the resulting patched or composite function has several continuous derivatives. Any such smooth piecewise polynomial function is called a Spline [19]. There are two commonly used ways to represent a Spline, the piece polynomial form (ppform) and B-form, which have been coded in the form of functions in MATLAB.

Determining the Starting Smoothing Point

Figures 17 and 18 show the difference between the original pressure trace and the smoothed pressure traces at various starting smoothing points using the Spline function and their corresponding RHR. At various starting smoothing points, the pressure and heat release values from 364.0 CAD to 369 CAD are significantly different. Accordingly, the starting point for smoothing has a great effect on the pressure trace oscillations and on the corresponding RHR.

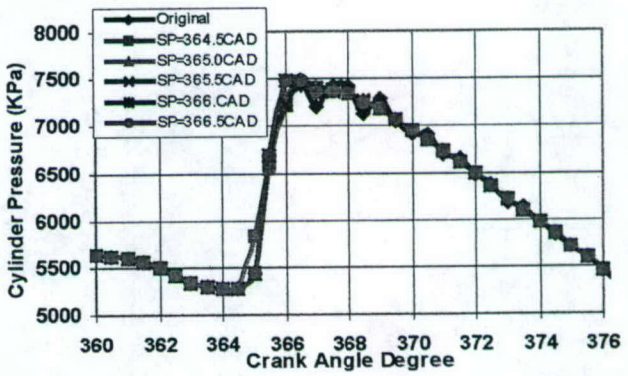

Figure 17. Pressure traces smoothed by Spline function at various starting smoothing points at engine speed 1500rpm, 0% EGR and 1300 bar injection pressure

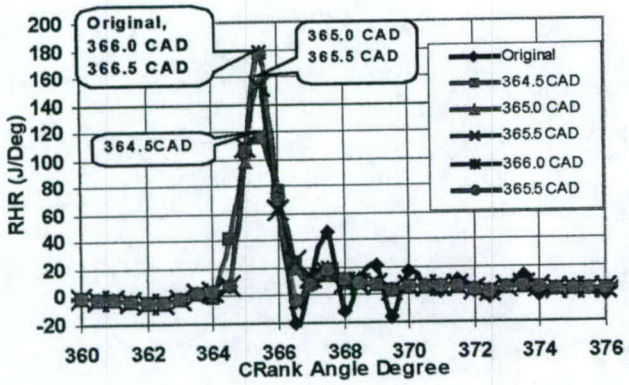

Figure 18. Rates of heat release corresponding to pressure traces in figure 17

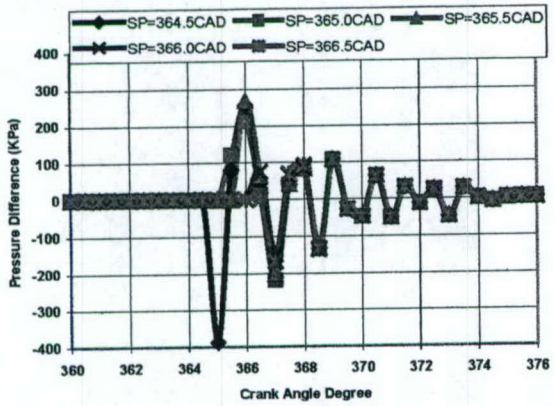

Figure 19.The deviation of smoothed pressure traces from the original pressure trace at engine speed 1500rpm, 0% EGR and 1300 bar injection pressure

Figure 19 shows the deviation of smoothed pressure traces at various smoothing starting points from the original pressure trace. The main differences in these curves are between 364.5CAD to 367.0CAD. However, if we apply power spectrum analysis, this difference becomes very clear as shown in Figure 20(a). As described earlier, the frequencies due to the combustion pressure wave were around 3012.5Hz, 5650 HZ and 7687.5 HZ. All the curves show the identical feature.

When smoothing starts at 364.5 CAD, the slope of pressure trace was changed as shown in figure 17, the values of the power spectrum at the frequencies between 2000 HZ and 5200 HZ are the highest compared to other curves. This indicates that part of useful signal in the pressure trace is removed. Therefore, this point is the not best smoothing starting point. Some noise still remains in the pressure trace when smoothing starts at 366.0 CAD and 366.5 CAD because of their low power spectrum values compared to other curves and the negative value at 366.5 CAD in RHR curves shown in figure 18. Figure 20(b) shows that the oscillation caused by combustion flame was completely removed and there are little losses in the available signal when the smoothing starts at 365.0 CAD and 365.5 CAD. Their RHR curves are shown in figure 21. Accordingly, these two points are the optimal starting smoothing points.

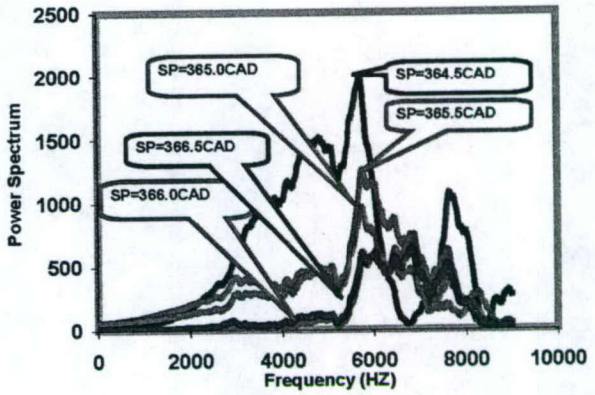

Figure 20(a). The power spectrum of the difference from the original pressure trace to the smoothed one at different starting smoothing points at engine speed 1500rpm, 0% EGR and 1300 bar injection pressure

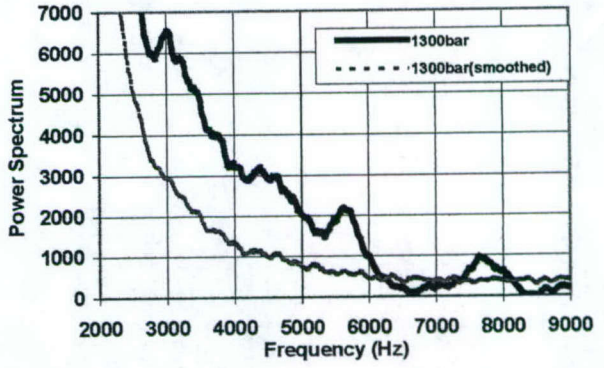

Figure 20(b). Power spectrum of pressure trace at engine speed 1500 rpm, 0%EGR, IMEP 300 KPa and 1300 bar injection pressure

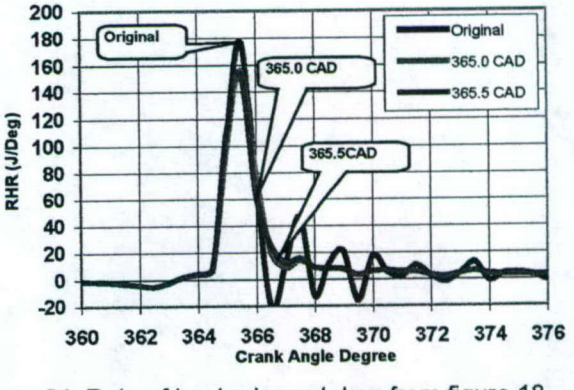

Figure 21. Rate of heat release taken from figure 18

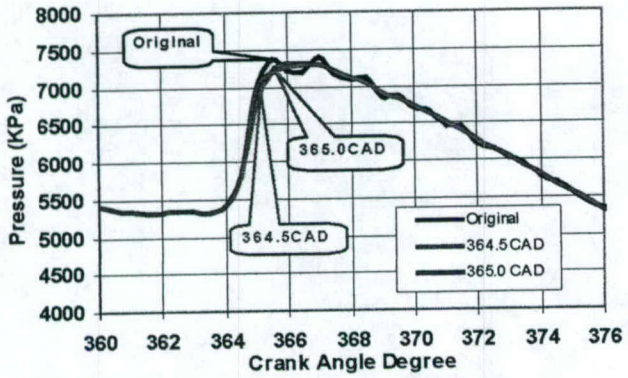

Figure 22(a). Pressure traces smoothed by Spline function at various starting smoothing points at engine speed 1500rpm, 45% EGR and 1300 bar injection pressure

Figure 21 shows the rate of heat release already shown in figure 16. The difference in RHR at starting smoothing points 365.0 CAD and 365.5 CAD is minor and can be neglected. Therefore, the optimal starting smoothing point for the pressure trace is the point locating 0.5 CAD or 1.0 CAD before the rapid raising peak of pressure (RRPOPT) trace at engine speed 1500 rpm.

Relation Between Starting Smoothing Point And Natural Frequency

The first pressure wave picked up by the pressure transducer may have a positive or negative value. However, studying the pressure traces carefully at different running conditions, EGR ratios and injection pressures, the authors found that all the pressure waves start at positive value although their magnitudes are different. Figure 7 gives two typical pressure waves (injection pressure 400 bar and 1200 bar) superposed on the cylinder pressure traces. The RRPOPT is located at or around the positive peak of the pressure wave. As described above, all the frequencies of the pressure waves are larger than the natural frequency, that is, 3 KHz. Therefore, the maximum period of the pressure waves is the natural period in crank angle degree (CAD) given in equation (3)

$$T = 6Ne / fn \qquad (3)$$

Where Ne is engine speed, fn is natural frequency. At engine speed 1500 rpm, T=3.0 CAD and at engine speed 2000 rpm, T=4.0 CAD. The pressure waves are composed of various frequency waves larger than 3 KHz and its period varied from 1.0 CAD to 2.5 CAD shown in figure 19 at engine speed 1500 rpm. Accordingly, it is an effective approach to apply natural period to estimate the starting point of pressure wave superposed on the cylinder pressure trace.

The pressure wave, therefore, may start at T/4 CAD before the RRPOPT and the starting smoothing point (SSPcad) can be given in equation (4):

$$SSPcad = \frac{3Ne}{2fn} \pm Dcad \qquad (4)$$

where Dcad is resolution of data acquisition system or the encoder. $\pm Dcad$ is used only if SSPcad doesn't equal to the multiple of resolutions. Accordingly, the starting smoothing point at engine speed 1500 rpm is 0.75 CAD, that is 0.5 CAD or 1.0 CAD for the resolution is 0.5 CAD and at engine speed 2000 rpm 1.0 CAD before the RRPOPT.

The conclusion was proved at engine speed 1500 rpm, 45%EGR, IMEP 300 KPa and 1300 bar injection pressure shown in figures 22(a), (b), (c) and at engine speed 2000 rpm, 45%EGR, IMEP 500 KPa and 1200 bar injection pressure shown in figures 23 (a), (b) and (c).

Discussion

The Spline function applied in this paper is cubic smoothing Spline. The smoothing Spline minimizes equation (3):

$$P\sum_i w(i)[y(i)-s(x(i))]^2 + (1-P)\int \lambda(t)(D^2 s)(t)^2 dt \qquad (3)$$

Where
w(i) is the optionally specified weight and its default value is 1;$\lambda(t)$ is the piecewise constant weight function in the error measure and its default value is 1;
P is the specified smoothing parameter (SSP) and its value is between 0 and 1. For P=0, s is the least-squares straight line fit to the data, while, on the other extreme, for P=1, s is the natural cubic Spline interpolation. Therefore LPA method and weighted smoothing method [6] are the special cases in Spline function. The value of P has a significant influence on smoothing result.

Figures 24, 25, and 26 show the effect of SSP on pressure trace, RHR, and power spectrum. When SSP value regulates from 1.0 to 0.2, the smoothed pressure trace deviates from the original pressure trace greatly; part of valuable signal in pressure trace was filtered shown in figure 24; the peak of RHR becomes more

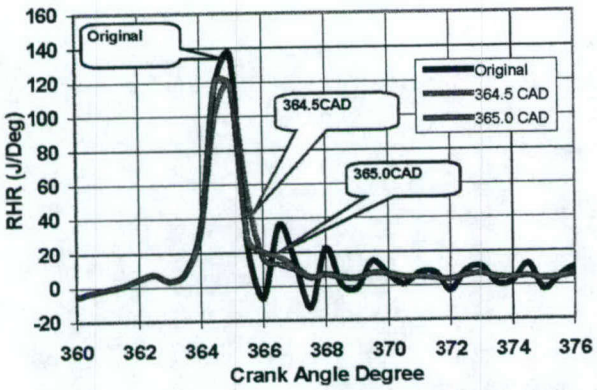

Figure 22(b). Rate of heat release corresponding to figure 22(a)

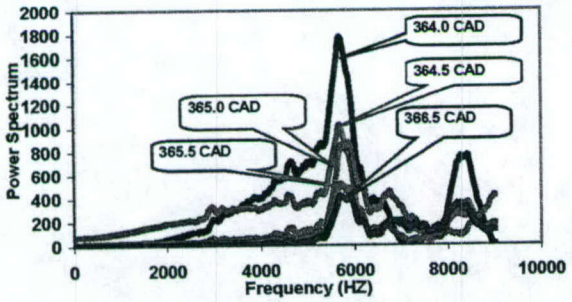

Figure 22(c). Relationship between power spectrum and frequency at different starting smoothing points at engine speed 1500rpm, 45% EGR and 1300 bar injection pressure.

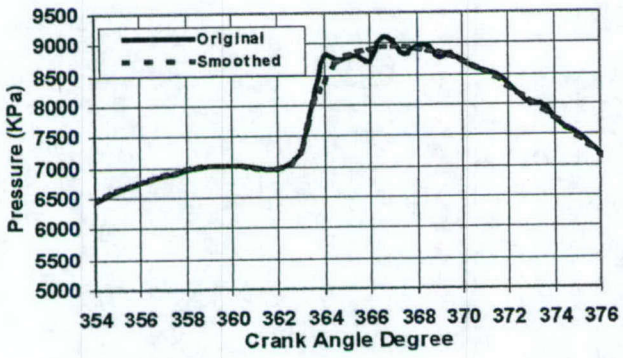

Figure 23(a). Pressure traces smoothed by Spline function at 1.0 CAD before RRPOPT at engine speed 2000rpm, 0% EGR, IMEP 500KPa and 1200 bar injection pressure

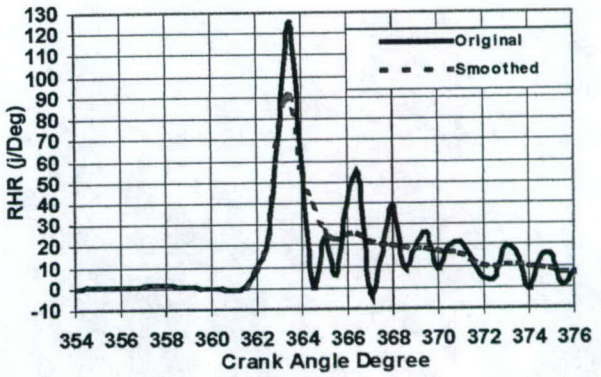

Figure 23(b). Rate of heat release corresponding to figure 23(a)

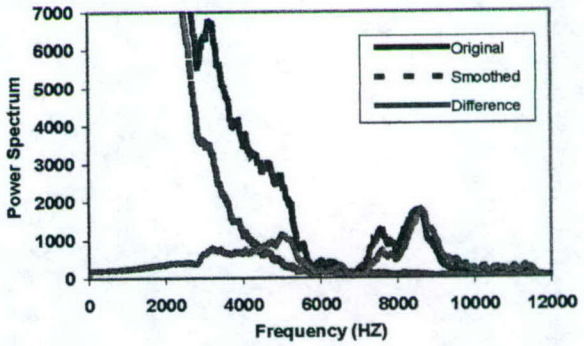

Figure 23(c). Power spectrum at 1.0CAD before RRPOPT at engine speed 2000rpm, 0% EGR, IMEP 500KPa and 1200 bar injection pressure.

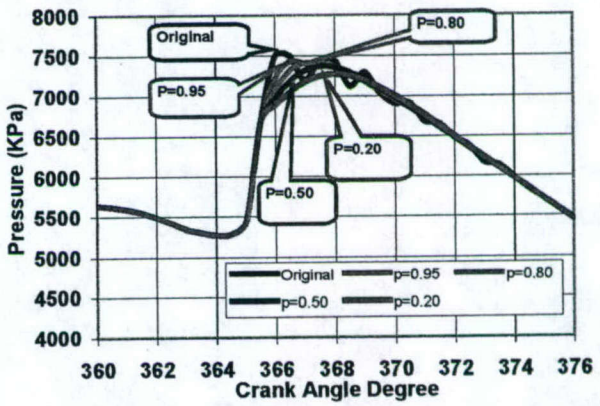

Figure 24. Effect of SSP on smoothed pressure trace at engine speed 1500 rpm, 0%EGR and 1300 bar injection pressure

flat, and the fraction of diffusion combustion increases that is, the selection of SSP value can arbitrarily change the distribution of calculated fuel burnt in premixed combustion and diffusion combustion. Therefore, the SSP value also has a significant effect on the smoothing pressure trace and the analysis of RHR. The higher is the SSP value, the less noise is filtered. On the contrary, the lower is the SSP value, the more is the useful signal filtered shown in figure 26. The rule to select SSP value is (a) to keep the magnitude of power spectrum of pressure difference between original pressure trace and smoothed pressure trace in relatively low value as frequency is less than the natural frequency in power spectrum-frequency map, or (b) to get maximum SSP value as all the disturbances in power spectrum curve of smoothed pressure trace are removed mostly. The optimal SSP value at this running condition ranges from 0.85 to 0.95. And the optimal SSP value will change with engine running condition such as engine load. Figure 27 show the effect of SSP value on smoothing quality at engine speed 2000 rpm, 0%EGR, 500 KPa and injection pressure 1200 bar. When engine load increases, the amount of fuel burned in premixed combustion increases and pressure trace oscillation increases either.

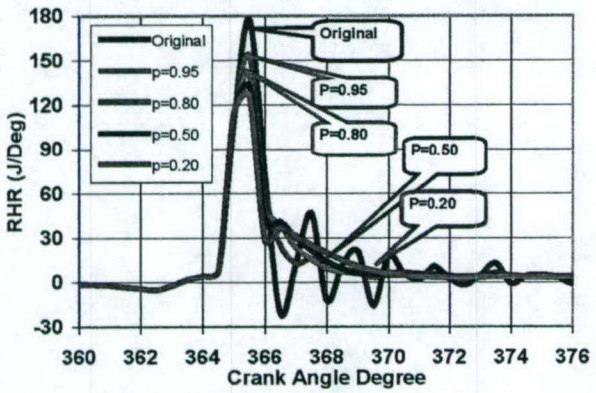

Figure 25. RHR corresponding to figure 24

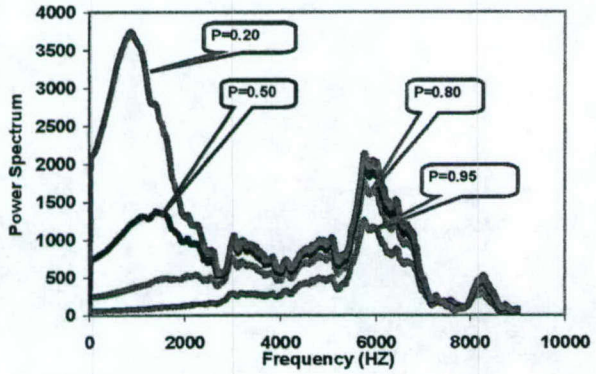

Figure 26. Relation between power spectrum and frequency corresponding to pressure difference in figure 24 between original and smoothed pressure traces

Application

The Spline function is applied to smooth cylinder pressure trace under the running condition of engine speed 2000 rpm, 0% & 45% EGR ratios and injection pressures 800 bar, 1000 bar & 1200 bar, starting smoothing point at 1.0 CAD before the RRPOPT. Figures 28(a) &(b) show the original pressure trace, smoothed pressure trace and their RHR at 0% EGR and injection pressures 1000bar & 1200 bar. The oscillation in pressure trace and RHR curve is reduced significantly. The Spline function filtered most of the disturbance at the high frequency shown in figure 29(a) &(b) and kept useful low frequency signal.

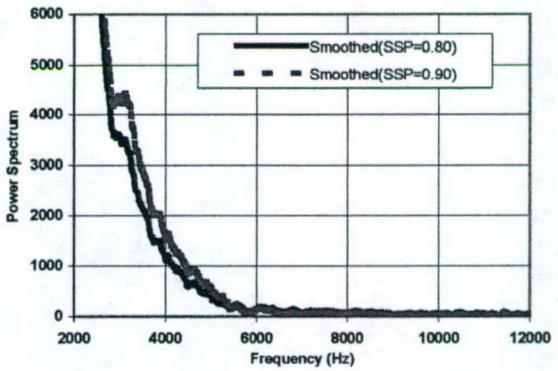

Figure 27. Effect of SSP value on smoothing quality at engine speed 2000 rpm, 0%EGR, 500 KPa and injection pressure 1200 bar.

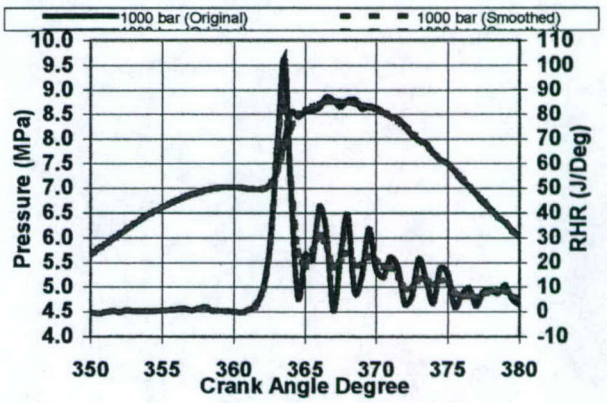

Figure 28(a). Original and smoothed pressure traces and their RHR at engine speed 2000 rpm, 0%EGR, 1000 bar injection pressure

The identical conclusion can be derived at engine speed 2000 rpm, 45% EGR and various injection pressures shown in figures 30 and 31. Compared to the running condition of engine speed 1500rpm, the following results can be obtained: (1) The SSP value is reduced to 0.65~0.80; (2) The frequencies of the disturbance larger than 3000 Hertz caused by combustion flame are different to those at 1500 rpm;

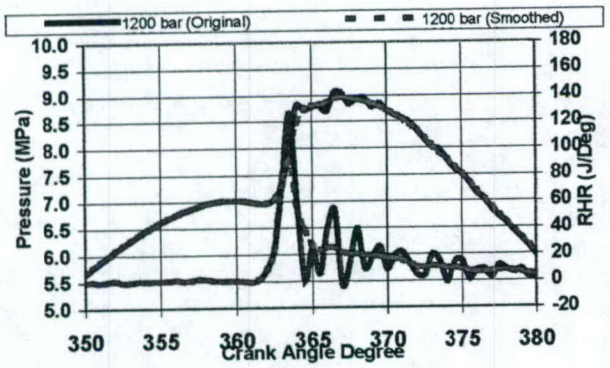

Figure 28(b). Original and smoothed pressure traces and their RHR at engine speed 2000 rpm, 0%EGR, 1200 bar injection pressure

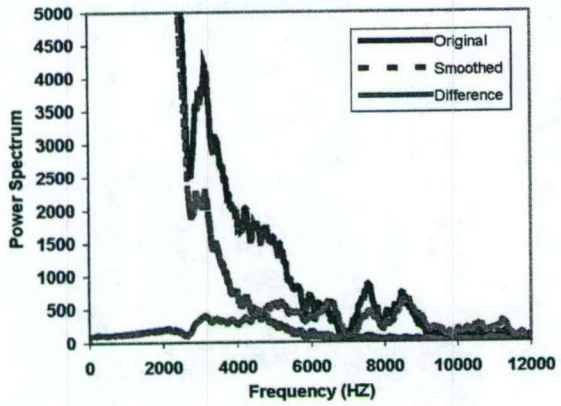

Figure 29(a). Relation between power spectrums of original pressure trace, smoothed pressure and their difference and frequency corresponding to figure 28 (a)

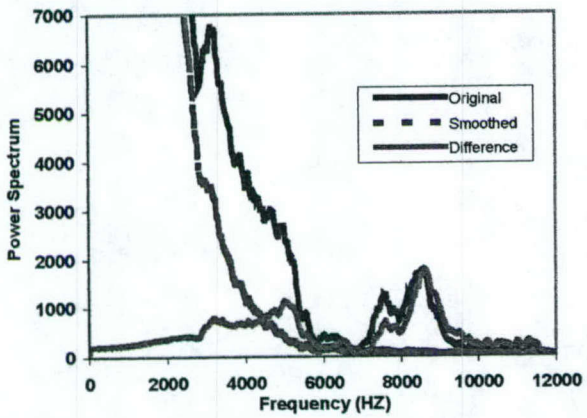

Figure 29(b). Relation between power spectrums of original pressure trace, smoothed pressure and their difference and frequency corresponding to figure 28(b)

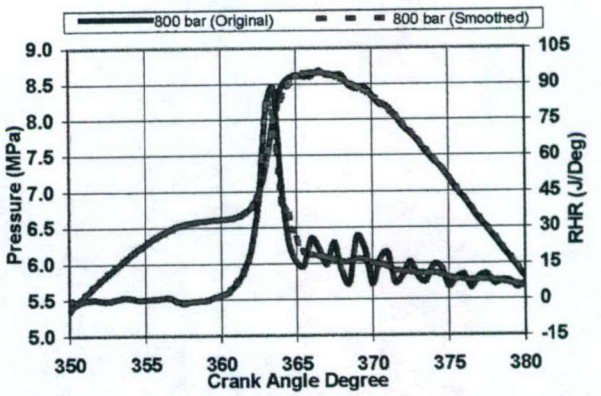

Figure 30(a). Original and smoothed pressure traces and their RHR at engine speed 2000 rpm, 45%EGR, 800 bar injection pressure

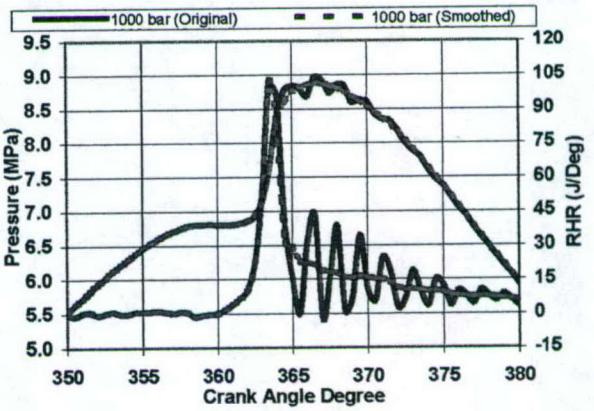

Figure 30(b). Original and smoothed pressure traces and their RHR at engine speed 2000 rpm, 45%EGR, 1000 bar injection pressure

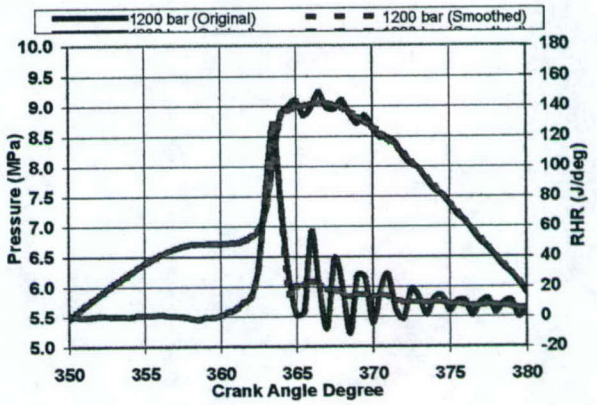

Figure 30(c). Original and smoothed pressure traces and their RHR at engine speed 2000 rpm, 45%EGR, 1200 bar injection pressure

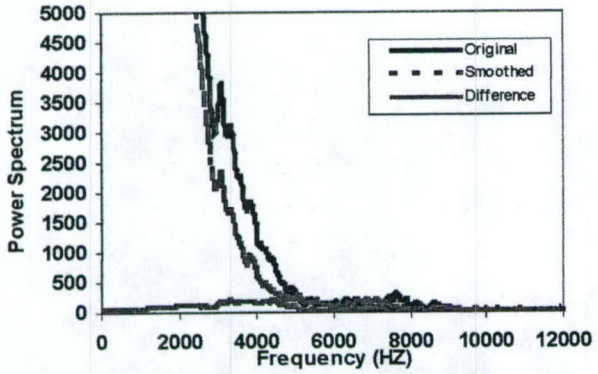

Figure 31(a). Relation between power spectrums of original pressure trace, smoothed pressure and their difference and frequency corresponding to figure 30(a)

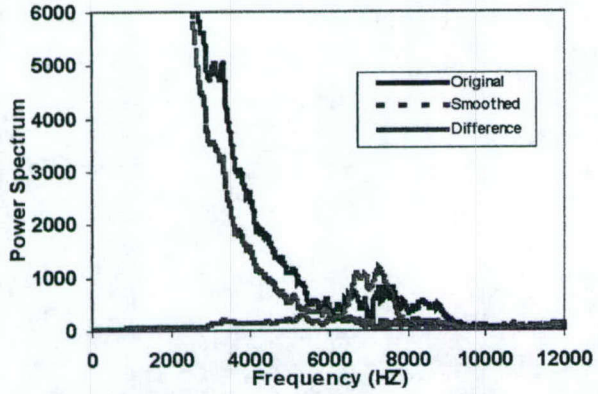

Figure 31(b). Relation between power spectrums of original pressure trace, smoothed pressure and their difference and frequency corresponding to figure 30(b)

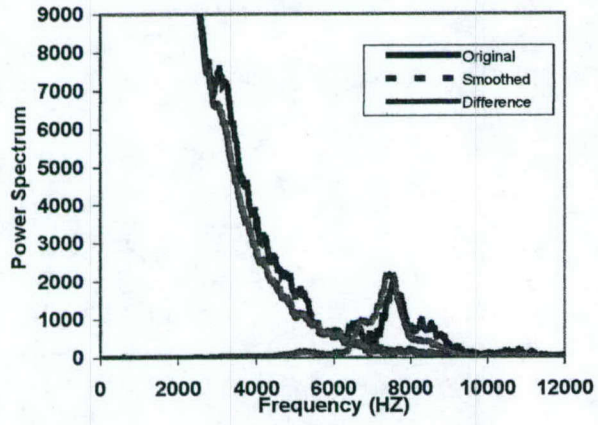

Figure 31(c). Relation between power spectrums of original pressure trace, smoothed pressure and their difference and frequency corresponding to figure 30(c)

(3) The peaks of the disturbance of power spectrum increase with the increase of engine load, EGR percentage and injection pressure. Clearly, the peaks of the disturbance of power spectrum at frequency lager than 2000 hertz are the source of combustion noise. Therefore, reducing the peaks of the disturbance is one of the most available approaches to eliminate engine emission noise when designing combustion system of diesel engines.

Figures 32 (a)&(b) show 4 consecutive cyclic pressure traces at engine speed 2000 rpm, 0%EGR and 1200 bar injection pressure, smoothed 1.0 CAD before the RRPOPT. The pressure data oscillation at each cycle is different, which causes their corresponding RHR oscillations. Figure 33 shows power spectrum analysis of these original pressure traces and of the difference between original and smoothed pressure traces. At various cycles, the distribution of disturbance in some frequencies is completely different, and in other frequencies is almost identical, compared to figure 29(c), which shows the power spectrum of averaged cylinder pressure trace of 35 cycles. It is clear that some of the disturbances are random noises that can be removed by averaged cycle number of data acquired; the others are systematic error, which cannot be eliminated through this method. Figures 32(a)&(b) show that the smoothing method is also very effective for smoothing transient data.

Injection timing has significant effect on premixed combustion, which has great influence on NOx formation and engine emission noise. Figure 34 shows the power spectrum of pressure traces at various injection timings under engine speed 2000 rpm, 0%EGR, IMEP 700 KPa and 1200 bar injection pressure (the pressure traces are shown in figure 12). As analyzed above, the magnitude of power spectrum of these disturbances is related to the engine emission noise. Therefore, reducing injection-timing retarding can lower engine emission noise. The approach to lower engine emission noise is to reduce the pressure trace oscillation during fuel combustion. The combination of pilot injection and main injection with injection timing retarding is one of the most effective approaches to reduce engine emission noise and improve engine fuel economy [23,24,25].

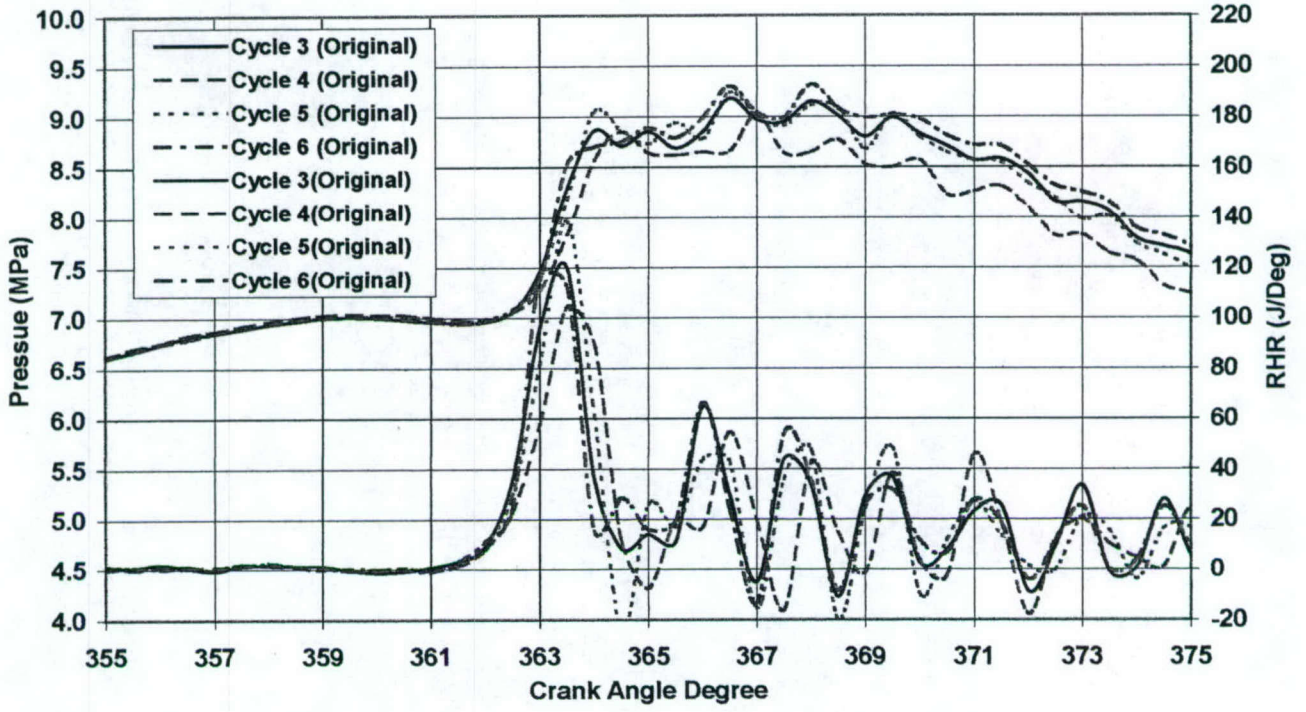

Figure 32 (a). Non-smoothed consecutive pressure traces and their RHR at engine speed 2000 rpm, 0% EGR and 1200 bar injection pressure

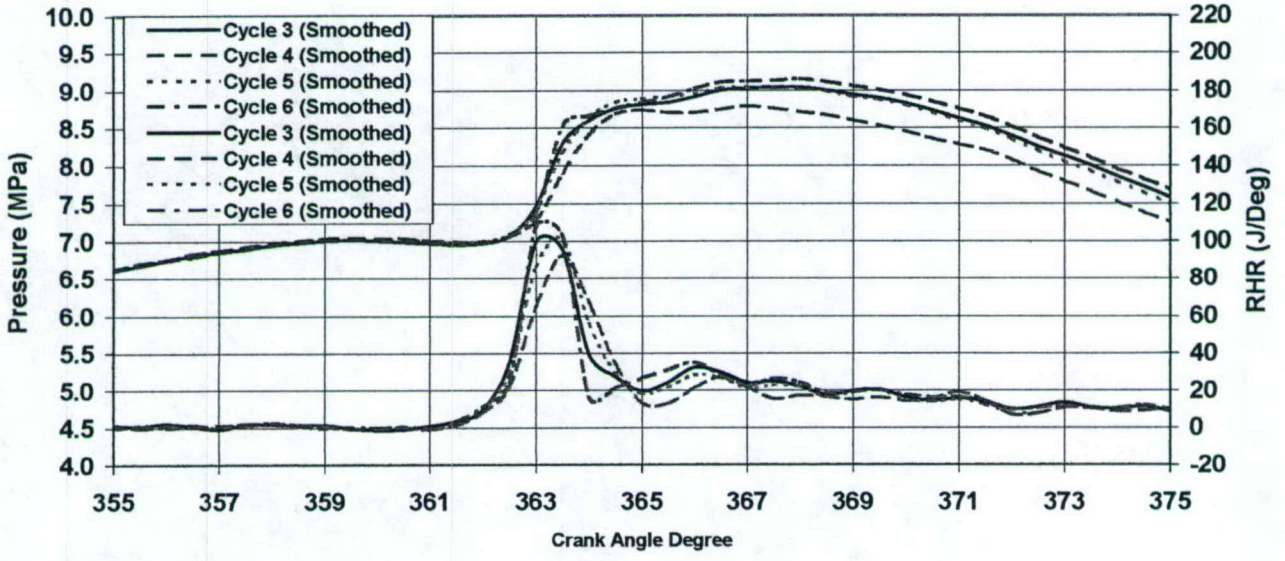

Figure 32 (b). Smoothed consecutive pressure traces and their RHR at engine speed 2000 rpm, 0% EGR and 1200 bar injection pressure

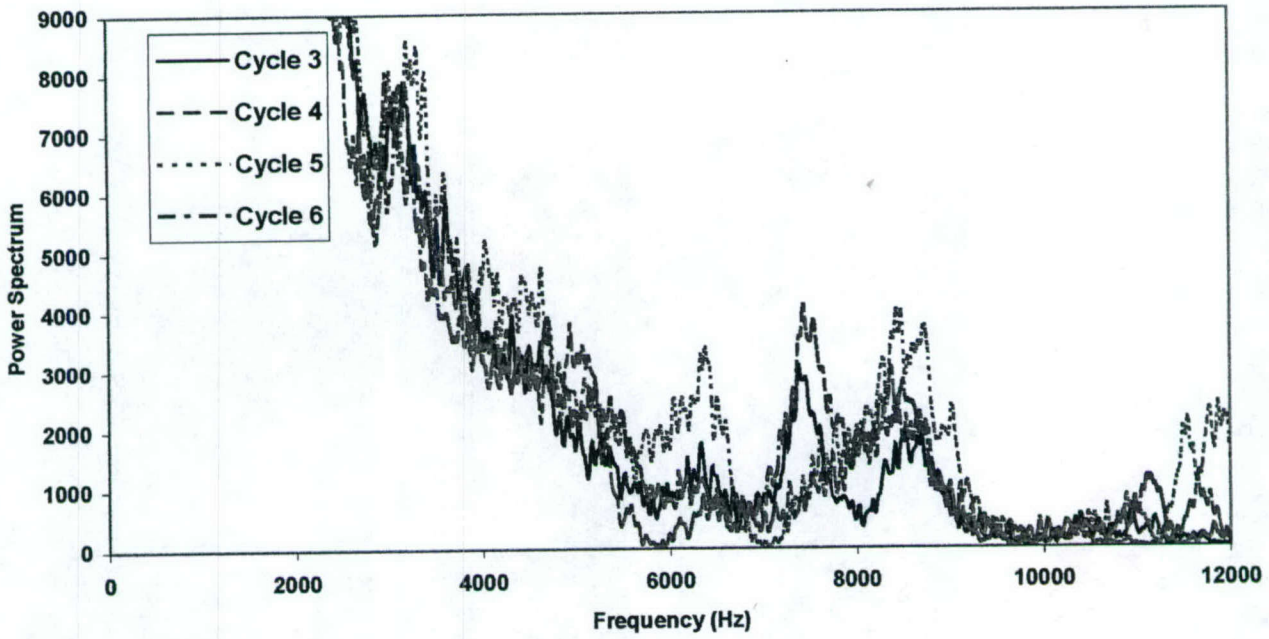

Figure 33(a). Power spectrum of original cylinder pressure traces at engine speed 2000 rpm, 0%EGR and 1200 bar injection pressure

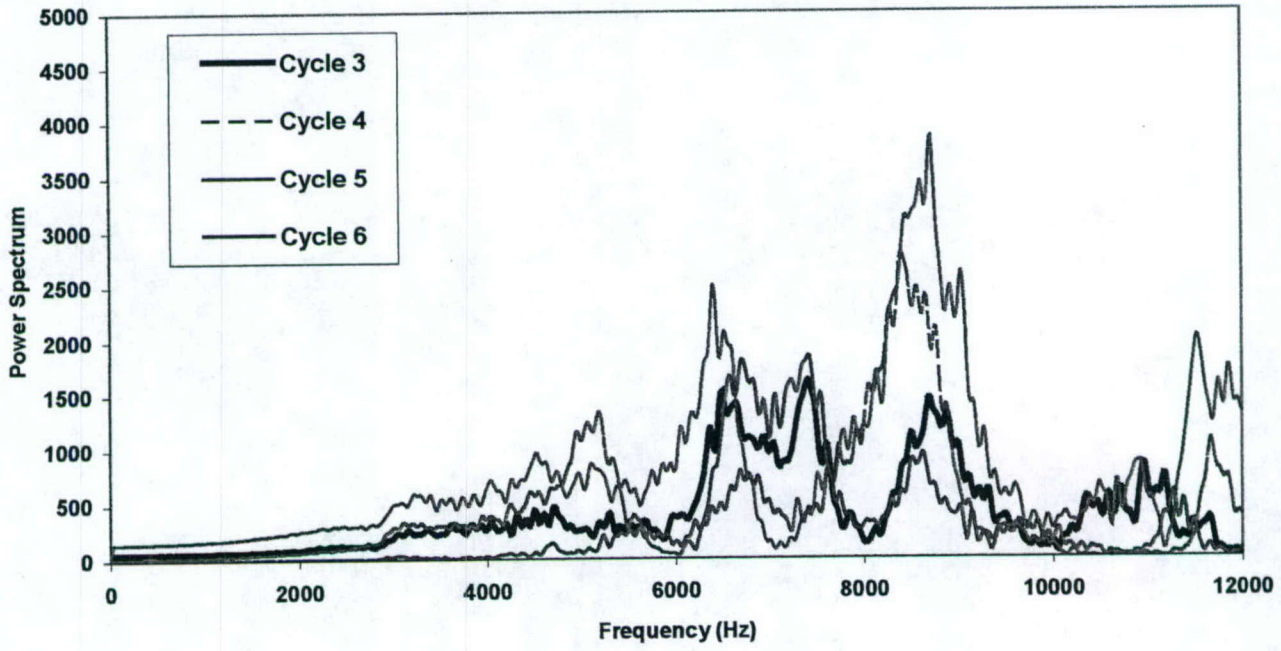

Figure 33(b). Power spectrum of cylinder pressure difference between original and smoothed pressure traces at engine speed 2000 rpm, 0%EGR and 1200 bar injection pressure

LIST OF SYMBOLS

CAD: Crank angle degree
CRS: Common rail fuel injection system
EGR: Exhaust gas recirculation
FFT: Faster Fourier Transform
FIR: Finite impulse response
IIR: Infinite impulse response
IMEP: Indicated mean effective pressure
LPA: Least-square polynomial approximation
MIP: Mean indicated pressure
PM: Particulate matter
RHR: Rate of heat release
RRPOPT: Rapid raising peak of pressure trace
SSP: Specified smoothing parameter

APPENDIX A

The tests covered conditions shown in table 1. For all tests, the injection timing was adjusted to ensure that the cycle peak cylinder pressure is located between 6 and 7 crank angle degree after TDC.

Table 1 Test conditions for engine

Specifications			
Engine speed	rpm	1500	2000
IMEP	KPa	300	500
Intake pressure	Bar	1.2	1.4
Exhaust pressure	Bar	1.5	1.8
Intake temperature	°F	170	170
Coolant temperature	°F	180	180
Oil temperature	°F	140	140
Specifications	Units	Description	
Combustion system	units	Direct injection	
Total piston displacement	Cm^3	421.932	
Working cycle		4-stroke	
Bore	mm	79.5	
Stroke	mm	85	
Direction of rotation		Counterclockwise	
No. of cylinder		1	
Rated speed (max)	rpm	4000	
Compression ratio		20:1	
Valve system		2 In./ 2 Exh.	
Cooling system		External water pump	
Lubricating system		External oil pump	
Injection system		Bosch common rail (Max. injection pressure 1350bar)	
Length of connecting rod	mm	179	
Swirl ratio		1.5 to 3.5	

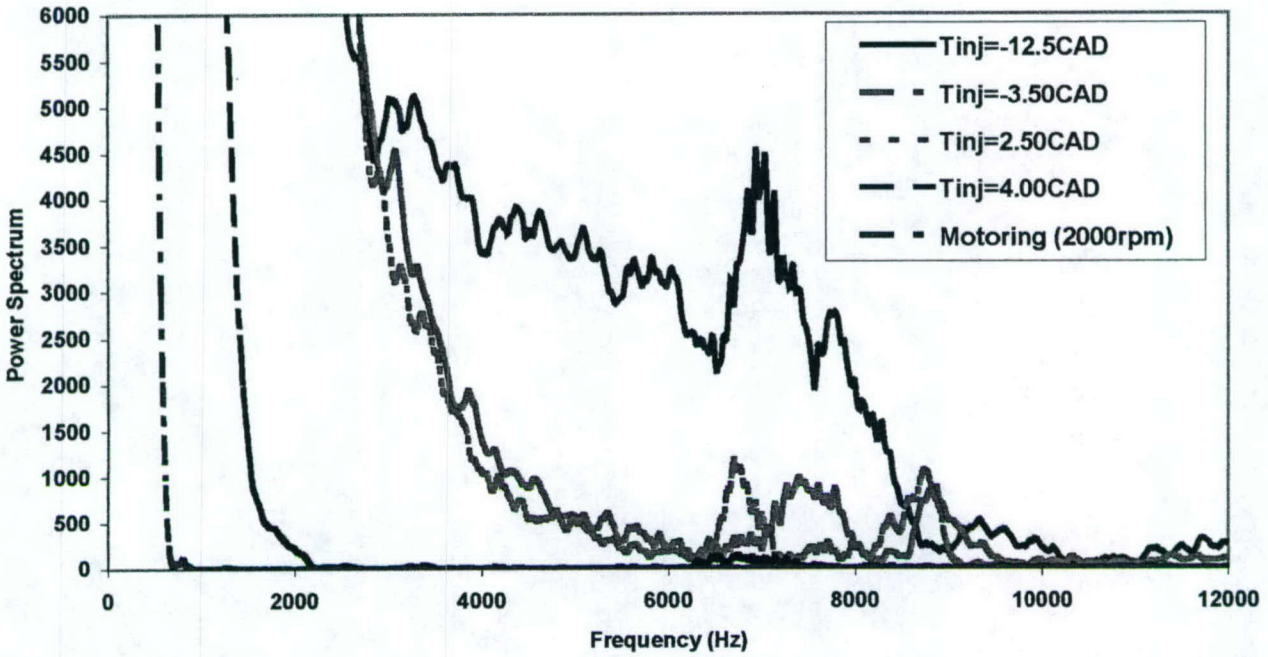

Figure 34. Power spectrum of cylinder pressure traces at various injection timing and at engine speed 2000 rpm, 0%EGR, IMEP 700 KPa and 1200 bar injection pressure

CONCLUSION

The following conclusions are based on an investigation conducted on a single-cylinder, small bore, high-speed, direct injection diesel engine. Tests were conducted under simulated turbocharged conditions using min-sac 320 nozzle and VCO 430 nozzle at two sets of loads and speeds, and covered a wide range of injection pressures, EGR ratios and injection timings.

1. It is necessary to smooth cylinder pressure trace for calculating RHR and analyzing engine combustion.
2. The natural frequency of the combustion pressure wave is located around 3000 Hertz for the engine, and injection pressure has little direct effect on the disturbance.
3. The oscillation in pressure traces increases with the increase of injection pressure, EGR percentage and engine load.
4. Retarding injection timing can reduce the magnitude of the disturbance related to engine emission noise
5. Among the smoothed methods discussed in this paper, the Spline function is the most effective one for smoothing both steady and transient cylinder pressure traces. Meanwhile, the starting smoothing point and SSP have a significant effect on the accuracy to analyze RHR and to eliminate system error. The optimal starting smoothing point is at the point of ¼ natural period in crank angle degree before the rapid rising peak of cylinder pressure and SSP should be changed with the change of engine load.
6. The rule to select optimal SSP value is to get maximum SSP value when the disturbance in power spectrum of smoothed pressure trace is removed mostly.

ACKNOWLEDGEMENT

The U S Department of Energy, Office of Transportation Technologies, Office of Advanced Automotive Technologies, support this program. This is a part of the PNGV program, conducted under the technical sponsorship of Sandia National Laboratories. The continuous technical support and help of Dr. Paul Miles, in running this program and supplying engine parts and instruments is gratefully acknowledged and appreciated.

Also, the support of the U.S. Army TARDEC, ARO and ARC is acknowledged. The cooperation and help of Lydia Nedeltcheva, Inderpal Singh and other members of the Center for Automotive Research and the machine shop at Wayne State University is appreciated.

REFERENCE

1. Miles, P., "The influence of Swirl on HSDI Diesel Combustion at Moderate and Load", SAE Paper 2000-01-1829, 2000.
2. Oppenheim, A.V., and R.W. Schafer. Discrete-Time Signal Processing. Englewood Cliffs, NJ: Prentice Hall, 1989. Pgs. 311-312.
3. Rohrer, R. and Chehroudi, B. " Preliminary Heat Release Analysis in a Single-cylinder Two-stroke Production Engine", SAE Paper 932431, 1993.
4. Andrew,L.R., "Cylinder Pressure Based Combustion Analysis in Race Engines", SAE Paper 942487, 1994.
5. Ullrich, W., " The Influence of Error in Finding TDC on the determination of Mean Indicated Pressure (MIP)", MTZ, Vol. 44, 1983.
6. Harndorf, H., Klösel, R. and Volkart, A., "Optimization of Parameters Concerning Measurement and Analysis of Cylinder Pressure Data", MTZ, Vol. 53, 1993.
7. Schmillen, K., Flotho, A. and Schlünder, " Determination of the Sound Transmission Rate of Diesel Engines By Means of Cyclic Fluctuations", SAE Paper 931331, 1993.
8. Hsu, D.B., " Practical Diesel-Engine Combustion Analysis", SAE International, 2002.
9. Grimm, B.M., and Johnson, R.T., " Review of Simple Heat Release Computations", SAE Paper 900445, 1990.
10. Deshpande, S.R., and Narasimhan, R.," Heat Release Analysis of a Two-stroke Engine", SAE Paper 880175, 1988.
11. Lancaster, D. R., Krieger, R.B. and Lienesch, J.H., " Measurement and Analysis of Engine Pressure Data", SAE Paper 750026, 1975.
12. Gatowski, J.A., Balles, E.N., Chun, K.M., Nelson, F.E., Ekchian, J.A., and Heywood, J.B., " Heat Release Analysis of Engine Pressure Data", SAE Paper, 841359, SAE Trans., Vol. 93, 1984.
13. N.A.Henein, M.C.Lai, I.Singh, D.H.Wang, L.Liu, "Emission trade-off and combustion characteristics of a high-speed direct injection diesel engine", SAE paper No. 2001-01-0197, 2001.
14. N.A. Henein, M.C Lai, I.P. Singh,L. Zhong, J. Han,"Characteristics of A Common Rail Diesel Injection System Under Pilot and Post Injection Modes", SAE paper No. 2002-01-0218, 2002
15. N. A. Henein, I.P. Singh, L. Zhong, M-C. Lai, W. Bryzik, "New Integrated "O.P.E.R.A.S." Strategies for Low Emissions in HSDI Diesel Engines ", SAE Paper 2003-01-0261, 2003.
16. Heywood, J.B., Internal Combustion Engine Fundamentals, McGraw-Hill, 1988.
17. Schneider, M., Schmillen, K., and Pischinger, F., " Regularities of Cylinder Pressure Oscillations and Their Effects on the Combustion Process and Noise", SAE Paper 872248, 1987.
18. Zhong, L., Singh, I.P., Han, J., Lai, M-C, Henein, N.A., Bryzik, W., "Effect of Cycle-to-Cycle Variation in the Injection Pressure in a Common Rail Diesel Injection System on Engine Performance ", SAE Paper 2003-01-0699, 2003.
19. De Boor, C., A Practical Guide to Splines, Springer-Verlag, 1978.
20. Forsythe, G. E., M. A. Malcolm, and C. B. Moler, Computer Methods for Mathematical Computations, Prentice-Hall, 1976.
21. Schihl, P., Tasdemir, J., Schwarz, E., and Bryzic, W., "Development of a Zero-Dimensional Heat Release Model for Application to Small Bore Diesel Engines", SAE Paper 2002-01-0073, 2002.
22. Akihama, K., Takatori, Y., Inagaki, K., Sasaki, S., Dean, A.M., " Mechanism of the Smokeless Rich Diesel Combustion by Reducing Temperature", SAE Paper 2001-01-0655, 2001.
23. Sasaki, S., Ito, T., Goto, M., Yoshizaki, K., " A Study of Low Temperature Diesel Combustion System", TOYOTA Technical Review, Vol. 50 NO. 2 Mar. 2001.
24. Kimura, S., Aoki, O., Kitahara, Y. and Aiyoshizawa, E., " Ultra-Clean Combustion Technology Combining a Low-Temperature and Premixed Combustion Concept for Meeting Future Emission Standards", SAE Paper 2001-01-0200, 2001.
25. Singh, I.P., Zhong, L., Lai,M.-C., Henein, N.A. and Bryzik, W. " Effect of Nozzle Hole Geometry on A HSDI Diesel Engine-out Emissions", SAE Paper 2003-01-0704, 2003.
26. Kuratle, R.H., " Measuring Spark Plugs With Integrated Cylinder Pressure Sensor", C465/019, ImechE, 1993.
27. Puzinauskas, P.V., Eves, J.C., and Tiuman, N.F., " Measuring Absolute-Cylinder Pressure and Pressure Drop Across Intake Valves of Firing Engines", SAE Paper 941881, 1994